# Structural Basis of Arrestin Mediated GPCR Signaling

By

Qiuyan Chen

Dissertation
Submitted to the Faculty of the
Graduate School of Vanderbilt University
in partial fulfillment of the requirements
for the degree of

DOCTOR OF PHILOSOPHY
in

Pharmacology
December 2015
Nashville, Tennessee

Approved:

Brian Wadzinski, Ph. D

Tina M. Iverson, Ph. D

Vsevolod V. Gurevich, Ph. D

Charles R. Sanders, Ph. D

Heidi E. Hamm, Ph. D

# ACKNOWLEDGEMENTS

I’d like to thank everyone who appears in my life.

I AM WHO I AM BECAUSE I KNOW YOU.

TABLE OF CONTENTS

Page

LIST OF FIGURES

Chapter 1



Chapter 2



Chapter 3



Chapter 4

# Chapter 1

# INTRODUCTION

A portion of this introduction here was published as part of a review in Methods in Molecular Biology – Springer [1]. Sergey A. Vishnivetskiy, Tiandi Zhuang, Min-Kyu Cho, Tarjani M. Thaker, Charles R. Sanders, Vsevolod V. Gurevich, and TM Iverson contributed to the work.

## G protein coupled receptor signaling

G protein coupled receptors (GPCRs) [2, 3] are located in the cell membrane and respond to thousands of stimuli [4], thus mediating critical physiological processes, such as vision, blood pressure regulation, mood control and so on. Abnormal modulation of GPCR signaling leads to pathological conditions [5] and small molecules targeting GPCRs are widely used for therapeutic purposes [6, 7]. Understanding the structural basis of GPCR signaling regulation will help guide the drug design.

There are more than 800 different GPCRs in the human genome [8]. The best-characterized receptor is perhaps the photoreceptor rhodopsin, which is located in the disk membranes of rod outer segments in the retina [9]. In the dark state, rhodopsin is covalently attached to its inverse agonist, an 11-*cis*-retinal chromophore. Upon activation, the 11-*cis*-retinal absorbs a photon of light, converting it to all-*trans*-retinal [10, 11]. This promotes a conformational change in rhodopsin that couples to the G protein transducin and catalyzes the exchange of GDP to GTP of the α subunit of transducin [12-14]. GTP bound Gα subunit then dissociates from rhodopsin and Gβγ and activate its downstream effector phosphodiesterase, which eventually results in an electrical signal that allows dim light vision [15].

## The role of arrestin-1 in rhodopsin signaling

Rhodopsin signaling is quenched by visual arrestin-1 (**Figure 1**) [16, 17]. This involves two steps. In the first step, light-activated rhodopsin is phosphorylated at multiple sites by G protein receptor kinase 1 (GRK1) [18, 19]. Arrestin-1 requires a minimum of three rhodopsin-attached phosphates for high affinity binding [20, 21]. In the second step, arrestin-1 binds to light-activated, phosphorylated rhodopsin (p-*Rh) and blocks further transducin coupling (**Figure 1,2**) [17]. The direct competition between arrestin-1 and transducin led to the hypothesis that they share common receptor-binding motif even before any structural information was available. Indeed, it was verified later that the C terminus of G proteins and an inter-domain loop (finger loop) of arrestins contain a consensus motif which folds into a α-helix and inserts into a cytoplasmic crevice of the receptor upon activation [22-25].

Receptor binding triggers the transition of arrestin-1 from the basal to the active state(s). Arrestin-1 has two distinctly folded domains, termed the N- and C-domains (**Figure 3**) [26-28]. In the basal, non-receptor-binding state, the distal C-terminal segment binds to the N-domain through two major interaction interfaces. One is the polar core comprising five charged residues in the N-domain (D30, R175), the C-domain (D296, D303) and the distal C-terminus (R382) (**Figure 3**) [27]. The other is the hydrophobic three-element interaction between β-strand I (V11, I12, F13) and α-helix I (L103, L107, L111) in the N-domain and F375, V376, F377 in the C-terminus (**Figure 3**) [27]. Receptor binding is proposed to disrupt the polar core and destabilize the three-element interaction, which results in the release of the distal C-terminus [29-32]. Complementary

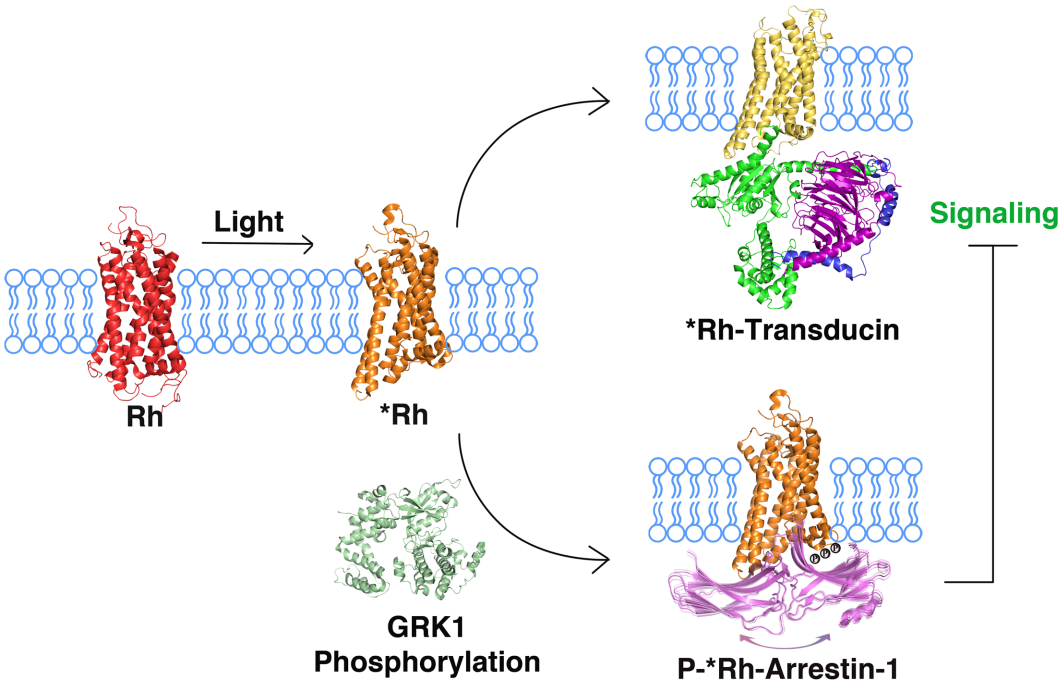


**Figure 1. Role of arrestin-1 in rhodopsin signaling.** Rhodopsin is located in the disk membranes of the outer segments of rod photoreceptor cells. Upon light activation, dark rhodopsin (PDB: 1F88) undergoes conformational change to the active state (PDB: 3PQR). Its cognate G protein, transducin, binds to the active rhodopsin and initiates the downstream signaling (structure from molecular simulation). Active rhodopsin also recruits and activates GRK1 (PDB: 3C50). *Rh is phosphorylated at multiple sites by GRK1. Arrestin-1 binds to active phosphorylated rhodopsin (p-*Rh), blocking further transducin activation by steric exclusion. The displayed p-*Rh-arrestin-1 complex is the assembly of *Rh (PDB: 3PQR) and pre-activated arrestin-1 (PDB: 4J2Q) in Pymol. Arrestin-1 gains conformational flexibility in the receptor bound state.

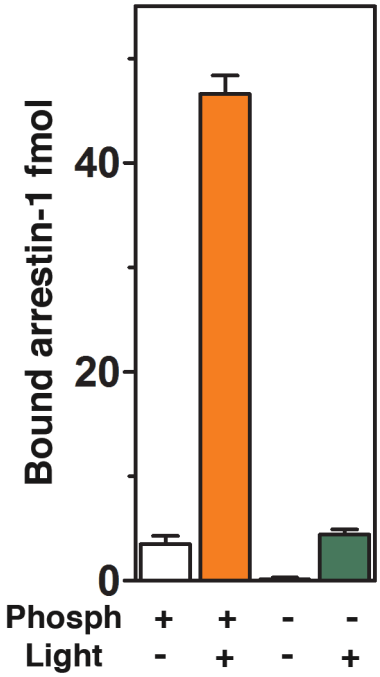


**Figure 2. Arrestin-1 has very high selectivity for phosphorylated active rhodopsin.** Its binding to phosphorylated active rhodopsin is about 10-20 fold higher than to only-activated or only-phosphorylated rhodopsin, while its binding to dark rhodopsin is barely detectable.

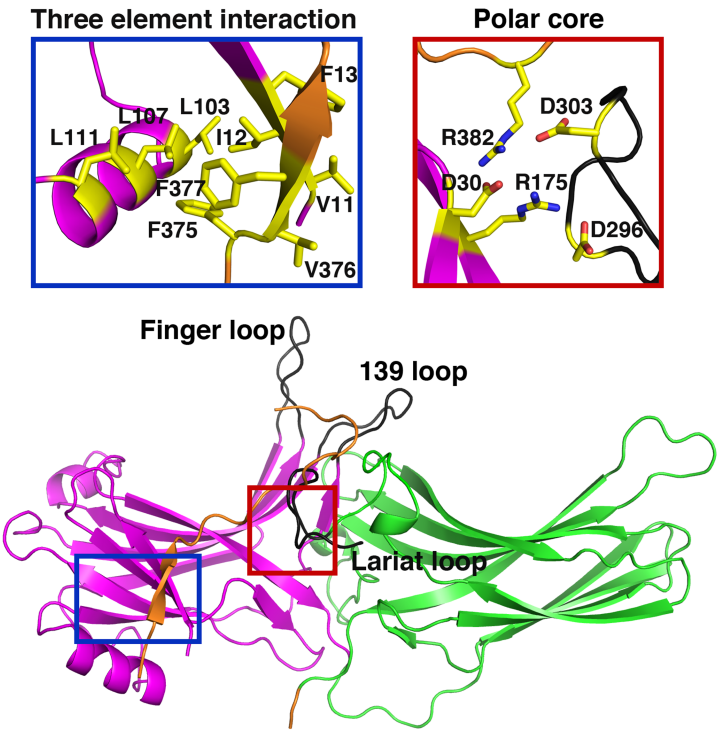


**Figure 3. The crystal structure of arrestin-1 (PDB: 1CF1).** The N-domain is colored magenta, the C-domain is colored green and the C-terminus is colored orange. Three loops have been reported to be involved in receptor binding: the finger loop, the 139 loop (referred to as the middle loop for non-visual arrestins) and the lariat loop, are shown in dark grey. Two major interactions that stabilize arrestin-1 in the basal state are displayed in details. The polar core comprises five charged residues distributed between the N-domain (D30, R175), the C-domain (D296, D303) and the C-terminus (R382). The hydrophobic three-element interaction is between β-strand I (V11, I12, F13) and α-helix I (L103, L107, L111) in the N-domain and F375, V376, F377 in the C-terminus.

studies employing site-directed spin labeling and electron paramagnetic resonance, functional mapping of arrestin-1 at single amino acid resolution, X-ray crystallography of pre-activated arrestin-1 and arrestin-1-rhodopsin complex, have also suggested that loops in between the two domains: the finger loop (residue 68-78), the middle loop (residue132-142) and the lariat loop (residue 293-306), are involved in receptor binding [2, 22, 33, 34]. In addition to these discrete conformational changes, recent evidence strongly suggests that arrestin-1 gains significant conformational flexibility upon binding to p-*Rh [32, 35].

**Arrestin-2 and arrestin-3 mediated signaling**

There are four known vertebrate arrestins, two visual arrestins (arrestin-1 and arrestin-4) [36, 37] and two non-visual arrestins (arrestin-2 and arrestin-3) [38, 39]. Arrestin-2 and -3 are ubiquitously expressed and each can mediate the signaling of ~800 GPCRs. They compete with G protein for active receptor binding and mediate the internalization of the active receptor to terminate G protein mediated signaling [40, 41]. It was later discovered that receptor bound arrestin is in its active conformation [22, 32] and is able to initiate G protein independent signaling [42]. Arrestin-2 and -3 serve as adaptors and scaffolds and bring a board range of cellular partners [43], such as E3 ubiquitin ligases [44, 45], mitogen-activated protein kinases (MAPKs) [46, 47], and Src [48, 49], to the activated receptors. Interestingly, it has also been revealed that arrestin can mediate the signaling independent of receptor, for example, arrestin-3 mediated c-Jun NH2-terminal protein kinase (JNK)3 activation was detected in the absence of receptor agonist [50]. However, it is remains largely unknown whether arrestin can be activated by other components in the cells.

Arrestin-2 and -3 share 88% similarity in the amino acid sequence and the mice with either β-arrestin1 or -2 knockout are viable, whereas the double-knockout phenotype is embryonic lethal [51, 52]. This indicates that arrestin-2 and -3 can at least partially substitute each other. Intriguingly, each isoform has some unique functions. For example, only arrestin-3 promotes the activation of c-Jun NH2-terminal protein kinase (JNK)3 [53], as well as ubiquitous JNK1/2 in cells [54], acting as a scaffold that brings together the MAP kinase cascade MAPKKK ASK1, MAPKKs MKK4 and MKK7, and several isoforms of JNK1/2/3 [50, 53-58]. The mechanism under the functional divergence between arrestin-2 and -3 remains unexplored. Further investigation will advance our knowledge in isoform selectively signaling and guide the drug design for biased agonist targeting one specific pathway.

# CHAPTER 2

# DEVELOPMENT OF MEMBRANE MODEL SYSTEM TO STUDY THE RECEPTOR-ARRESTIN INTERACTION

A portion of the text in this chapter is published as a review in Methods in Molecular Biology – Springer [1]. Sergey A. Vishnivetskiy, Tiandi Zhuang, Min-Kyu Cho, Tarjani M. Thaker, Charles R. Sanders, Vsevolod V. Gurevich, and TM Iverson contributed to the work.

## Introduction

Structure-function studies of both rhodopsin and arrestin-1 have advanced our understanding of the molecular mechanisms of vision. However, caution should be taken when applying these *in vitro* findings to the interpretation of the physiological process of vision. A major concern comes from fact that most studies begin by extracting the receptor or the receptor complex from the lipid bilayer into detergent micelles, and thus the influence of the membrane is not accounted for. However, the lipid composition of the highly specialized disk membranes dramatically affects rhodopsin signaling [59, 60]. For this reason, several alternative membrane model systems have been explored that may be more native-like than micelles. Here we focused on the reconstitution of rhodopsin into bicelles and its consequences for rhodopsin signaling, particularly arrestin-1-mediated signal termination. In particular, I am focused on the methods to reconstitute rhodopsin into bicelles and perform binding and functional studies in bicelles. A detailed material list and methods are the main part of this chapter.

### Introduction to bicelles

Bicelles, first introduced by the Prestegard lab [61-64], have a central planar bilayer formed by long-chain lipids and edges shielded by either short-chain lipids or detergents (Figure 1). The planar surface of bicelles and bilayered interior mimics the

biological membrane much better than detergent micelles, while due to their small size and monodispersity the attractive features of conventional micelles are retained. Indeed, bicelles have been successfully used to crystallize several membrane proteins [64], particularly the GPCR β2 adrenergic receptor, after decades of efforts using traditional detergent crystallization failed [65].

The long-chain lipid determines the thickness of the lipid bilayer, while phospholipids with different head groups can tailor the charge characteristics of the surface and provide lipid composition versatility. Both the total phospholipid concentration (*c*) and ratio (*q*) of long-chain:short-chain phospholipid (or long-chain phospholipid:detergent) play an important role in shaping bicelles. Intuitively, a high *q* value indicates an extended bilayer while bicelles with a low *q* value (e. x. $q<1$) more closely resemble round isotropic spheres (Figure 1). It is a matter of some debate as to whether bicelles with $q \leq 0.5$ retain any of the characteristics of ideal bicelles or whether they should be regarded as classical mixed micelles [66, 67]. Interestingly, it has been reported that mixtures of n-dodecyl β-D-maltoside (DDM) and cholesteryl hemmisuccinate [22] [22] have an architecture more reminiscent of bicelles than micelles. The modulation of micelle morphology was shown to contribute significantly to stabilizing GPCRs, such as opioid-like receptor ORL-1 [68]. In fact, it is now common practice to include 10% CHS in detergent micelle solutions for the purification and structural characterization of GPCRs [69].

**Introduction to reconstitution of rhodopsin into bicelles**

The idea of including phospholipids in detergent micelles was applied to the study of rhodopsin as early as 1995, although at that time, what are termed bicelles were

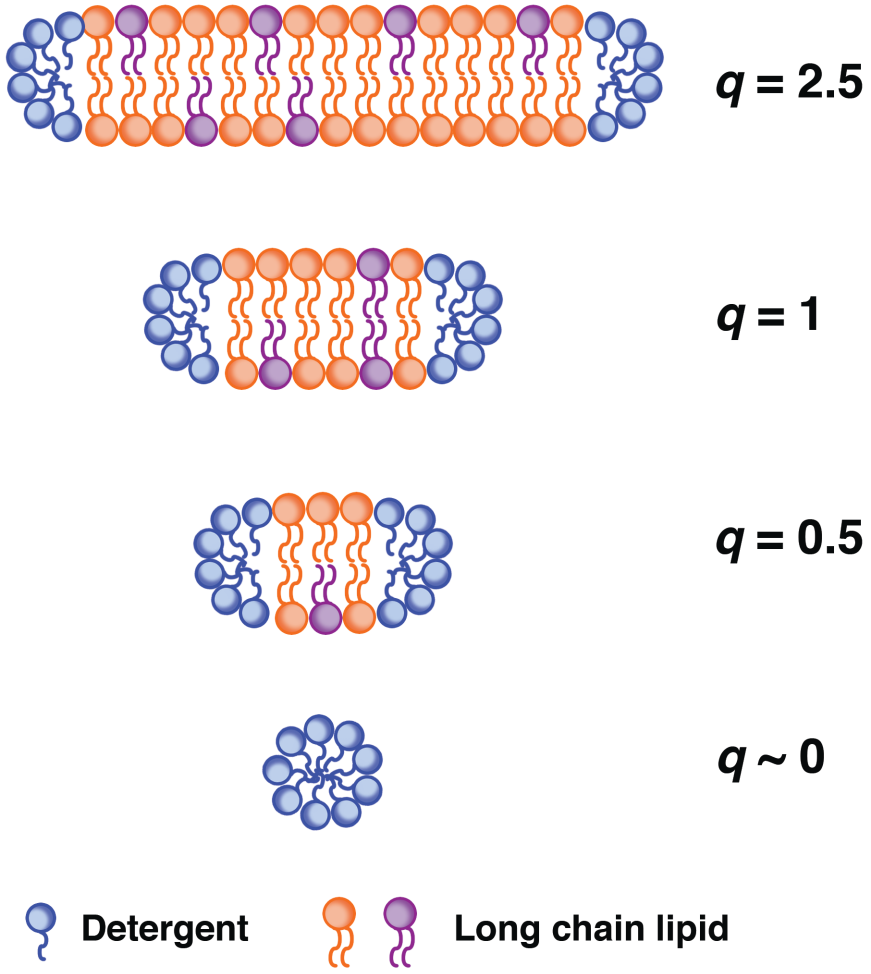


**Figure 1. Bicelles.** Bicelles have a central planar bilayer formed by long-chain lipids (orange) with the edges stabilized by either short-chain lipids or detergents (blue). Phospholipids with different head groups (purple) can be used to tailor the charge characteristics of the surface and provide lipid composition versatility. The bicelles with a higher q value (e. g. q=2.5) have more extended lipid bilayers than ones with a lower q value (e. g. q=0.5). In this sense, detergent micelles can be viewed as bicelles with the q value equal to 0.

simply called a ‘phospholipid-detergent mixture’ [70]. In that study, the influence of lipids on the stability of opsin, the apoprotein of rhodopsin, was assessed. Opsin denatures rapidly in detergent solution, losing its ability to bind *11-cis* retinal and regenerate to rhodopsin [71]. However, the presence of asolectin, a mixture of phospholipids, significantly improved the stability of opsin such that the protein was functional following detergent extraction and subsequent purification [70]. Shortly thereafter, the Khorana group replaced asolectin with a single phospholipid, dimyristoylphosphatidylcholine (DMPC), while keeping the 3-[(cholamidopropyl) dimethyl-ammonio]-1-propane sulfonate (CHAPS) as the detergent component [72]. The DMPC/CHAPS bicelles successfully extracted opsin from membranes, and opsin reconstituted into these bicelles retained its retinal binding activity. The effects of DMPC/CHAPS and DMPC/dihexanoylphosphatidylcholine (DHPC) bicelles on rhodopsin and opsin were more extensively characterized in 2007 [73]. The authors showed that rhodopsin and opsin had significantly increased stability in both types of bicelles as compared to their stability in detergent micelles. The $q$ value modulated the opsin stability, which suggests that the bicelle size impacts opsin stability. Interestingly, the authors also showed that inclusion of CHAPS rather than DHPC in the DMPC/CHAPS bicelles further stabilized opsin. This indicates that the detergent component of bicelles can affect protein stability either by directly interacting with the protein or by altering the bilayer properties. Due to high working lipid:protein ratios, bicelles usually contain monomeric GPCRs [32]. While this could create problems for constitutively dimeric class C GPCRs [74], monomeric rhodopsin was shown to be sufficient for effective coupling to transducin [75, 76], efficient phosphorylation by

GRK1 [21], and also arrestin-1 binding with physiologically relevant nanomolar affinity [21], which leads to the same conformational rearrangements in bound arrestin-1 as its interaction with p-*Rh in native disk membranes. Mutations that select for monomeric only protomers of rhodopsin were also shown to be phosphorylated by GRK1 and bind arrestin-1 effectively [77].

Bicelles not only serve as an excellent model membrane system for rhodopsin, but also greatly facilitate structural and dynamics studies of the rhodopsin-arrestin-1 interaction. Indeed, prior to the application of bicelles to the rhodopsin-arrestin-1 interaction, studies of this complex in a defined, purified system were dramatically hindered since arrestin-1 binding to rhodopsin is severely diminished when the receptor is solubilized with commonly used detergents (unpublished results). Near-UV circular dichroism spectra indicate that detergents cause significant changes of arrestin-1 tertiary structure [32]. One possibility is that detergent penetration can potentially disrupt one of the two key interactions that hold arrestin-1 in the basal state and result in the "melting" of the arrestin-1 global structure. Interestingly, acidic phospholipids can restore the binding of arrestin-1 to rhodopsin purified in DDM. Moreover, arrestin-1 retains its selective binding to rhodopsin reconstituted in bicelles [78]. In addition to the fact that that bicelles provide a milder environment than detergents, they also have several other clear advantages over detergent micelles in case of rhodopsin-arrestin interactions. First, the central planar bilayer of bicelles creates an extended native membrane-like surface, while detergent micelles might cover some receptor elements involved in arrestin-1 binding. Second, bicelles contain phospholipids that can regulate the rhodopsin-arrestin-1 interaction either via electrostatics or by directly binding to either rhodopsin or arrestin-1.

It was found that acidic phospholipids significantly prolong the half-life of the rhodopsin-arrestin-1 complex and that 20-50% lipids with negatively charged head group are essential to promote maximum binding [21, 78].

## Materials

**Preparation of bicelles**

1. Buffer A: 25 mM Bis-Tris pH 6.5, 100 mM NaCl, 0.1 μM EDTA
2. 1,2-dimyristoyl-sn-glycero-3-phosphoglycerol (DMPG)
3. 1,2-dimyristoyl-sn-glycero-3-phosphocholine (DMPC)
4. 1,2-dihexanoyl-sn-glycero-3-phosphocholine (DHPC)

**Reconstitution of rhodopsin with bicelles**

1. Rod outer segment (ROS) membranes
2. Buffer A: 25 mM Bis-Tris pH 6.5, 100 mM NaCl, 0.1 μM EDTA

**Assess structural integrity of arrestin by near-UV circular dichroism (CD)**

1. Buffer A: 25 mM Bis-Tris pH 6.5, 100 mM NaCl, 0.1μM EDTA
2. Denaturing buffer: 8 M urea in buffer A

**Preparation of radiolabeled arrestin-1**

1. Transcription mix: 120 mM HEPES-K, pH 7.5, 2 mM spermidine, 16 mM $MgCl_2$, 40 mM dithiothreitol (DTT), 3 mM each of adenosine triphosphate (ATP), guanosine triphosphate (GTP), cytidine triphosphate (CTP), and uridine triphosphates (UTP), 2.5 U/ml inorganic pyrophosphatase, 200 U/ml RNasin, and 1500 U/ml SP6 RNA polymerase
2. 7.5 M LiCl
3. 2.5 M LiCl

4. 70% (v/v) ethanol
5. Ultrapure distilled water
6. 3 M sodium acetate pH 5.2
7. 100% ethanol
8. Translation mix: 70% rabbit reticulocyte lysate, 120 mM potassium acetate, 30 mM creatine phosphate, 200 μg/ml creatine kinase, 200 U/ml RNasin or Prime RNase inhibitor, 0.1 μg/ml pepstatin, 0.1 μg/ml leupeptin, 0.1 mg/ml soybean trypsin inhibitor, 5 mM cAMP, 50 μM 19 unlabeled amino acids and 40-50 μM [$^{14}$C] leucine (14,000-35,000 dpm/ml). When [$^{3}$H] leucine is used, 800,000-1,000,000 dpm/ml is added along with [$^{14}$C] leucine to a final concentration of 30-50 μM.
9. 40 mM ATP
10. 40 mM GTP
11. 10 % (w/v) trichloroacetic acid (TCA)
12. 5 % (w/v) trichloroacetic acid (TCA)
13. Scintillation fluid
14. Buffer B: 50 mM Tris pH 7.5, 50 mM potassium acetate and 2 mM EDTA
15. Buffer C: 10 mM Tris-HCl, pH 7.5, 100 mM NaCl

**Direct binding assay in bicelles with radiolabeled arrestin-1**

1. Binding buffer: 50 mM Tris-HCl, pH 7.5, 0.5 mM $MgCl_2$, 1.5 mM dithiothreitol, 100 mM potassium acetate
2. Buffer C: 10 mM Tris-HCl, pH 7.5, 100 mM NaCl
3. Scintillation fluid

**Expression of isotopically-labeled arrestin-1**

1. BL21(DE3) cells
2. LB agar plate with 100 mg/L ampicillin
3. LB with 100 mg/L ampicillin (LB/A)
4. 1L M9 minimal media prepared in $D_2O$ supplement with 1 g/L of $^{15}NH_4Cl$: dissolve 6 g $Na_2HPO_4$, 3 g $KH_2PO_4$, 0.5 g NaCl, 4 g glucose, 1 mM $MgSO_4$, 0.1 mM $CaCl_2$and 1 g of $^{15}NH_4Cl$ in $D_2O$.
5. 100 mM Isopropyl-β-D-thiogalactopyranoside (IPTG)
6. $^{15}N$, $^{2}H$-Bioexpress
7. 1 L LB prepared in $D_2O$ with 100 mg/L ampicillin: dissolve 10 g tryptone, 5 g yeast extract and 10 g NaCl in 950 ml $D_2O$.
8. glucose-D6, α-ketovaleric acid salt (3-methyl-$^{13}$C,3,4,4,4-D4), α-ketobutyric acid salt (methyl-$^{13}$C,3,3-D2)

**NMR study of arrestin-1 binding to rhodopsin in different states**

1. Buffer D:25 mM Bis-Tris pH 6.5, 100 mM NaCl, 0.1 mM EDTA
2. 1 M dithiothreitol (DTT)
3. $D_2O$

## Methods

**Preparation of bicelles**

Two different methods of bicelle preparation are used, depending on the stock solution concentration, as well as *q* value. For relatively low stock concentration (< 20% w/v) or low *q* value ($q$<1), we varied the temperature to induce phase transitions. The gel-to-liquid crystalline phase transition temperature for DMPG-DMPC mixtures is roughly

24°C. For relatively high stock concentration (>20% w/v) or high *q* value (*q*>1), we use a custom extrusion apparatus to mix bicelles in addition to varying the temperature change to induce phase transition.

**Preparation of bicelles at low stock concentration or low *q* value**

1. Calculate the amount of each component needed. For 1 ml 12.5% w/v stock solution with *q* = 0.33 (molar ratio), this means 1 mole lipid (DMPC+DMPG) per 3 moles DHPC at a ratio of 1 mole DMPG per 4 moles DMPC: 32 mg of DMPC, 8 mg of DMPG and 85 mg of DHPC.
2. Dissolve 85 mg of DHPC in 500 µl of buffer A in one tube and mix 8 mg of DMPG and 32 mg of DMPC in 500 µl of buffer A in another tube by vortexing. DHPC solution will become clear, while the DMPG and DMPC mixture remains cloudy.
3. Combine the solutions in these two tubes and mix them well by vortexing.
4. Cycle by incubating the mixture at 42°C for 2 min, then at 0°C (on ice) for 2 min. Repeat this cycle until the solution is completely clear (typically 3-4 times).
5. Spin at 13,000xg in a tabletop centrifuge for 10 min to remove of any insoluble material. The supernatant is the bicelle solution, now ready to use.

**Preparation of bicelles at a high stock concentration or a high q value**

1. Calculate the amount of each component needed. For 1 ml of 35% w/v stock solution with *q* = 3 (molar ratio), that is 3 moles of lipid (DMPC+DMPG) per 1

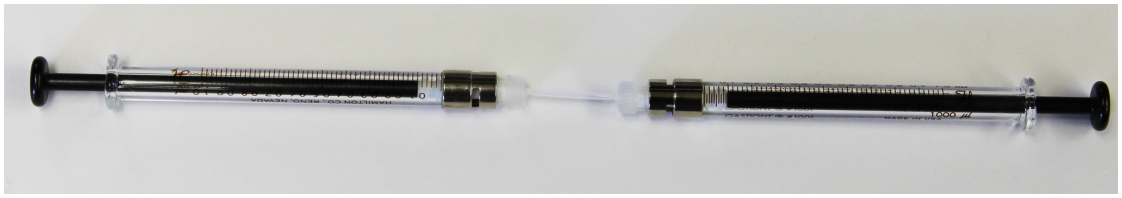

**Figure 2 Apparatus to make bicelles.** Two Hampton syringes are connected by a plastic coupler for extrusion. For example, to make 1000 µl 35% (w/v) bicelle stock, add 500 µl of DHPC solution to one syringe and 500 µl of DHPC solution homogenized with 224 mg of DMPC and 57 mg of DMPG to another syringe. The bicelles are homogenized by passing the contents back and forth between syringes multiple times. For this process, the entire apparatus is incubated at 4°C and 55°C after equilibration at each temperature.

mole of DHPC at a ratio of 1 mole of DMPG per 4 moles DMPC: 224 mg of DMPC, 57 mg of DMPG and 66 mg of DHPC.

2. Dissolve 66 mg of DHPC in 1 ml of buffer A.
3. Weigh 224 mg of DMPC and 57 mg of DMPG in one tube, add 500 µl of DHPC solution, mix by vortexing, and add it to one syringe **(Figure 2)**.
4. Add the remaining 500 µl DHPC solution to another syringe, which is then attached nose-to-nose with the other (lipid solution containing) syringe. Mix by extruding the solution back and forth between the syringes, effectively extruding the mixture through the narrow connecting tube.
5. Cycle the bicelle mixture through its phase transition temperature (24°C) four times by incubating the entire apparatus at 4°C and 55°C; homogenize between cycles.
6. Dispense the bicelle mixture to a tube on ice and centrifuge at 13,000xg for 10 min to remove bubbles and insoluble material. The supernatant is the bicelle solution, now ready for use.

**Reconstitution of rhodopsin into bicelles**

1. All steps are performed in the dark under dim red light at 4°C.
2. Measure the rhodopsin 500 nm absorption in the dark (extinction coefficient: 40,600 $M^{-1}cm^{-1}$) to determine the rhodopsin concentration.
3. Pellet ROS membranes by centrifugation at 13,000xg for 30 min, discard supernatant, and wash the pellet twice with buffer A.
4. Pellet ROS membranes after washing and estimate the volume of the membrane pellet by weighing in a pre-weighted 1.5 ml eppendorf tube (1 µl ~ 1 mg). Add

equal volume of 11.25% stock of bicelles to the membranes, pipette up and down to dissolve the membranes and incubate on a shaker in dark cold room for 30 min. The solution should become clear.

5. Centrifuge as above to remove insoluble material and save the supernatant.
6. Determine the concentration of rhodopsin in the supernatant (using absorption at 500 nm) and calculate the bicelle concentration using 11.25%* bicelle volume added / final solution volume (measure it with a pipette).
7. Typically, 70 µl of 11.25% bicelle stock are added to ROS membranes containing 1 mg of rhodopsin, which yields a final rhodopsin concentration around 8 mg/ml and bicelle concentration around 8%. The lipid from ROS membrane is also dissolved in bicelles and the concentration is around 8 mg/ml.

**Assess the structural integrity of arrestin-1 by near UV CD spectroscopy**

1. Prepare 500 µl arrestin-1 protein samples at the concentration of 50 µM in buffer A, denaturing buffer, and the model membrane conditions of choice: for example, 0.2% DM micelles, or 4% bicelle mixtures prepared as described in 3.1. Incubate arrestin-1 in these conditions at room temperature overnight, ~ 12 hours.
2. Transfer the samples to a masked cell (1-cm pathlength) with a minimum volume of 500 µl and collect the near-UV CD spectra over the wavelength range of 250-320 nm using the CD spectro-polarimeter with the bandwidth of 1 nm. Average five scans for each sample to achieve reasonable signal-to-noise. For each protein sample, collect the near-UV CD spectrum of the same buffer without

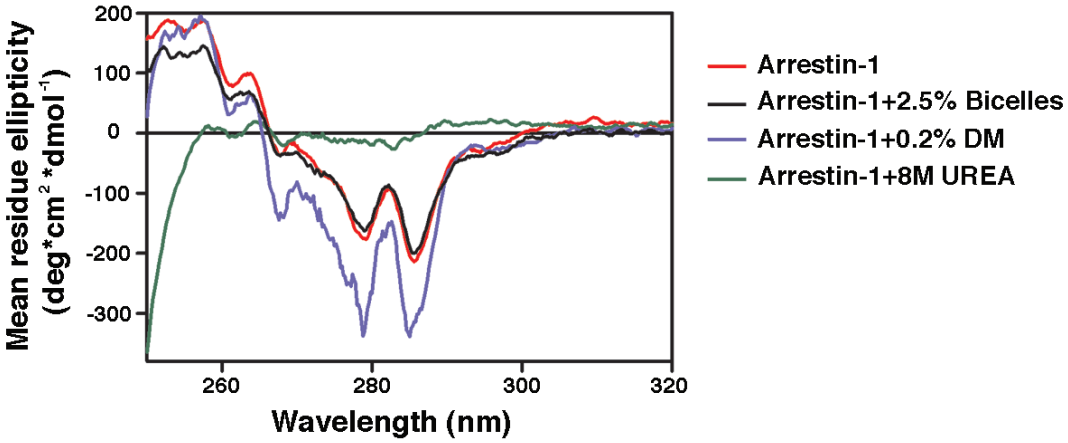


**Figure 3. Near-UV CD spectra of arrestin-1 in the presence of model membranes.** Arrestin-1 (50 μM) samples were prepared in detergent micelles composed of n-decyl-β-D-maltopyranoside(blue) and DMPC/DHPC bicelles (black). The reference spectrum for native conformation of arrestin-1 in buffer A is shown in red. The spectrum of fully denatured arrestin-1 in 8 M urea is shown in green.

protein, which yields the blank signal that should be subtracted from the spectrum of protein sample to reveal the signal from protein only.

3. The raw data from Jasco J-810 is given in ellipticity (measured in millidegrees). Apply the following equation: $[\theta] = \frac{100*(signal)}{c*n*l}$ (c is protein concentration in mM, n is the total number of amino acid residues and l is the cell pathlength in cm) to convert the output to units of mean residue ellipticity (degrees squared centimeters per decimole) (Figure 3).

**Preparation of radiolabeled arrestin-1**

1. Purify and linearize plasmid DNA where arrestin-1 coding sequence is under control of a SP6 promoter.
2. Incubate 10 µg of linearized DNA in 300 µl of the transcription mix at 38°C for 90 min.
3. Add 150 µl of 7.5 M LiCl, incubate on ice for 10 min, and centrifuge for 10 min at 16,100 x *g* and 4° C to pellet mRNA.
4. Wash the pellet with 1 ml of 2.5 M LiCl at 4° C.
5. Wash the pellet with 1 ml of 70% (v/v) ethanol at room temperature.
6. Let the pellet dry for 5-7 min or until it is completely dry, then dissolve it in 300 µl of ultrapure distilled water (we use a volume equal to that of the transcription reaction). Remove an aliquot to measure the amount of mRNA via absorption at 260 nm.
7. Add 30 µl of 3 M sodium acetate pH 5.2 and 960 µl of ethanol. Then vortex and incubate on ice for 10 min. mRNAs in this suspension can be stored at -80°C for several years.

8. Before translation, pellet the necessary amount (~24 μg for 0.2 ml translation) of mRNA from this suspension, wash with 70% ethanol, dry for 5-7 min, and dissolve in 16 μl of ultrapure distilled water.
9. Incubate mRNA with 184 μl translation mix for 2 h at 22.5° C.
10. Add 4 μl of 40 mM ATP and 4 μl of 40 mM GTP (1 mM final concentrations) and incubate at 37° C for 7 min (ribosome runoff).
11. Cool the samples on ice and centrifuge at 600,000xg for 60 min at 4° C (in TLA 120.1 rotor, Beckman TLA tabletop ultracentrifuge) to pellet ribosomes and aggregated proteins. The supernatant contains [$^{14}$C]- and [$^{3}$H]- labeled arrestin-1 and free [$^{14}$C]- and [$^{3}$H]- leucine.
12. Take a 2 μl aliquot, add it to 18 μl water (10-fold dilution), and spot 5 μl of diluted sample onto Whatman 3MM paper (1 cm x 1 cm square), incubate the paper in ice-cold 10 % (w/v) TCA for >10 min (to wash away free radiolabeled leucine), then in boiling 5% TCA for exactly 10 min (hydrolyzes aminoacyl-tRNA and removes radiolabeled leucine attached to tRNA). Then, let the paper dry and add each square to a separate scintillation vial, let the protein dissolve in 0.5 ml of buffer B, then add 5 ml of scintillation fluid, briefly shake, and quantify protein-incorporated radioactivity using scintillation counter capable of quantifying $^{3}$H and $^{14}$C separately.
13. Measure the radioactivity of the control sample (translation mix without mRNA).
14. Calculate protein yield based on specific activity of the radiolabeled leucine used. Dividing the total protein-incorporated radioactivity (dpm per microliter of

translation mix with the value from the control sample subtracted) by the specific activity (dpm/fmol) of the arrestin-1 gives the yield in fmol/µl.

15. To separate the free [$^{14}$C]- and [$^{3}$H]- leucine from [$^{14}$C]- and [$^{3}$H]- labeled arrestin-1, load the supernatant onto a 2 ml Sephadex G-75 column equilibrated with buffer C. Add 100 µl of buffer C and collect the eluted 100 µl buffer. Repeat this for 15 times. For the last elution, add 500 µl of buffer C and collect the eluted 500 µl buffer.
16. Take 2 µl of each elution and add it to 18 µl $H_2O$, add 5 ml of scintillation fluid, and determine the radioactivity in each elution fraction to get the elution profile and pool the fractions containing arrestin-1 together. This is translated arrestin-1 ready for use.

**Direct binding assay in bicelles with radiolabeled arrestin-1**

1. Incubate 100 fmol of radiolabeled arrestin-1 with the 7.5 pmol of p-*Rh in bicelles in a final volume of 50 µl of binding buffer at 30° C under ambient light.
2. Cool the samples on ice and load them on 2 ml Sephadex G-75 columns equilibrated with buffer C.
3. Wash the column with 100 µl and then 500 µl buffer C.
4. Elute with 600 µl buffer C into scintillation vials, add 5 ml of scintillation fluid, and count the radioactivity from bound arrestin-1as total binding.
5. Determine the non-specific binding in the presence of equal amount of empty bicelles.

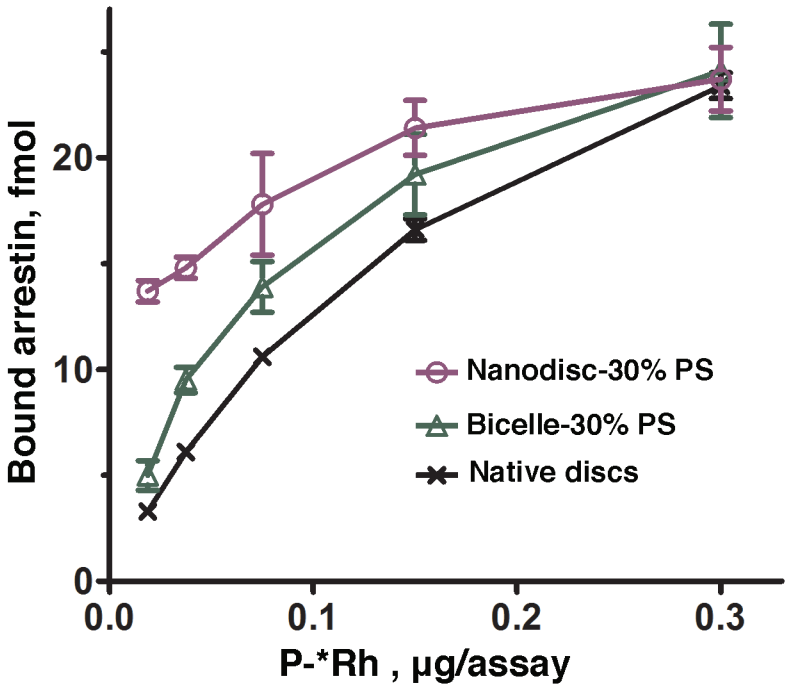


**Figure 4. Arrestin-1 binding to P-*Rh.** P-Rh from the same batch (0.3 µg) in native disc membranes (black crosses), or solubilized and reconstituted in DMPC bicelles with 30% DMPS (green triangles), or solubilized and reconstituted in POPC nanodiscs with 30% POPS (purple circles) was incubated with radiolabeled arrestin-1 (100 fmol) in 50 µl at 30$^{o}$C for 5 min. The samples were light activated, cooled on ice, and bound and free arrestin-1 were separated by gel-filtration on Sephadex G-75 (bicelles and nanodiscs) or Sepharose 2B (native disc memebranes). Means ± SD from three experiments performed in duplicate are shown.

6. Subtract the non-specific binding from total binding to obtain the specific binding. Dividing specific binding (dpm) by arrestin-1 specific activity (dpm/fmol) gives the fmol of arrestin bound to the p-*Rh (Figure 4).

**Expression of NMR isotopically-labeled arrestin-1**

**Preparation of $^{2}H$, $^{15}N$ labeled arrestin-1**

1. Transform a pTrc-based plasmid encoding arrestin-1 to BL21(DE3) cells and plate on LB agar with 100 mg/L ampicillin.
2. Start a 10 ml small culture from a single colony in LB with 100 mg/L ampicillin (LB/A) at 30 $^{o}$C overnight.
3. Centrifuge the 10 ml small culture for 3-5 min at 2000 rpm. Resuspend the cell pellet in 1 L M9 minimal media prepared in $D_2O$ supplemented with 1 g/L of $^{15}NH_4Cl$.
4. Incubate the culture at 30 °C with vigorous shaking at 250 rpm until OD reaches 0.8.
5. Add 250 µl of 100 mM IPTG to 1L culture. The final IPTG concentration is 25 µM. Continue shaking for another 18 hours.
6. Optional: 5-10 ml of $^{15}N$, $^{2}H$-Bioexpress can be added to the M9 minimal media. This can significantly shorten the cell growth time in step 4 from 3 days to 1 day.

**Preparation of $^{13}C$, $^{1}H$-methyl-labeled perdeuterated arrestin-1**

1. Transform a pTrc-based plasmid encoding arrestin-1 to BL21 (*DE3*) cells and plate on LB agar with 100 mg/L ampicillin.
2. Start a 5 ml small culture from a single colony in a LB prepared in $D_2O$ with 100 mg/L ampicillin at 30 °C overnight.

3. Transfer 50 µl of overnight cultures prepared in step 2 into 5 ml M9 minimal medium prepared in $D_2O$ and contains 4 g/L glucose-D6.
4. Inoculate 5 ml of cultures in step 3 to 500 ml of M9 minimal medium that is prepared in $D_2O$ and contains 4 g/L glucose-D6, 37.5 mg/L 3-methyl-$^{13}C$, 3,4,4,4-$D_4$-α-ketovaleric acid salt and 22.5 mg/L methyl-$^{13}C$, 3,3-$D_2$-α-ketobutyric acid salt.
5. Shake the cultures at 30° C until OD600 reaches 0.6. Add additional 3-methyl-$^{13}C$, 3,4,4,4-$D_4$-α-ketovaleric acid salt and methyl-$^{13}C$, 3,3-$D_2$-α-ketobutyric acid salt to the culture to make the final concentration 75 mg/L and 45 mg/L respectively.
6. Continue shaking for 30 more minutes.
7. Add 250 µl of 100 mM IPTG to 1 L culture. The final IPTG concentration is 25 µM.
8. Harvest the cells by centrifugation after induction for 18 hours.
9. Purify the proteins.

**NMR study of arrestin-1 binding to rhodopsin in different states**

**Sample preparation**

1. Buffer exchange arrestin-1 to buffer D using the Amicon Ultra centrifugal filters with 30 kDa molecular-weight cutoff.
2. Concentrate arrestin-1 sample to the desired concentration. Ideally the concentration should be at least double the concentration in final working solution. The arrestin-1 F85/197A mutant used in the NMR study can be concentrated up to 640 µM without any visible precipitation.

3. Mix arrestin-1 and rhodopsin reconstituted into bicelles at the molar ratios of 1:1, 1:3 and 1: 5 in dark. The final volume is 200 µl. Add 1 µl of 1 M DTT and 10 µl of $D_2O$. Adjust the final bicelle concentration to 4% with the bicelle stock. The solution should contain 30 µM arrestin-1, 30, 90 or 150 µM rhodopsin, 5 mM DTT, 5% $D_2O$, 4% bicelle.
4. To investigate arrestin-1 binding to activated rhodopsin or phosphorylated rhodopsin, light activate the sample on ice for 30 min or until the A500nm absorption decreases to the base line. Phosphorylate rhodopsin.
5. To investigate arrestin-1 binding to rhodopsin or phosphorylated rhodopsin in an inactive state, everything should be kept in the dark during sample preparation, sample transfer and data collection.
6. Add 200 µl sample to a 5 mm Shigemi NMR or to a 3 mm conventional tube. It is ready for NMR experiments.

**NMR titration experiments**

1. All NMR data are obtained in Bruker Avance spectrometers with $^{1}H$ resonance frequency of either 800 MHz or 600 MHz at 308 K. Collect the two-dimensional $^{1}H$-$^{15}N$ correlated spectra using sensitivity-enhanced, phase-sensitive transverse relaxation optimized spectroscopy (TROSY) pulse sequence. It is important to use a version of this sequence that filters out all extraneous signal (from protons not directly attached to an $^{15}N$) using pulsed field gradients rather than via phase cycling. Typical TROSY spectra for NMR titration experiments are obtained using 1024*128 complex points with 200 scans per increment, which requires total acquisition time of 20 hours for one spectrum. Key NMR parameters include

the $^{1}H$ and $^{15}N$ 90 degree pulse widths and the relaxation recovery delay between scans, which are kept the same during the same series of titration points.

2. Two-dimensional methyl-TROSY spectra were obtained using heteronuclear multiple-quantum correlated spectroscopy ($^{1}H$, $^{13}C$-HMQC) pulse sequence. Set the $^{1}H$ and $^{13}C$ spectra widths at 14 and 22 PPM respectively, with the $^{13}C$ carrier frequency corresponding to 20 PPM. Typical HMQC spectrum contains 1024x256 complex points with 128 scans per increment, which requires total acquisition time of 20 hours for one spectrum.
3. Collect one-dimensional TROSY spectra before and after each titration point to monitor the decaying of rhodopsin in different states. Process $^{1}H$,$^{15}N$-TROSY data using a program such as nmrPipe (Delaglio, Grzesiek et al. 1995) with zero filling, Gaussian apodization and linear prediction in indirect dimension ($^{15}N$) before Fourier transformation. For $^{1}H$,$^{13}C$-methyl-TROSY spectra, process the data with one-time zero filling and squared sine-bell function. Visualize and analyze the using programs such as nmrDraw, NMRview and Sparky.
4. Plot the titration curve as arrestin NMR peak chemical shift against the concentration of rhodopsin. The calculation of $K_d$ from the concentration dependence of NMR resonance chemical shift changes has been described previously.

# CHAPTER 3

# NMR STUDY OF FREE AND RECEPTOR-BOUND ARRESTIN

Much of this chapter was published in *Proceeddings of the National Academy of Sciences U S A* [32]. Tiandi Zhuang, Min-Kyu Cho, Sergey A. Vishnivetskiy, T. M. Iverson, Vsevolod V. Gurevich, and Charles R. Sanders contributed to this work.

## Introduction

Arrestin-1, also known as visual or rod arrestin, was the first member of the family discovered [79]. It preferentially binds light-activated phosphorylated rhodopsin (P-Rh*) and prevents further signaling by direct competition with transudin, the visual G protein [16, 17]. Arrestin-1 also specifically binds dark phosphorylated (P-Rh) and light-activated unphosphorylated rhodopsin, albeit with much lower affinity [29, 80]. These interactions, as well as arrestin-1 binding to phospho-opsin (P-opsin) remain largely unexplored, despite their biological importance. Rh* is directly produced by light, P-Rh is generated by high-gain phosphorylation of multiple rhodopsin molecules upon activation of a modest sub-population [81, 82], and P-opsin is generated by the decay of P-Rh*. Arrestin-1 is the second most abundant protein in rod photoreceptors, expressed at a ~0.8:1 molar ratio to rhodopsin [83-85]. In dark-adapted rods the bulk of arrestin-1 is localized away from the rhodopsin-containing outer segment. Light induces massive translocation of arrestin-1 into this compartment due to its tight binding to P-Rh* [86, 87].

Mammalian arrestin-1 self-associates, forming significant populations of dimers and tetramers at physiological concentrations [88-90]. Only the arrestin-1 monomer binds rhodopsin [88], because the receptor-binding elements are shielded by quaternary structural contacts in tetramers and both possible dimers. Arrestin-1 monomers, dimers,

and tetramers have very different sizes, while the space between rhodopsin-containing discs in the outer segment is fairly small [91]. It appears that only monomeric arrestin-1 is small enough to easily diffuse into the inter-discal space, and this has been proposed to be the major factor limiting arrestin concentration in the outer segment in the dark [91]. The binding of arrestin-1 to any form of rhodopsin affects the arrestin-1 distribution in rod photoreceptors and determines the concentration of the active monomer in the outer segment, which likely contributes to the kinetics of photoresponse and recovery [92]. Thus, to fully understand receptor signaling it is important to determine the affinities of these interactions and identify the arrestin-1 residues involved. This is necessary for the elucidation of the molecular mechanisms of arrestin-1 function in the visual system and for building a comprehensive model of its behavior in photoreceptors [93]. These data are also critical for the design of arrestin-1 mutants capable of compensating for the effects of rhodopsin mutations that cause congenital human disorders. In light of the high homology among arrestins novel insight from studies of arrestin-1 is likely applicable to the interactions of other arrestin family members with their cognate receptors [94].

Nuclear magnetic resonance spectroscopy (NMR) is well suited for the study of dynamic and relatively low-affinity interactions [95], which constitute the majority of biologically important protein-protein and ligand-protein interactions. Here we took advantage of our recent assignment of >140 amide $^{1}H$, $^{15}N$ correlation resonances in the NMR spectrum of arrestin-1 [96] to probe its binding interface and affinity for different functional forms of rhodopsin. These studies also revealed a global conformational change in arrestin-1 resulting from complex formation with P-Rh*and P-opsin.

## Methods

### Preparation of arrestin-1 samples

Constitutively monomeric arrestin-1-(F85A/F197A) and single-cysteine mutants constructed in the background of fully functional cysteine-less arrestin-1 were expressed and purified as described. Constitutively monomeric arrestin-1-(F85A/F197A) was purified used for all experiments, except for those that involving PRE measurements, for which single-cysteine mutant forms were prepared and spin-labeled.

### NMR spectroscopy of arrestin-1

$^{1}H,^{15}N$-TROSY NMR titrations of $^{2}H,^{15}N$-labeled arrestin-1 with various forms of rhodopsin (P-Rh, P-Rh*, Rh* or P-opsin) were carried out at pH 6.5 and 308 K in the presence of 100 mM NaCl. Samples with different ratios of arrestin-1 and rhodopsin were made using a constant arrestin-1 concentration of 30 μM. $^{1}H,^{13}C$-Me-TROSY NMR spectra were collected of arrestin-1 that was uniformly perdeuterated except for the side chain methyl groups of isoleucine, leucine, and valine residues, which were also $^{13}C$-labeled.

### Determination of dissociation constants

A 1:1 binding model was fit to NMR titration data to estimate $K_D$ for complex formation of arrestin-1 with various forms of rhodopsin. To determine the affinity by an alternative method, we used direct binding assay with radiolabeled arrestin-1 generated in cell-free translation, as described [97]. Increasing amounts of P-Rh* or P-opsin were added to fixed concentration of arrestin-1 and the amount of bound arrestin was determined upon incubation at 37$^{o}$C for 5 min (P-Rh*) or for 30 min (P-opsin). Since the

equilibrium cannot be achieved with P-Rh* due to its decay, these data yielded an apparent $K_D$, whereas P-opsin binding was measured at equilibrium, yielding a true $K_D$.

## Results

### Arrestin-1 retains native structure in the presence of negatively charged bicelles

Investigation of the arrestin-1 interactions with different functional forms of rhodopsin by solution NMR requires that rhodopsin be solubilized in an isotropic model membrane system. Detergent micelles [98] and lipid-detergent bicelles [99] have been successfully used to solubilize rhodopsin in a native-like functional state. However, detergents tend to disrupt the native structure of arrestins. We examined arrestin-1 structure and stability using near-UV circular dichroism (CD) in the presence of different types of micelles, bicelles, and amphipols (Figure 1) [100]. Arrestin-1 has 16 phenylalanines, 1 tryptophan, and 14 tyrosines, all of which contribute to its near-UV CD spectrum. The spectrum of arrestin-1 in native conformation in neutral buffer exhibits pronounced negative signals in the 270-290 nm range, whereas the spectrum of denatured protein in 8M urea is near zero in this range (Figure 1). We found that detergents and amphipols destabilized arrestin-1, whereas three different types of bicelles yielded CD spectra very similar to those observed in buffer (Figure 1). Thus, isotropic bicelles are suitable for solution NMR-based studies of arrestin-rhodopsin interactions.

Rhodopsin was shown to be stable and functional in negatively charged bicelles [99]. Similarly, rhodopsin in bicelle-like nanodiscs containing negatively charged lipids binds arrestin-1 with a physiologically relevant affinity ($K_D$~3-4 nM) [21]. We therefore acquired a 2D $^{1}H$-$^{15}N$ TROSY spectrum of 50 mM $^{2}H$,$^{15}N$-labeled arrestin-1 in the

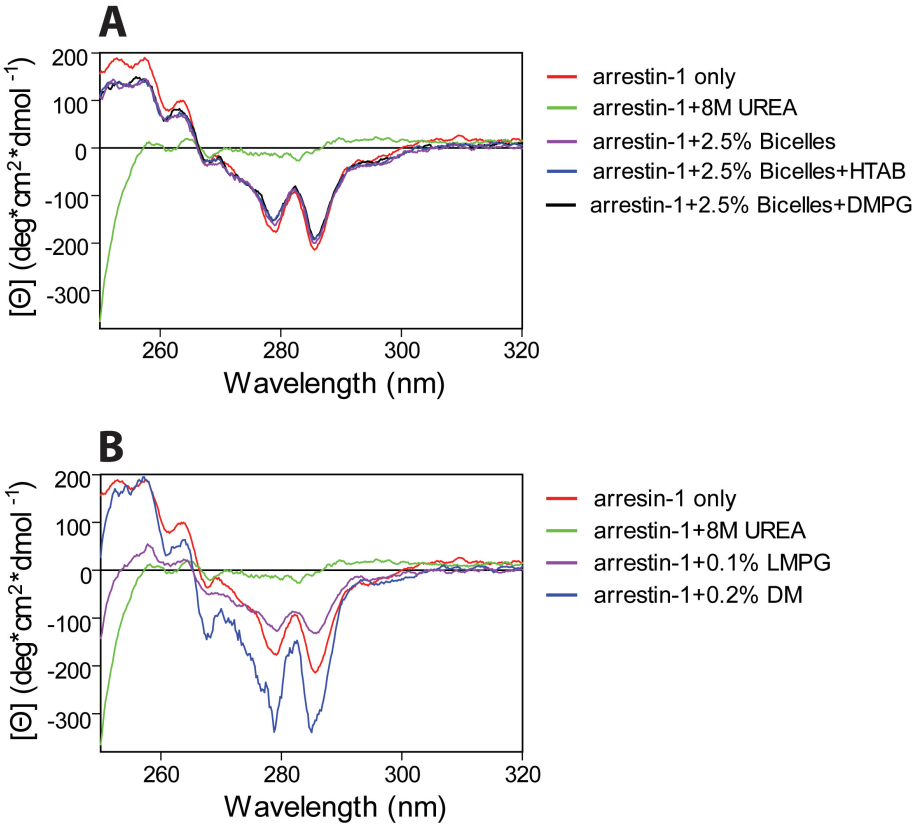


**Figure 1. Near-UV CD spectra of arrestin-1 in the presence of NMR-compatible model membranes.** A. Arrestin-1 (50 μM) samples were prepared in zwitterionic bicelles (purple), cationic bicelles (blue), and anionic bicelles (black). The reference spectrum for a sample in buffer is colored in red. The spectrum of denatured arrestin-1 in 8 M urea is colored in green. B. The reference spectrum for a sample in buffer-only is colored in red. The spectrum of denatured arrestin-1 in 8 M urea is colored in green. Spectra of arrestin-1 in detergent micelles composed of LMPG (purple) or DM (blue).

presence of 4.2% dimyristoylphosphatidylcholine/diheptanoylphosphatidylcholine (DMPC/D7PC) bicelles containing 20% lipid-mol% of negatively charged dimyristoylphosphatidylglycerol (DMPG). The NMR spectrum of arrestin-1 in the presence of bicelles was similar to that in buffer, indicating lack of a bicelle-induce global structural perturbation. Negatively charged bicelles were therefore selected as the model membrane for titrations of arrestin-1 with various forms of rhodopsin.

**Arrestin-1 binding to dark state phosphorylated rhodopsin**

Two-dimensional $^{1}H$-$^{15}N$ correlation NMR (HSQC or TROSY) has long been used to monitor protein-protein or protein-ligand binding and to map protein residues involved in complex formation. Arrestin-1 binds P-Rh* with high selectivity [19], and arrestin-1 residues engaged by P-Rh* were extensively mapped [2, 101-107]. *In vivo*, light activation and subsequent phosphorylation of rhodopsin by GRK1 are essential for high affinity arrestin-1 binding, which effectively shuts off further signaling [108]. Both light-induced Rh* and inactive P-Rh are produced in photoreceptors *in vivo* [82], but bind arrestin-1 less avidly than P-Rh* [80, 97]. However, the dissociation constants ($K_D$) and the elements that interact with Rh* and dark P-Rh remain to be fully elucidated. Here we used NMR titration experiments to investigate the binding of $^{2}H$-$^{15}N$-arrestin-1 to P-Rh and Rh*.

Figure 2 shows the titration of NMR-labeled arrestin-1 by dark P-Rh. A number of peaks broadened and/or shifted in response to complex formation. Many of the peaks broadened beyond detection at the higher levels of R-Ph; therefore, we focused our analysis on the 1:2 arrestin-1: P-Rh sample, where most peaks were still detected. The peaks shifted rather than split, which indicates that binding was rapid on the NMR time

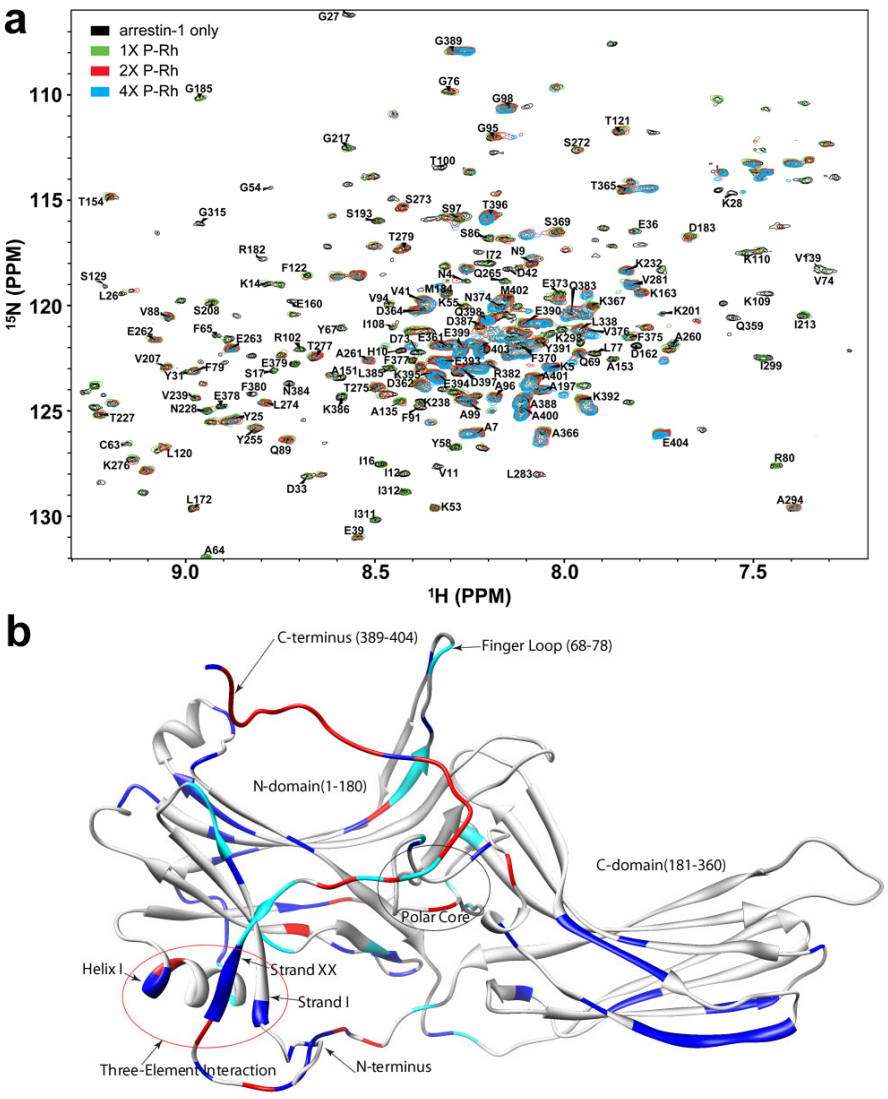


**Figure 2. Arrestin-1 binding to dark-state P-Rh.** (a) Superimposed $^{1}$H,$^{15}$N-TROSY spectra of 30 μM $^{2}$H,$^{15}$N-labeled arrestin-1 titrated by P-Rh in 4.2% anionic bicelles, 25 mM BisTris, 100 mM NaCl, 0.1 mM EDTA, 5 mM DTT pH 6.5 at 308 K. The bicelles contained DMPC:DMPG = 4:1 (mol:mol), $q$ = 0.3, where $q$ is the mol:mol ratio of the detergent-like D7PC to DMPC+DMPG. All samples in this work were examined in the same buffer and bicelles and at the same temperature. The molar ratio of arrestin-1 to P-Rh was varied: 1:0 (black), 1:1 (green), 1:2, and 1:4 (cyan). (b) Mapping of P-Rh–induced site-specific NMR chemical-shift changes onto the 3D structure of arrestin-1 (PDB ID 1CF1). Red sites are those for which the backbone amide chemical shifts changed by 0.010 ppm or more. Light blue sites are those for which peaks shifted by less than 0.010 ppm, but underwent significant line-broadening in response to P-Rh. Resonances for dark blue sites neither shifted significantly nor broadened. Because the crystal structure does not resolve residues 1–9, 363–373, and 394–404, these segments were modeled into the depicted structure using X-PLOR-NIH (http://nmr.cit.nih.gov/xplor-nih).

scale. The set of peaks that uniformly shifted the most in response to complex formation were from mostly from the C-tail of arrestin-1 (Figure 2b), indicating that binding to P-Rh changes the conformation of this element. This is consistent with significant changes in the arrestin-1 C-terminal segment detected in the presence of chemical mimics of the phosphorylated rhodopsin C-terminus, heparin and hexaphosphoinositol ($IP_6$) [96]. A few other peaks also shifted significantly or exhibited line broadening (Figure 2b). Those residues were mainly from the "polar core" and "three-element interaction" motifs that were previously shown to be perturbed by $IP_6$ and heparin. For three peaks that exhibited relatively large shifts but did not completely disappear, we plotted the variations in chemical shifts as a function of the P-Rh concentration (Figure 3). Fitting of the data by a 1:1 binding model [21, 83] yielded the $K_D$ of 80 ± 30 μM (Figure 3) for arrestin-1 and P-Rh.

**Binding of arrestin-1 to unphosphorylated light-activated rhodopsin**

Visual signal transduction is initiated when rhodopsin absorbs a photon, which isomerizes covalently bound 11-cis-retinal, converting rhodopsin into Rh*, which activates transducin and is then rapidly multi-phosphorylated at its C-terminus [79]. The structure of Rh* is significantly different from inactive rhodopsin [109-112]. High selectivity of arrestin-1 for P-Rh*, as compared to Rh*, indicates that arrestin-1 affinity for Rh* must be much lower, although this has not been previously quantitated. Figure 4a shows overlaid spectra of 30 mM $^{2}H,^{15}N$-arrestin-1 with and without 150 mM Rh*. Only a few residues exhibited significant chemical shift changes (Figure 4b). Analysis of a full titration (30, 60 and 150 mM Rh*) indicates that binding is relatively weak ($K_D$ >150 mM, see Figure 5). Most resonances exhibiting significant chemical shift changes

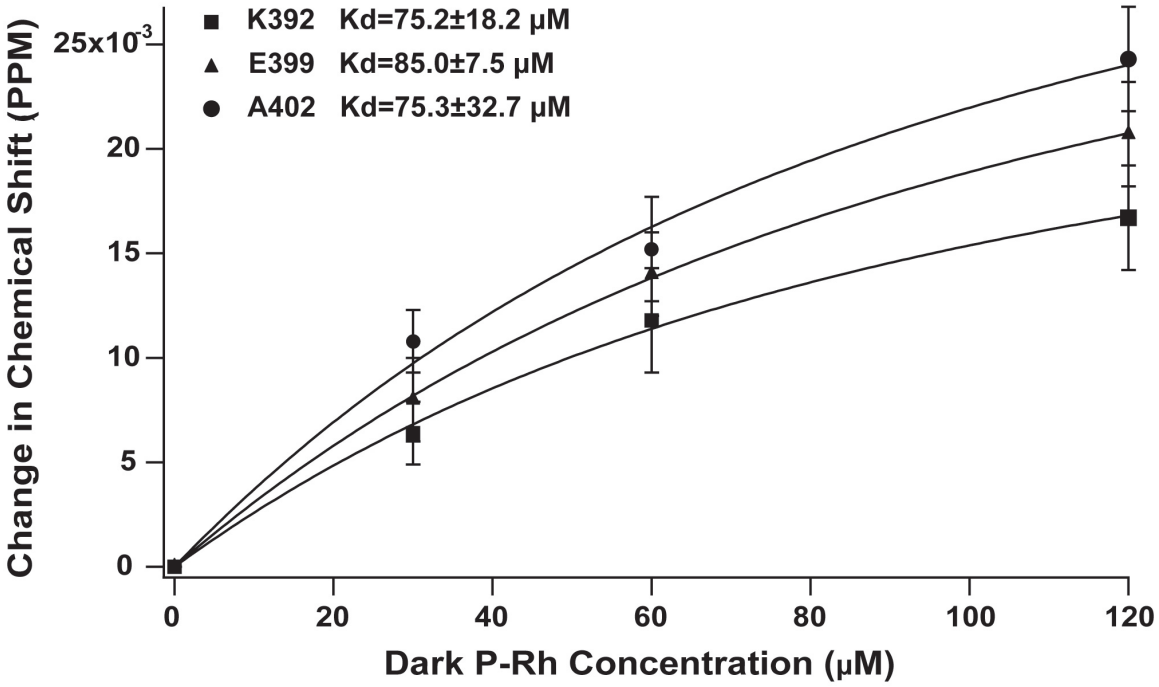


**Figure 3. Estimation of $K_D$ for binding of arrestin-1 to dark state P-Rh.** Changes in the TROSY NMR chemical shifts of arrestin-1 (Figure 2A) for the resonances from K392 (square), A402 (circle), and E399 (triangle) were plotted as a function of the P-Rh concentration. The $K_D$ for each curve was determined by fitting the model for 1:1 noncooperative binding to the data using nonlinear least squares analysis. Based on the three individual fits, the $K_D$ is estimated as 80 ± 30 µM.

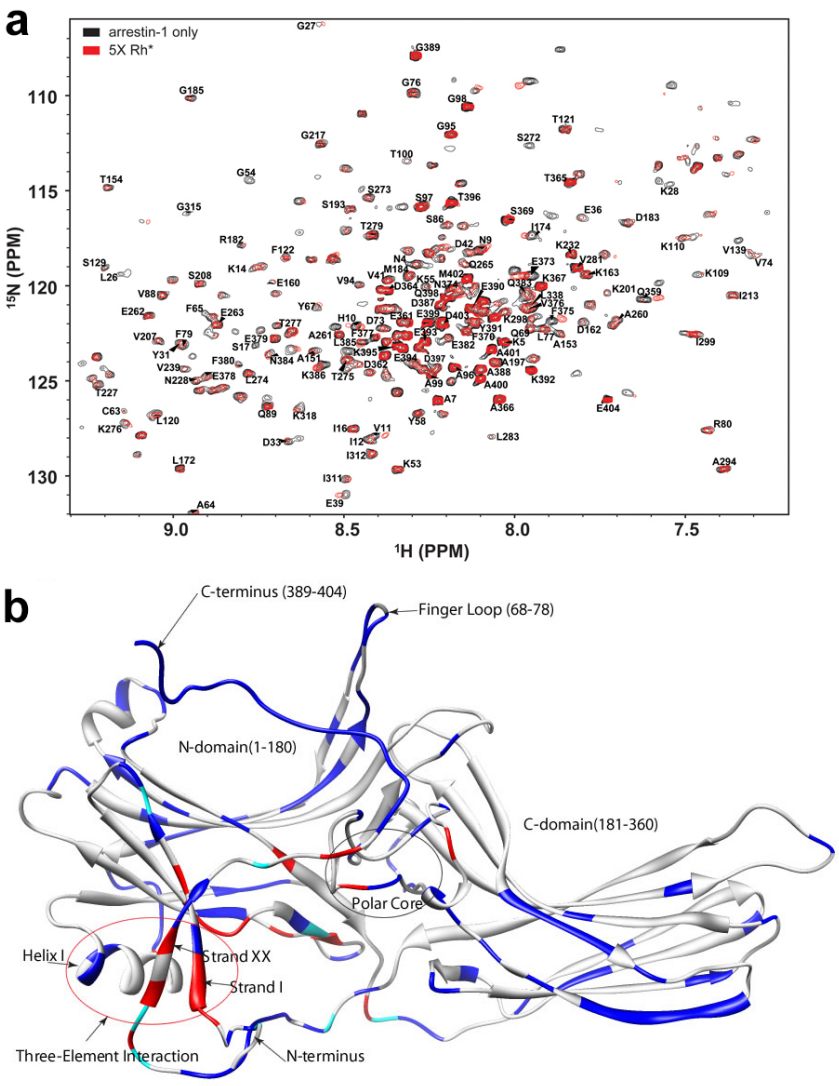


**Figure 4. Arrestin-1 Binding to Rh*.** TROSY spectra of 30 mM $^{2}$H,$^{15}$N-labeled arrestin-1 were acquired in the presence of varying amounts of Rh*. **(a)** The spectrum of arrestin-1 alone (black). Only very small chemical shift changes were observed in the presence of a 5-fold molar excess of Rh*. Assigned residues that exhibited the most significant dose-dependent chemical shift changes are labeled. **(b)** Mapping of P-Rh-induced site-specific NMR chemical shift changes onto the 3-D structure of arrestin-1 (PDB 1CF1). Red sites are those for which the backbone amide absolute chemical shifts changed by 0.010 PPM or more. Cyan sites are those for which peaks shifted by less than 0.010 PPM, but underwent significant line-broadening in response to P-Rh. Resonances for blue sites neither shifted significant nor broadened.

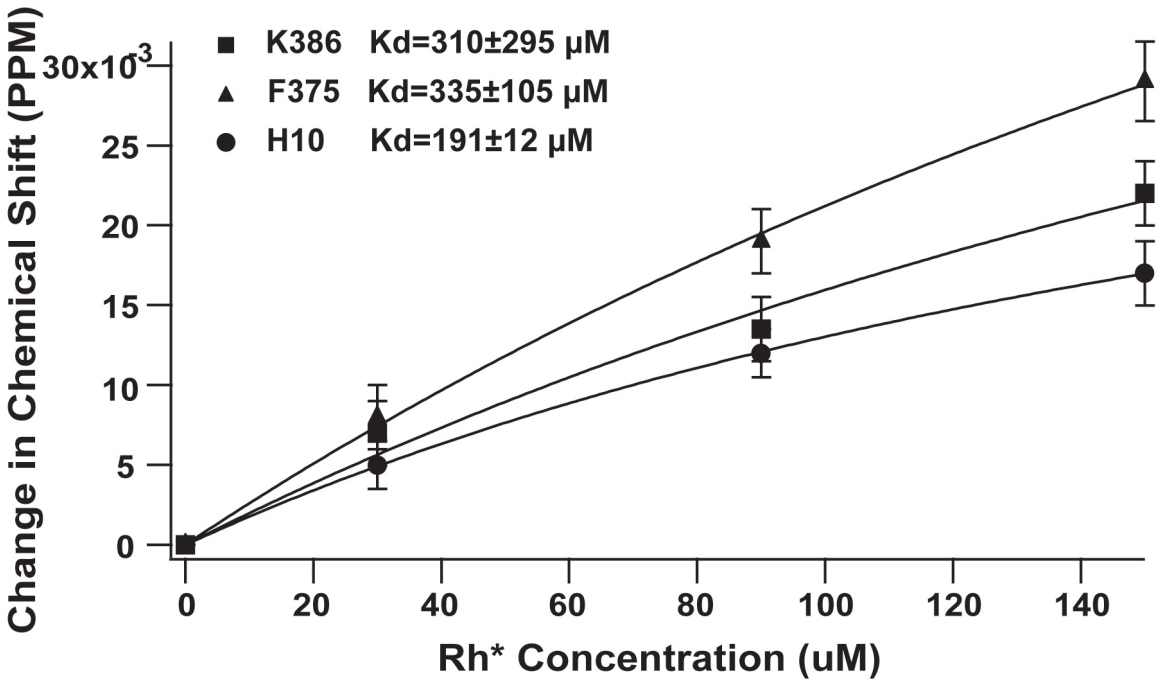


**Figure 5. Estimation of $K_D$ for arrestin-1 binding to Rh*.** The dose-dependent chemical-shift changes in arrestin-1 peaks positions were plotted as a function of the concentration of Rh* for residues K386 (square), F375 (triangle), and H10 (circle). The $K_D$ for each curve was determined by fitting the model for 1:1 noncooperative binding to the data using nonlinear least squares analysis. The large uncertainties associated with two of three fits plus the fact that the lowest of the three $K_D$ was determined to be larger than the highest Rh* concentration reached in the titration leads to the conclusion that $K_D$ is very reliably determined to be larger than 0.15 mM by these data.

corresponded to residues in the 10-70 and 370-385 ranges. These segments include two of three sets of residues known to be involved in the "three-element interaction" between the N-terminal b-strand I (residues 9-14), α-helix I (103-111) and β-strand in the C-tail (373-380) (Figure 4b). This data for the Rh*/arrestin-1 complex suggests that the known destabilization of the three-element interaction by P-Rh* is not directly triggered by the phosphorylated rhodopsin C-terminus, but by the interactions with elements of rhodopsin that change conformation upon light activation. In light of the fact that binding of P-Rh (Figure 2) or P-Rh* results in release of the distal C-tail (385-404) it is notable that binding of Rh* does not do so [2, 3].

**High-affinity binding of arrestin-1 to phosphorylated active rhodopsin**

Arrestin-1 associates with P-Rh* with very high affinity [21, 113, 114], blocking transducin binding sites on rhodopsin. To probe structural changes that occur in arrestin-1 upon binding, we titrated $^{2}H,^{15}N$-labeled arrestin-1 with P-Rh*.

Figure 6 shows the TROSY spectrum of 30 mM $^{2}H,^{15}N$-labeled arrestin-1 in the presence and absence of saturating P-Rh*. Binding of P-Rh* resulted in a dramatic change in the spectrum in which the majority of peaks disappeared (Figure 6b). The remaining peaks were assigned by tracing the chemical shift changes seen in Figure 1, which appeared to shift from their assigned positions in free arrestin-1 in the same direction upon complex formation with either P-Rh or P-Rh*. The assignments (Figure 6b) reveal that the observed arrestin-1 peaks originate from domains shown to be flexible in free arrestin-1, particularly the C-terminal residues 360 to 404. Several residues in the body of the N-domain (G95, A96, S97 and G98) were also observed, as well as the N-terminal residues K5, A7, and A10. Resonances from most other peaks disappeared upon

complex formation due to extensive line broadening. The high intensity of the peaks from the C-tail after complex formation suggests that binding of arrestin-1 to P-Rh* results in freeing of the C-tail of arrestin-1 from tertiary structural interactions, in agreement with distance measurements between the C-tail and the body of the N-domain by EPR and NMR experiments reported below. P-Rh* induced chemical shift changes for residues G95, S97 and G98, which are located on a short connector between the body of the N-domain and the a-helix I (Figure 6b). Thus, a structural rearrangement of the N domain takes place upon complex formation. This effect was not seen in the titration of arrestin-1 with $IP_6$ or heparin [96], suggesting a possible shift of the a-helix I resulting from disruption of the three-element interaction. Previous EPR and limited proteolysis results indicated that the C-tail of arrestin-1 is displaced upon binding P-Rh* [2, 3, 115]. Our data confirm that formation of the complex results in a conformational change in the C-tail that enhances its local motional freedom. Because light-activated rhodopsin decays faster than equilibrium can be reached, true $K_D$ cannot be determined in a simple binding experiment. The apparent $K_D$ for arrestin-1 binding to P-Rh* was determined to be 49 ± 11 nM (Figure 6c), which is similar to 25-50 nM previously measured using extra Meta II assay. Some comment on the stoichiometry of the complex is merited. Monomeric rhodopsin was shown to be necessary and sufficient for high-affinity arrestin-1 binding. However, recent reports suggest that two types of arrestin-1-rhodopsin complexes are formed upon activation of a high fraction of rhodopsin in native disc membranes, with 1:1 and 1:2 arrestin:rhodopsin stoichiometries. In the latter, arrestin-1 apparently binds only one rhodopsin with high affinity, stabilizing its Meta II state and trapping all-trans-retinal, whereas the other molecule is engaged with much lower affinity by distinct

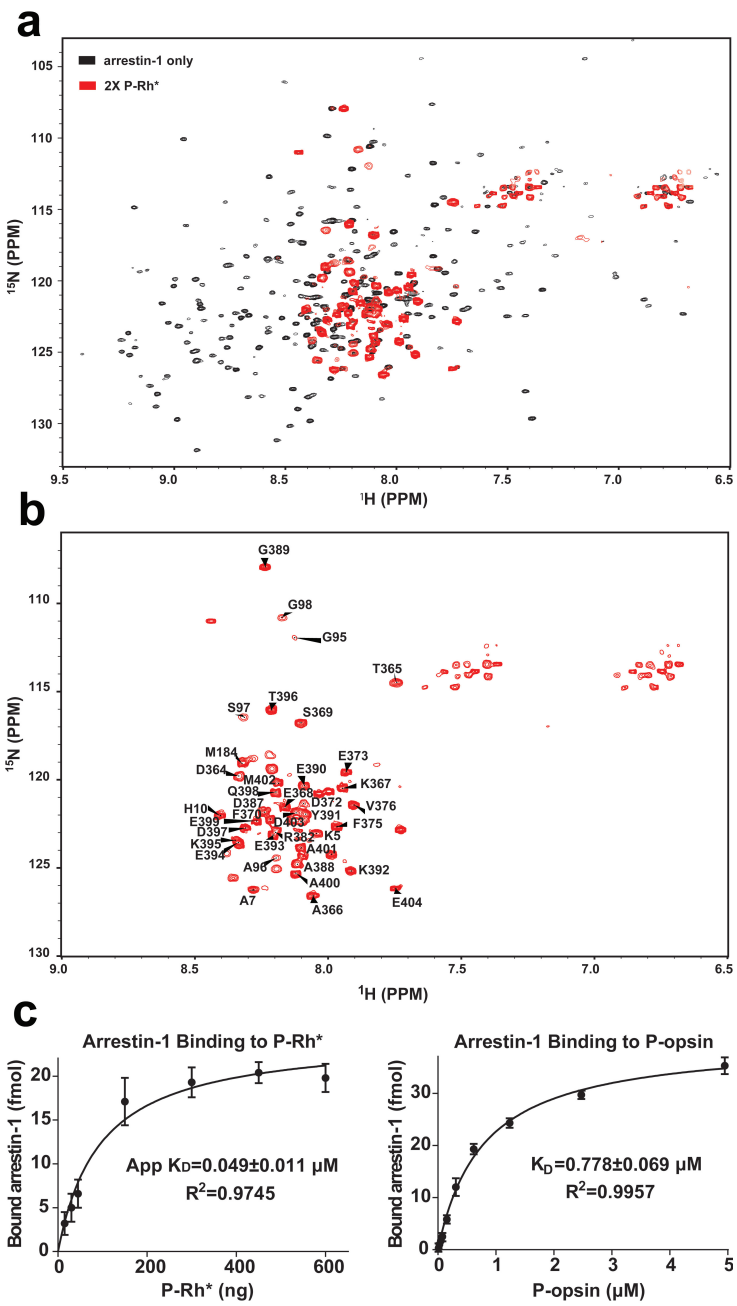


**Figure 6 Binding of arrestin-1 to P-Rh*.** (a) TROSY spectrum of 30 μM 2H, 15N-labeled arrestin-1. The spectrum of 30 μM $^{2}H$, $^{15}N$-labeled free arrestin-1 (black) shows substantial chemical shift differences for the residues that remain observable. (b) Spectrum of arrestin-1 bound to P-Rh* from (a), with labeling of the assigned peaks. (c)Determination of $K_D$ for binding of arrestin-1 with P-Rh* (left) or with P-opsin.

arrestin-1 elements localized in the C-domain. Since all forms of rhodopsin used here were solubilized by a large excess of bicelles, most of the perturbations we observed were in the N-domain of arrestin-1 and the C-tail that is anchored to this part of the molecule, and all data points to a 1:1 stoichiometry. It is highly unlikely that "auxiliary" interaction with a second rhodopsin contributed to our results.

**Binding to P-Rh* induces a major change in the global dynamics of arrestin-1**

Most arrestin-1 peaks disappear upon complex formation with P-Rh* (Figure 6b). *A priori*, this phenomenon could be due to the large correlation time associated with the ~200 kDa size of the arrestin/P-Rh*/bicelle complex. Alternatively, complex formation might result in a global change of conformational dynamics within arrestin-1, with the induced motions occurring in the intermediate rate regime ($msec^{-1}$- $\mu sec^{-1}$) of the NMR time scale. To determine which line broadening mechanism actually pertains we collected $^{1}H,^{13}C$-methyl-TROSY spectra of ILV-$^{13}C$-methyl-protonated arrestin-1 in the presence and absence of P-Rh* (Figure 7). It is well established that high quality methyl-TROSY spectra can be acquired even for complexes with molecular weights well in excess of 200 kDa [116]. However, our data revealed the same general disappearance of peaks in the methyl-TROSY spectrum that is observed in the $^{1}H,^{15}N$-TROSY spectrum of backbone amide peaks. This indicates that NMR peak disappearance for arrestin-1 upon binding to P-Rh* must be due to widespread conformational exchange in the intermediate rate regime, leading to extensive exchange-broadening. This is not an unusual phenomenon in protein structure and dynamics: global exchange-broadening is a hallmark of proteins in molten globule-like conformational states [117]. Binding of P-Rh* apparently induces

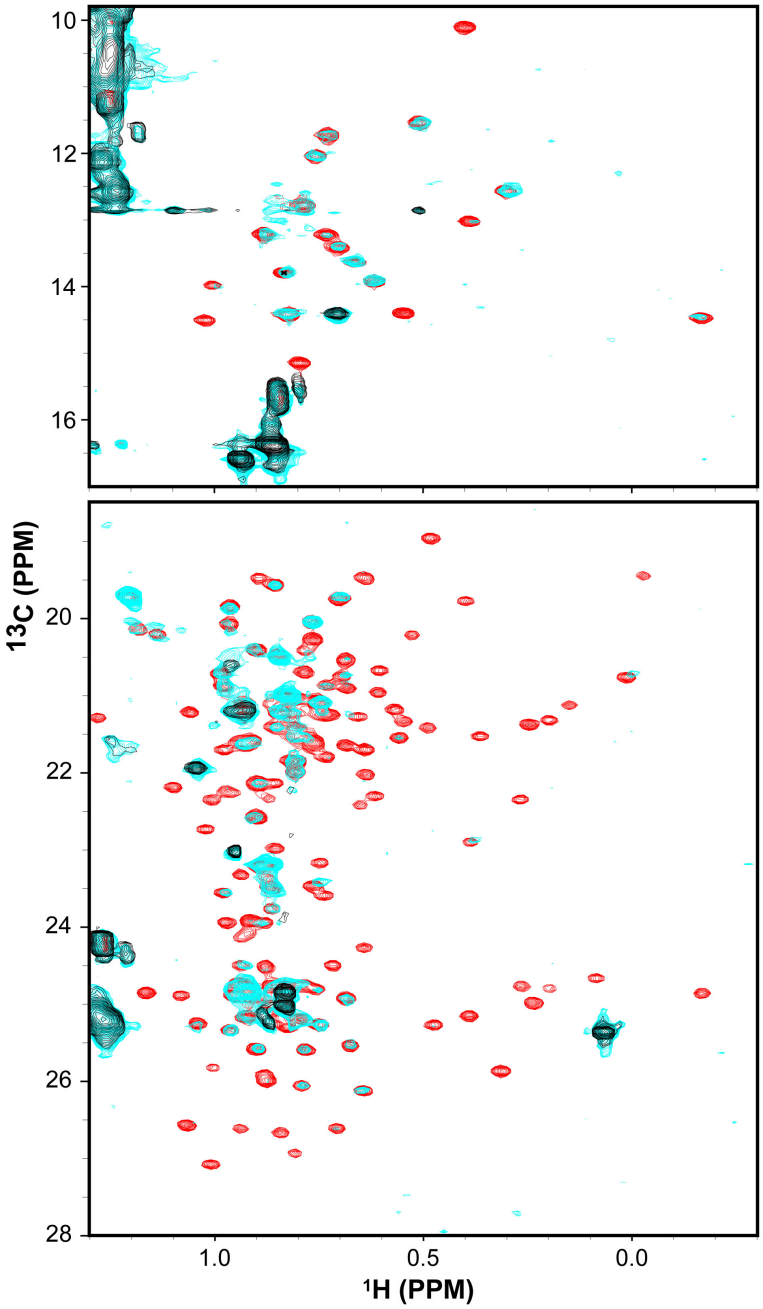


**Figure 7. Binding to P-Rh* induces a major change in the global dynamics of arrestin-1. Upper Panel:** Isoleucine region of arrestin-1 spectrum. **Lower Panel:** Leucine and valine region of spectrum. All three samples contained 4% bicelles at 308K and pH 6.5. Arrestin-1 was perdeuterated except for the methyl groups of isoleucine, leucine, and valine, which are also $^{13}$C-labeled. The sample represented by the black spectrum contained 90 μM of unlabeled P-Rh*, but no arrestin-1. The sample represented by the red spectrum contained 30 μM arrestin-1 but no P-Rh*. The cyan spectrum corresponds to a sample containing both 30 μM of arrestin-1 and 90 μM of unlabeled P-Rh*.

transition of arrestin-1 to such a state, which evidently encompasses both its N- and C-domains.

**Comparison of binding affinity, structure, and dynamics of arrestin-1 bound to phosphorylated opsin versus P-Rh***

The regeneration of rhodopsin following photoactivation requires the release of all-trans retinal, which occurs while arrestin-1 is still associated with P-Rh*. Previous studies indicated that arrestin-1 binds retinal-free phosphorylated opsin [80]; however it has not been clear whether the conversion of P-Rh* to P-opsin induces additional changes in bound arrestin-1 or even triggers arrestin-1 release, as was hypothesized previously [80, 118]. Figure 6c shows determination of $K_D$ for arrestin-1 binding to both P-Rh* and P-opsin in anionic bicelles. Binding to P-opsin was indeed strong ($K_D$ = 780 ± 70 nM; which is close to recently reported $K_D$ = 1.5 μM [119]), but less avid by an order of magnitude than the binding to P-Rh* (apparent $K_D$ = 49 ± 11 nM). The $^{1}H$-$^{15}N$ TROSY spectrum of arrestin-1 in the presence of a 3-fold molar excess of P-opsin was nearly identical to that in complex with P-Rh*, indicating remarkable similarity in the structure and dynamics of arrestin-1 in the two complexes. Opsin exists in a pH-dependent equilibrium between active-like and inactive conformations, with lower pH favoring the former [120]. Since both transducin [121] and arrestin-1 stabilize the active Meta II state of rhodopsin it is likely that, similar to binding to rhodopsin of the C-terminal peptide of the transducin a-subunit [120], bound arrestin-1 shifts this equilibrium towards active-like state. Apparently, subtle structural differences remaining between P-opsin and P-Rh* do not significantly affect the structure of bound arrestin-1.

## Discussion

High-affinity binding of arrestin-1 to P-Rh* is a necessary step for rapid termination of rhodopsin signaling [108]. Arrestin-1 elements engaged by P-Rh* and the conformational changes in the arrestin-1 molecule induced by P-Rh* binding have previously been extensively characterized [93]. In contrast, while arrestin-1 binding to other functional forms of rhodopsin—Rh*, dark P-Rh, and P-opsin—has been reported [80], the $K_D$ values for most of these interactions have not been determined and the impact of complex formation on the structure of arrestin-1 has not been studied. Here we took advantage of unique suitability of NMR to explore protein-protein interactions of modest affinity as a route to identifying arrestin-1 elements engaged by non-preferred forms of rhodopsin and the nature of conformational changes these interactions induce. The fact that these solution NMR studies focused on complex formation between a large soluble protein and a large membrane protein and were carried out using only 30 μM arrestin-1 also exemplifies the advances in NMR sensitivity that have taken place during in recent years thanks to the availability of very high field magnets, exploitation of TROSY spin physics [122, 123], and cryoprobe detectors [124].

This work shows that binding to Rh* affects the N-terminus and proximal C-terminus (370-385) of arrestin-1, likely destabilizing the three-element interaction. Rh* binding did not result in the freeing of the distal C-tail (385-404), in contrast to binding of the phosphorylated forms of rhodopsin. This provides evidence that a unique conformational change in arrestin is induced by Rh* and that active but unphosphorylated receptor destabilizes the three-element interaction previously believed to be disrupted solely by receptor-attached phosphates [31]. It also indicates that the proximal C-tail can

be perturbed without the displacement of the distal C-tail. Finally, our estimate of arrestin-1 affinity for Rh* ($K_D$>150 μM) is consistent with physiological data that wild-type arrestin-1 cannot effectively quench Rh* signaling.

We found that both dark P-Rh and P-opsin displace the distal C-tail of arrestin-1, similar to P-Rh* [2, 3] and the phospho-mimics heparin and $IP_6$ [96]. These data show that receptor-attached phosphates are necessary and sufficient for this conformational rearrangement. The affinity of arrestin-1 for dark P-Rh measured in this work ($K_D$~80 μM) [86, 88] is comparable to the arrestin-1 homodimerization constant. This suggests that the interaction with P-Rh can significantly affect the arrestin-1 monomer-dimer-tetramer equilibrium in photoreceptors. Only the monomeric form of arrestin-1 binds rhodopsin [115]. The concentration of arrestin-1 monomer in the outer segments calculated based on arrestin distribution in rods and its self-association constants yielded values that are insufficient to explain the unexpectedly short lifetime of active rhodopsin [92]. Low-affinity binding of arrestin-1 to additional partners, such as non-preferred forms of rhodopsin, would increase the supply of arrestin-1 monomer available to P-Rh*, reconciling biochemical and physiological evidence.

Perhaps the most important finding of this work is that complex formation between arrestin-1 and P-Rh* results in a dramatic "loosening" of the arrestin-1 conformation, as manifested both by direct observation of NMR resonances from mobile elements (N-terminal 10 residues, sites 95-98, and the distal C-terminus) and by the disappearance of all other resonances due to intermediate timescale conformational exchange (in both $^{1}H,^{15}N$-TROSY and $^{1}H,^{13}C$-methyl-TROSY spectra). The global conformation of arrestin-1 is evidently destabilized by high affinity binding of P-Rh*,

with the consequence that the protein transitions into a molten globule-like structure. Whether a similar transition to a much more globally dynamic state occurs for other arrestins upon complex formation with the agonist-simulated and phosphorylated forms of their cognate GPCRs is not yet known but is an intriguing possibility. A transition from a largely well-ordered structure to a much looser ensemble of conformations might be the central mechanism underlying the "activation" of arrestins that enables association with many signaling proteins. This would explain how the same arrestin with the same receptor can form distinct complexes, leading to different functional outcomes.

Finally, we also found that P-opsin binds to arrestin-1 with relatively high affinity ($K_D$ = 780 nM) and induces the same changes in its structure and dynamics as P-Rh*. These data suggest that it is regeneration of rhodopsin with 11-cis-retinal, rather than the loss of all-trans-retinal by P-Rh*, that promotes arrestin-1 dissociation [118]. Considering that opsin can activate transducin, delayed arrestin-1 release makes perfect biological sense in rods, where high sensitivity requires efficient noise suppression [125].

# CHAPTER 4

# THE CRYSTAL STRUCTURE OF ACTIVE ARRESTIN-3 AND ITS FUNCTIONAL CONSEQUENCES

This chapter is in preparation for publication. Nathaniel C. Gilbert, Nicole A. Perry, Sandra Berndt, Ya Zhuo, Sergey A. Vishniveteskiy, Candice S. Klug, Vsevolod V. Gurevich, TM Iverson contributed to the work.

## Introduction

Arrestins were first discovered for their ability to bind active, phosphorylated G protein-coupled receptors (GPCRs) and suppress G protein-mediated signaling [40]. Subsequent findings showed that the arrestin-GPCR complex additionally initiates a second, G protein-independent wave of signaling [126]that likely requires an activated form of arrestin-3 [127]. The conformations of free (basal) and active arrestins are quite different at the global level [22, 28, 128]. However, the active arrestin structures reported to date involved artificial stabilization. As a result, no study has yet explained the most pressing questions on the role of arrestins in GPCR signaling: how arrestins are activated, how non-visual arrestins interact with hundreds of receptors, and how the activated form of arrestins promotes signaling. Here, we use inositol hexakisphosphate ($IP_6$) to activate arrestin-3 and report the 2.4 Å resolution structure. The resolution of this structure allows an unprecedented view of the details of activation while the lack of artificial stabilization methods gives confidence that we are analyzing a physiologically relevant state. The structure identifies how both the binding of phosphates and the induced-folding of the receptor-binding finger loop contribute to the stabilization of the active form and suggests a mechanism of arrestin activation. Moreover, the structure reveals the basis for arrestin-3 to form productive interactions with numerous receptors based upon helicity,

hydrophobicity, and flexibility of the finger loop. Excitingly, the structure reveals previously unidentified activation-associated conformational changes in the proposed effector-binding regions, suggesting that arrestin uses molecular switches to modulate the availability of binding sites for downstream effectors and to scaffold signaling cascades.

## Methods

### Purification of arrestin-3

Arrestin-3 was cloned into the pTrcHisB vector (Invitrogen; Carlsbad, CA) with a stop codon (TGA) introduced at L394 to generate a truncated version of arrestin-3 that still retains the C-tail. The pTrc-HisB plasmid containing arrestin-3 (1-393) was then transformed into E. coli BL21 Gold. Expression was performed by growing 1L cultures in Luria Broth at 30° C overnight with shaking until stationary phase was reached. Expression was induced with the addition of 35 μM IPTG and allowed to proceed for 4 hrs. Cells were harvested by centrifugation and the pellet was frozen at -80°C for later purification.

Arrestin-3 was purified using a modification of a previously described protocol. Briefly, cell pellets were resuspended in buffer containing 50 mM MOPS, pH 7.2, 5 mM EGTA, 2 mM dithiothreitol (DTT), and a protease inhibitor cocktail (Sigma) containing AEBSF at 23 mM, EDTA at 100 mM, Bestatin at 2 mM, Pepstatin A at 0.3 mM, and E-64 at 0.3 mM and disrupted by sonication at 4 °C. The lysate was clarified by centrifugation at 12,000 rcf for 60 min, and $(NH_4)_2SO_4$ was added to the supernatant to a final concentration 0.32 mg/ml. After centrifugation at 12,000 rcf for 90 min, the pellet containing precipitated arrestin-3 was collected and resuspended in buffer containing 10 mM MOPS pH 7.2, 2 mM EGTA, 1 mM DTT and 2 mM benzamidine. This resuspended

mixture was again centrifuged at 12,000 rcf for 60 min, and the supernatant containing arrestin-3 was applied onto a heparin column and eluted with a linear salt gradient. The fractions containing arrestin-3 were identified by SDS-PAGE and combined. The salt concentration of the pooled fractions was adjusted to 100 mM, and the solution was loaded onto a linked Q and SP column. At a NaCl concentration of 100 mM, arrrestin-3 flows through the Q column (while most contaminants bind), but binds the SP column. The columns were uncoupled and a liner NaCl gradient was used to elute arrestin-3 from the SP column. The fractions containing arrestin-3 were identified by SDS-PAGE and were combined, concentrated with a 30 kDa cutoff concentrator, then further purified using a Superdex 200 10/30 GL column equilibrated with 20 mM MOPS pH 7.2, 150 mM NaCl, 2mM tris(2-carboxyethyl) phosphine (TCEP), and 2 mM benzamidine.

**Crystallization of arrestin-3 in the presence of IP6**

Purified arrestin-3 (residues 1-393) was concentrated to 5 mg/ml and incubated with IP6 at the molar ratio of 1:20 for 30 min. Hexagonal crystals in space group P63 were grown by the vapor diffusion method in sitting drops containing 2 µl of protein-IP6 mix and 2 µl of reservoir solution (100 mM Succinate/Phosphate/Glycine (SPG; Rigaku) pH 8.5 and 25% PEG 1500). Microcrystals appeared within 24 hours and were used for seeding using the same reservoir solution. Crystals were harvested after 7 days, cryoprotected in 50% w/v glycerol (and none of the crystallization chemicals) and cryocooled by plunging in liquid nitrogen.

**Crystallographic data collection, structure determination, and analysis**

Diffraction data were collected at the Advanced Photon Source LS-CAT beamline ID-D. All images were indexed, integrated and scaled using HKL2000 and the CCP4

suite of programs. MrBUMP was used to identify and prune models for molecular replacement in an automated fashion, and suggested that bovine arrestin-2 (PDB entry 1G4M) was the best search model. The coordinates of bovine arrestin-2 were then pruned by the MOLREP 36 subroutine and used for molecular replacement in the PHASER 37 subroutine. The best solution was associated with an R/Rfree of 0.34/0.37 and was iteratively improved by model building in COOT and refining in PHENIX. Both IP6 molecules were placed into the coordinates using the LigandFit subroutine in PHENIX. MolProbity was used to assess statistics for the final coordinates. Figures were prepared in PYMOL. Domain rotation was measured and analyzed using DynDom.

**DEER distance measurements**

Double electron electron resonance (DEER) spectroscopy data were collected using a Bruker ELEXSYS E580 operating at Q-band and equipped with an EN5107D2 resonator. Samples contained 20% deuterated glycerol as a cryoprotectant and 100 μM protein and varying amounts of IP6 and were run at 80 K following flash freezing in a dry ice and acetone mixture. Acquired raw data after phase correction were background corrected, plotted and analyzed in the same way for each data set using the LongDistances software program written by C. Altenbach (University of California-Los Angeles, CA). Distance distributions were determined by fitting the corrected dipolar evolution data using the algorithms included in the LongDistances program. The upper reliable distance limit of 65 Å was determined based on the maximum data collection time (t=4.5 μs) of the DEER experiments according to the equation d $\approx$ 5(t/2)1/3 41 and is reflected in the x-axis of the distance distribution plot. The release of the C-tail causes the distances to spread out and possibly become longer than the observable range of our data.

**BRET measurements of arrestin-3 binding to the M2 muscarinic receptor**

The interactions of N-terminally Venus-tagged WT and mutant arrestin-3 with C-terminally RLuc8-tagged M2 muscarinic cholinergic receptor was determined by BRET, as described, using the highest (saturating) arrestin-3 concentrations. Absolute levels of luminescence were used as the measure of the expression levels of RLuc-tagged M2 receptor, whereas direct fluorescence was used to determine the expression of Venus-tagged arrestins, as described. BRET was measured 15 minutes after the addition of 25 μM M2 agonist carbamylcholine, which was added 5 min prior to 5 μM luciferase substrate coelenterazine. Luminescence and fluorescence were measured using an Infinite F500 multimode plate reader (Tecan). Net BRET was calculated as the difference between BRET signal in the presence and absence of agonist.

## Results and discussion

**Arrestin-3 activation by $IP_6$**

Arrestin-3 mediated signaling can be either receptor-dependent or receptor-independent. One proposed mechanism of receptor-independent arrestin-3 activation is by polyanions [129]. Indirect methods have demonstrated that polyanions can induce release of the arrestin C-tail, one of several requirements for activation. $IP_6$ is one of the most abundant polyanions in the cytoplasm, with concentrations ranging from 35 to 105 μM [130, 131]. As arrestin-3 can bind IP6 and can interact with downstream effectors in a receptor-independent fashion, we reasoned that a signaling-active form of arrestin-3 could be induced by $IP_6$. To test this hypothesis, we used site-directed spin labeling (SDSL) and double electron electron resonance (DEER) spectroscopy to measure inter-spin distances (Figure 1a) between spin labels on the N-domain (at Ser13) and the C-tail

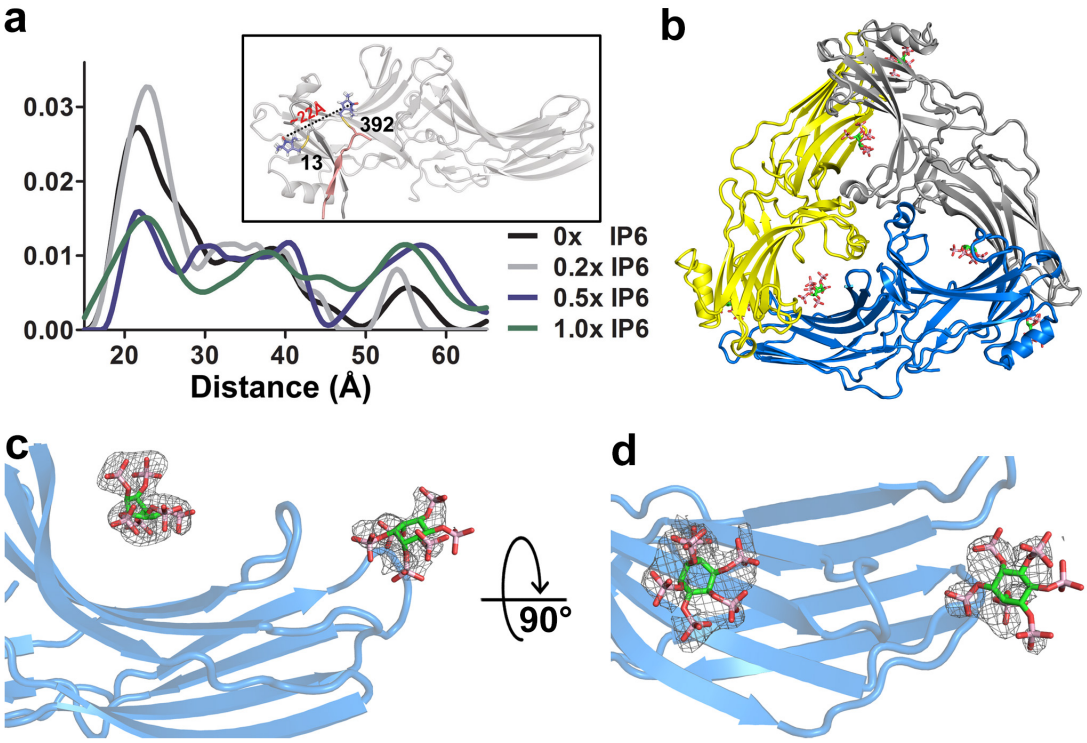


**Figure 1. arrestin-3 activation by $IP_6$** (a) Plot of the probability of the distances between spin labels (at S13 and A392) for 100 μM arrestin-3 in the presence of the indicated molar ratios of $IP_6$; inset shows the location of the spin labels in basal arrestin-3 (PDB entry 3P2D) after reaction of the cysteines with 1-oxyl-2,2,5,5-tetramethyl-Δ3-pyrroline-3-methyl methanethiosulfonate spin label (MTSL). (b) Ribbons diagram of the IP6-activated arrestin-3 trimer. Each protomer is shown in a different color (grey, yellow, blue), with IP6 shown as sticks. The finger loop is circled. (c; d) Electron density for the two IP6 molecules bound to arrestin-3. $IP_6$ molecules are superimposed on a composite omit map calculated in Phenix and contoured at 1.2σ.

(at Ala392) to identify whether activation-associated C-tail release is observed in arrestin-3 upon IP6 binding. In the absence of IP6, the major population of the inter-spin distances is 22 Å (Figure 1a), which agrees with the crystal structure of the basal state [132]. Addition of IP6 to arrestin-3 at a molar ratio as low as 0.5:1 induced C-tail release, as evidenced by a decrease in the population of the 22 Å inter-spin distance and a concomitant increase in several of the observable longer distances, especially at 55 Å (Figure 1a). Under the conditions tested, approximately one in three proteins released its C-tail, suggesting that IP6 promotes arrestin-3 less effectively than phosphorhodopsin, where the C-tails of virtually all arrestin-3 molecules are released.

We activated arrestin-3 with $IP_6$ and determined the crystal structure at 2.4Å resolution. $IP_6$-activated arrestin-3 forms a trimer (3,053 $Å^2$ of buried surface area per protomer, Figure 1b) with each interface mediated by two $IP_6$ molecules (Figure 1c). Inspection of the structure identifies that $IP_6$ directly displaces the C-tail (Figure 2a) and that $IP_6$-bound arrestin-3 has an interdomain twist of ~18° (Figure 2b) with respect to the structure in the basal state, both of which are hallmarks of activated arrestin. The middle loop and the lariat loop also undergo large conformational changes in the $IP_6$-bound arrestin-3 structure. It is similar to the changes observed in previously reported arrestin active structures [22, 128].

The $IP_6$ binding sites highlight locations for all phosphorylated partners that bind arrestins under different physiological situations. For example, the two $IP_6$ interaction sites in the N-domain make nearly identical contacts with arrestin-3 as peptide-attached phosphates make with arrestin-2 (Figure 2a). Further, one $IP_6$ binding site in the C-domain includes residues proposed to be in close proximity to the membrane whe

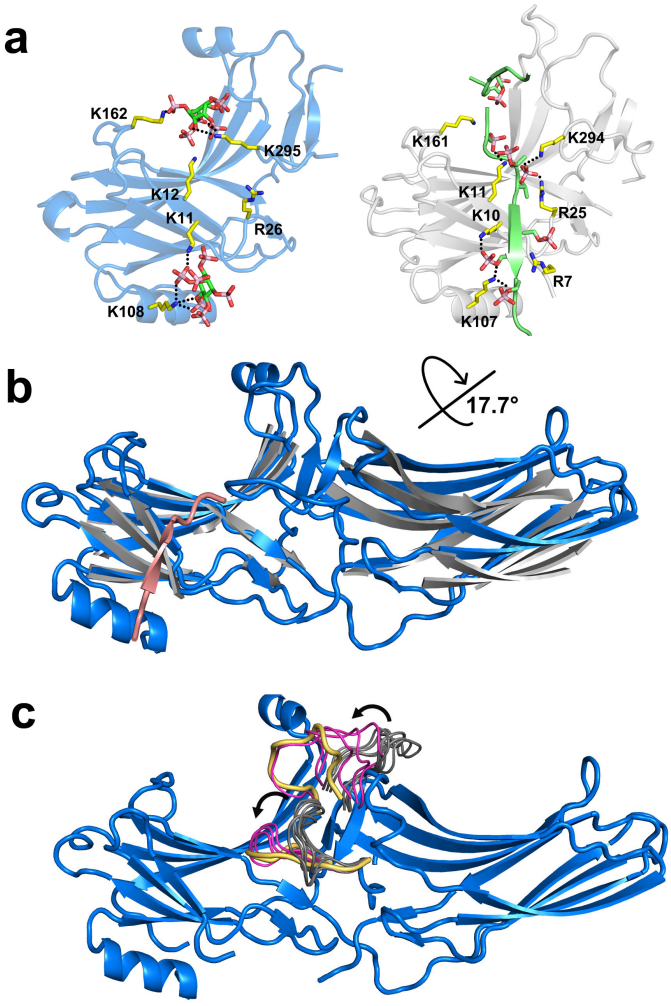


**Figure 2 Global conformational changes in activated arrestin-3. (a)** Comparison of the structure of arrestin-3 with IP6 and receptor peptide bound to arrestin-2 (PDB entry 4JQI) showing the promiscuous use of the same binding site. The binding of $IP_6$, receptor phosphopeptide, and the arrestin C-tail are anticipated to be mutually exclusive as they bind at the same location. **(b)** Overlay of the N-domain of $IP_6$-activated arrestin-3 (*blue*) with the secondary structural elements of basal arrestin-3 (*grey* with a *pink* C-tail, PDB entry 3P2D) highlights the 17.7° interdomain rotation. **(c)** Comparison the positions of the middle and lariat loops in active arrestin-3 (*yellow*), other active arrestins (*magenta*; PDB entries 4JQI, 4J2Q, and 4ZWJ and basal arrestins (*grey*; PDB entries 1CF1, 1JSY, 1ZSH, 1G4M, 3P2D). Arrows indicate the direction of loop movement upon arrestin activation.

arrestin is bound to receptor. It is possible that under some physiological conditions, this site may instead bind to phospholipids to pre-localize arrestin to the membrane.

**Mechanism of arrestin activation via the phosphate sensor**

Comparison of IP6-activated arrestin-3 to the structure of receptor-activated arrestin-1 suggests that activation by either receptors or polyanions promotes a similar conformation, which has not been previously suggested. Notably, we observe an activation-associated interdomain rotation of 17.7° as compared to the structure of basal arrestin-3 (Figure 2b) accompanied by changes in the positions of receptor-binding loops (Figure 2c). The resolution of this structure allows accurate placement of side chains, which reveals the mechanism of activation. The interdomain rotation centers around conformational changes that disrupt the polar core, a network of intra-molecular interactions proposed to determine the domain orientation in the basal state (Figure 3). Major conformational changes that directly involve IP6 include displacement of the C-tail from its binding site in the N-domain by IP6, and a conformational change of the lariat loop (a region important for receptor-association), with the new conformation stabilized by a direct interaction between IP6 and Lys295. This interaction shifts the backbone and displaces two of the three negative charges in the polar core, such that the interdomain angle observed in the basal state becomes unfavorable. In summary, the phosphates on the receptor or IP6 “pull” the lariat loop out of its basal position when they displace the C-tail. Together, these changes stabilize a conformation with a disrupted polar core, allowing the interdomain twist that we observe here, which has been reported previously for arrestin-1 and arrestin-2. This activation mechanism explains how

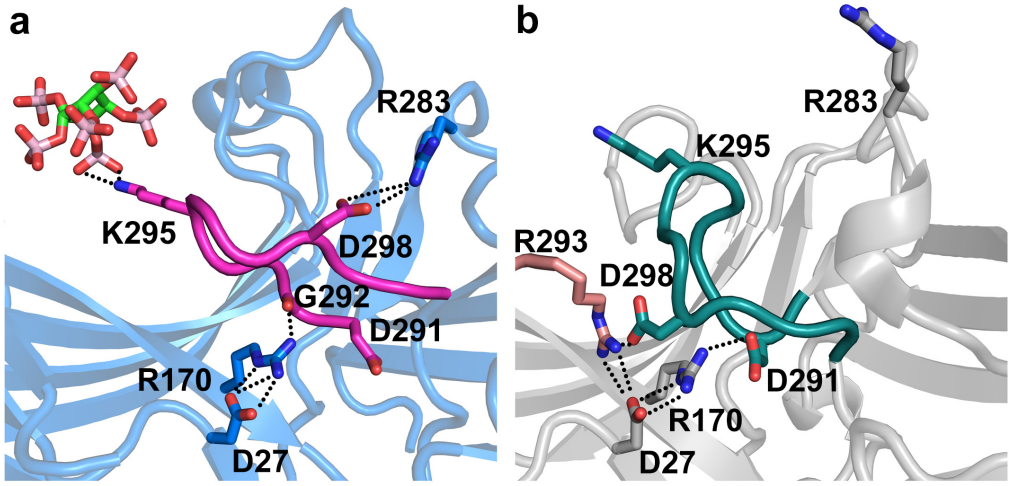


**Figure 3. Mechanism of arrestin activation promoted by the binding of phosphoryl groups in the N-domain.** (a) Conformation of the lariat loop in $IP_6$-activated arrestin-3 disrupts the polar core. (b) Conformation of the lariat loop in basal arrestin-3 (PDB entry 3P2D) with an intact polar core.

engineered arrestins that eliminate or reverse the charges in the polar core can be more easily activated and bind to active, unphosphorylated GPCRs.

**Finger loop properties in activation and receptor specificity**

During the arrestin-receptor interaction, the finger loop of arrestin-3 (Figure 1b) likely binds within a hydrophobic pocket in active cognate receptor. Upon receptor binding, a conserved ED(I/L)D motif in the finger loop (residues 68-71 of arrestin-3) is proposed to fold into a short α-helix that may be a characteristic of fully activated arrestin. NMR studies indicate that in partially active arrestins, the finger loop conformation is not altered [32]. This helix is absent in previous structures of the isolated active arrestins stabilized by mutations or antibodies, but stabilized in IP6-activated arrestin-3 by a coiled-coil around the crystallographic three-fold axis (Figure 2a) [22, 26, 128], suggesting that we have crystallized fully activated arrestin-3.

A key question in GPCR signaling is how non-visual arrestins (arrestin-2 and arrestin-3) recognize hundreds of GPCRs without a detectable conserved binding site on the receptors [126]. Our structure (Figure 4) suggests a model for receptor binding in which the activated finger loop is on a flexible tether that can be presented to cognate receptors at a range of angles (Figure 4c). Any hydrophobic environment then induces α-helix formation, which enhances receptor coupling (Figure 4a,b). If this model is correct, the helicity, hydrophobicity, and flexibility of this helix will all be key for receptor coupling. We therefore designed site-specific mutations to perturb these properties and measured receptor binding using a bioluminescence resonance energy transfer (BRET) assay in COS-7 cells cotransfected with luciferase-muscarinic M2 receptor and Venus-arrestin-3 [133] (Figure 4d). Wild-type Venus-arrestin-3 shows a robust increase in

BRET signal upon agonist stimulation, whereas arrestin-3-KNC (a negative control containing 12 substitutions of key receptor-binding residues) [134] does not (Figure 4d). We first assessed the role of the hydrophobic side chain of Leu69 using the Leu69Arg and Leu69Glu mutations. The Leu69Arg mutation completely abrogates binding (Figure 4d, e), while the Leu69Glu mutant shows binding similar to wild-type. This is consistent with the side chain charge of Glu being more easily neutralized by protonation. We next assessed whether helicity of this region is important by introducing the Asp70Pro mutation. Binding was not detectable with this assay (Figure 4d, e), suggesting that formation of the finger loop α-helix is important for receptor binding. Finally, we explored the role of helix flexibility with modification of Asp68. Asp68 is the first residue in the short α-helix formed by the tip of the finger loop, and does not interact with the receptor in the rhodopsin-arrestin complex. As a result, replacement of this Asp with Pro is not anticipated to affect helicity or directly influence receptor interaction, but is anticipated to restrict finger loop flexibility. We therefore designed the Asp69Pro mutation to modulate finger loop flexibility, and this mutation abolished detectable agonist-induced recruitment of arrestin-3 to the M2 muscarinic receptor (Figure 4d, e). Each of these variant arrestins expressed at levels somewhat higher than wild-type arrestin- 3 (Figure 4f) as assessed by measuring fluorescence of transfected cells such that loss of coupling cannot be explained by changes in expression levels. This supports a role for these finger loop properties in promoting broad receptor specificity [126].

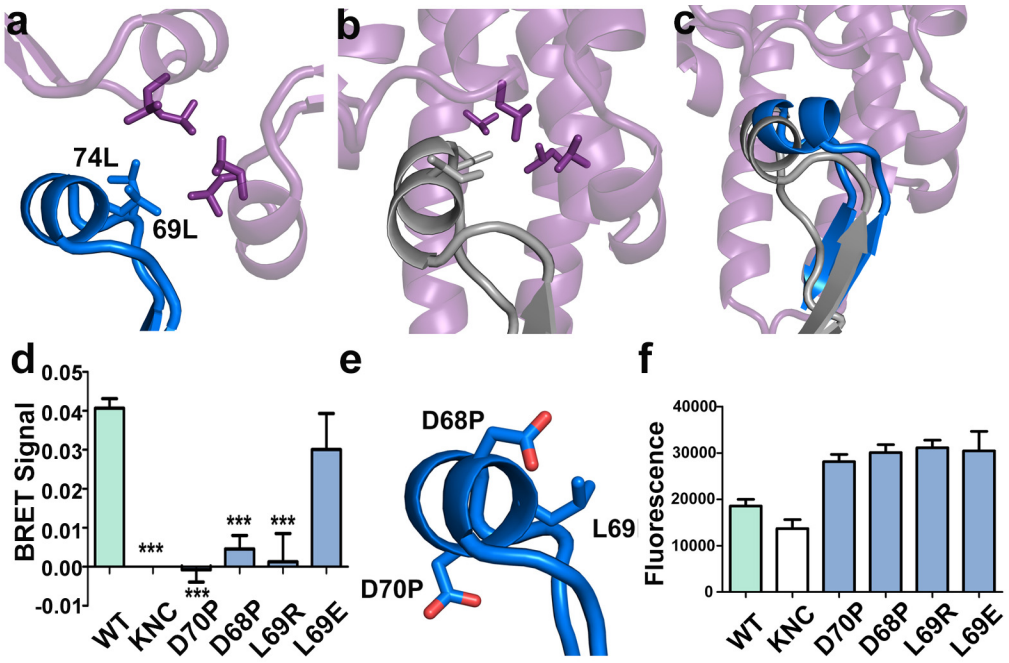


**Figure 4. Finger loop properties in activation and receptor specificity.** (a) Helical conformation of the receptor-binding finger loop as stabilized by the active arrestin-3 trimer. (b) The arrestin-1-rhodopsin interaction (PDB entry 4ZWJ) shows similar hydrophobic contacts induce the finger loop helix. (c) Comparison of the position of the helical finger loop in $IP_6$-activated arrestin-3 (*blue*) and rhodopsin-activated arrestin-1 (*grey*, PDB entry 4ZWJ]). (d) Evaluation of WT and mutant Venus-arrestin-3 binding to the luciferase-tagged M2 muscarinic receptor by BRET. a) Location of sites of mutations in the background of the active arrestin-3 structure. (e) Fluorescence of wild-type and mutant Venus-tagged arrestin-3 in COS-7 cells (reflecting expression level) was measured using $\lambda_{ex}$= 500 nm and $\lambda_{em}$= 535 nm.

**Arrestin switch regions in effector binding**

A major functional consequence of non-visual arrestin activation is the scaffolding and activation of downstream effectors, yet how the activated form of arrestins supports signaling has never been explained. As this is the highest resolution structure of any active arrestin, we identified conformational changes induced by activation in the effector binding surfaces (Figure. 5a). These conformational changes have not been previously reported, although inspection of the coordinates for the basal and active conformations of arrestin-1 and arrestin-2 suggests that activation-dependent conformational changes in equivalent regions are universal in arrestins. We suggest that these conformational changes act as molecular switches that are functionally analogous the switch regions of G proteins [reviewed in [135]]. In many signaling proteins the activation state is reflected in conformations of effector binding regions. However, the possibility of switch regions in arrestins has never previously been suggested. Our findings explain for the first time how activated arrestins support G protein-independent signaling. We termed elements subject to activation-associated conformational changes "arrestin switch" regions.

Arrestin switch I (aSwI; residues 89-97; Figure 5a) is strongly conserved in sequence in arrestin-3 from other organisms, but poorly conserved in the other three arrestin isoforms (Figure 5a, inset). This nine amino acid segment in arrestin-3 contains seven prolines, including two PPXP motifs that may be recognized by SH3 domains [136]. Comparison of the basal and activated arrestin-3 structures reveals a maximal displacement of 4.7 Å and both a *cis* to *trans* and *trans* to *cis* isomerization in different prolines; however, the electron density of this region is difficult to interpret, and not all of

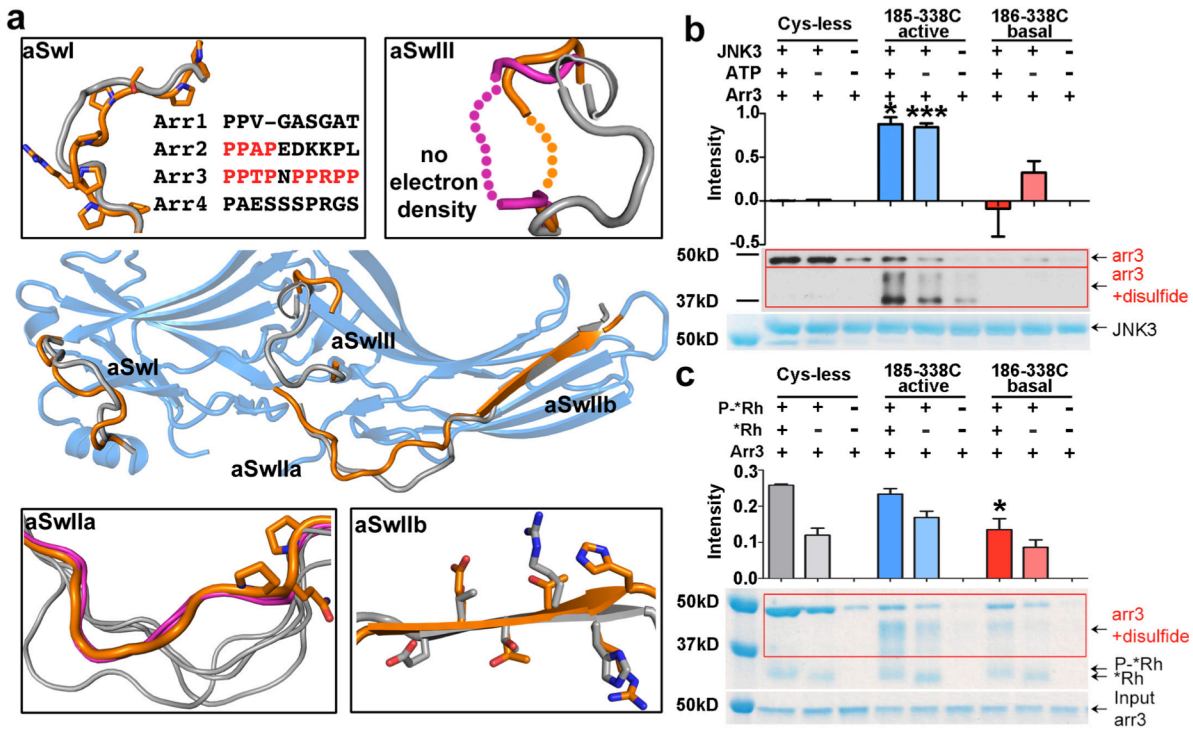


**Figure 5 Arrestin-3 switch regions.** (a) Conformations of the arrestin switch regions in the active form are shown in *orange* ($IP_6$-activated arrestin-3) or *magenta* (phosphopeptide-activated arrestin-2; PDB entry 4JQI) differ from those observed in basal arrestin-3 (*grey,* PDB entry 3P2D). Insets highlight these switch regions. (b) Evaluation of arrestin-3 variants binding to $His_6$-JNK3 in the presence and absence of ATP. Arrestin-3 that had formed disulfide bonds (lower red box) was quantified. Arrestin-3 that has not formed disulfide bonds (upper red box) is quantified in Figure S11. (c) Evaluation of arrestin-3 variants binding to active phosphorhodopsin (P-*Rh) or active rhodopsin (*Rh). Total arrestin-3 binding (red box) was quantified.

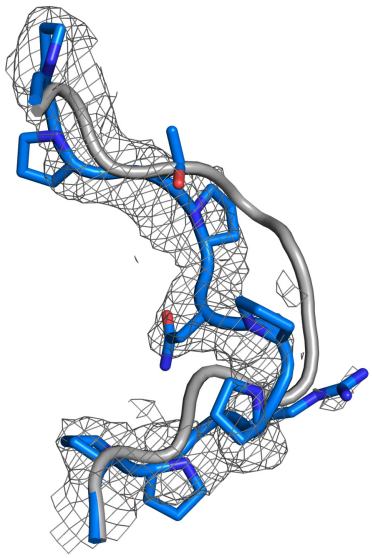

**Figure 6. Conformational changes in aSwI.** Composite omit electron density for $IP_6$-activated arrestin-3 contoured at 0.8σ shown superimposed on the structure of $IP_6$-activated arrestin-3 (*blue*) and basal arrestin-3 (*grey,* PDB entry 3P2D).

the residues could be modeled with confidence (Figure 6). Such flexibility may be important for adapting to different effectors.

Arrestin switch II (aSwII; residues 176-191 Figure 5a) contains two distinct parts: IIa (residues 176-183) and IIb (184- 191). ASwIIa connects the N- and C-domain, and has been proposed to act as a hinge between domains [137]. Like aSwI, aSwIIa contains a polyproline motif (PQP residues 181-183) that has been proposed as a putative non-canonical SH3 binding site in arrestin-2 [136]. The aSwIIa region shows a nearly identical conformation in all available active arrestin structures, in contrast to variable conformations observed in basal arrestins (Figure 5a).

ASwIIb includes the entirety of the first edge β-strand of the C-domain (residues 184-191) and superimposes in all active arrestin structures. As compared to most arrestins in the basal state, the β-strand of aSwII is register-shifted; the register shift moves the strand one position in arrestin-2 and -3 and two positions in arrestin-1 (Figure 5a). Register-shifted β-strands are unusual, but there is a precedent in RNA polymerase for register shifts regulating cognate protein-binding [138]. It should be noted, however, that the position of aSwIIb that correlates with the active state of arrestin was observed in one structure of basal arrestin-2 [136, 139], which may relate to known basal activity of the signaling cascade [32, 35].

Arrestin switch III (aSwIII, residues 307-316; Figure 5a) is an extension of the lariat loop, a region that is key for promoting activation-associated conformational changes and a part of the polar core that stabilizes the orientation of the two domains in the basal state. ASwIII becomes disordered in both activated arrestin-3 and arrestin-2, however

interaction with effector could promote a folded conformation as a part of the signaling process.

To test the role of the activation-associated conformational changes in the switch regions, we focused on aSwII, where the register-shifted β-strand can be stabilized by disulfide trapping. We introduced disulfides into a Cys-less version of arrestin-3 to trap aSwII in the basal and activated conformation, validated the formation of the disulfide bond and compared the binding of these variants and Cys-less arrestin-3 without disulfides to the JNK3 effector (Figure 5b, c). Densitometric quantitation of arrestin-3 binding to JNK3 shows that disulfide-trapping aSwII in the conformation observed in the active structure results in significantly higher effector binding, as compared to arrestin-3 with aSwII disulfide-trapped in the conformation of basal arrestin-3 (Figure 5b).

To assess whether the receptor binding sites and arrestin switch regions are allosterically connected, we evaluated in vitro binding of the disulfide-trapped arrestin-3 variants to light-activated phosphorhodopsin. Arrestin-3 with a disulfide that trapped aSwII in the conformation observed in the active structure bound to rhodopsin at a significantly higher level than arrestin-3 with aSwII trapped in the basal conformation (Figure 5c). These findings indicate the presence of an allosteric network between the receptor- and effector-binding sites in arrestin.

# CHAPTER 5

# ENGINEERING OF ARRESTIN WITH ENHANCED RECEPTOR BINDING

Much of this chapter was published in *The Journal of Biological Chemistry* [ref]. Sergey A. Vishnivetskiy, Maria C. Palazzo, Evan K. Brooks, Christian Altenbach, TM Iverson, Wayne L. Hubbell and Vsevolod V. Gurevich contributed to the work here.

## Introduction

Rod photoreceptors mediate night vision in vertebrates. Rods demonstrate remarkable single photon sensitivity and unusual reproducibility of a single photon response. These features require biochemically perfect signaling cascade with virtually no noise, enormous amplification, and extremely rapid shutoff. Light activates rhodopsin, which then sequentially catalyzes GDP/GTP exchange on numerous molecules of its cognate G protein transducin. Within 30–60 ms, active rhodopsin [140] is phosphorylated by GRK1, whereupon visual arrestin-1 specifically binds light-activated phosphorylated rhodopsin (P-Rh*), ensuring timely signaling shutoff.

Genetic defects in this rapid and efficient two-step shutoff mechanism invariably result in visual disorders. Loss-of-function mutations in arrestin-1 or GRK1 cause Oguchi disease, a form of stationary night blindness. Mutations in rhodopsin that lead to the loss of GRK1 phosphorylation sites result in retinal degeneration. Although in principle loss-of-function mutations can be cured by gene replacement therapy, in the case of gain-of-function defects, such as the loss of phosphorylation sites resulting in unquenchable signaling, viable therapeutic strategies remain to be developed.

We have recently proposed a compensational approach using enhanced arrestin-1 mutant that binds Rh* with much higher affinity than wild type (WT) arrestin-1 to reduce excessive signaling by unphosphorylated rhodopsin. Although, the first proof-of-principle

study showed that compensational gene therapy works in vivo, it also revealed the limitations of existing phosphorylation-independent arrestin-1 mutants. Enhanced arrestin-1 improved functional performance of phosphorylation-deficient rods, facilitated their recovery, and prolonged their survival, but "compensated" shutoff was still significantly slower than in WT animals with normal Rh* phosphorylation. Thus, improved enhanced arrestin-1 mutants with higher affinity binding to Rh* and sufficient stability for in vivo expression have to be designed.

Mammalian arrestin-1 at physiological concentrations found in rods robustly self-associates, forming dimers and tetramers. Only monomeric arrestin-1 binds rhodopsin, because receptor binding surfaces in the tetramer and both possible dimers are shielded by sister subunits. Arrestin-1 is the only signaling protein in the visual system that forms inactive "storage" oligomers, and the biological significance of this phenomenon is unclear. To elucidate the role of arrestin-1 self-association in photoreceptors, the consequences of the replacement of WT arrestin-1 with a constitutively monomeric mutant in vivo must be determined. In addition, it is unknown whether oligomerization needs to be preserved in a therapeutically effective enhanced mutant with high Rh* affinity. These in vivo experiments require a stable constitutively monomeric version of arrestin-1 as well as enhanced mutants both with normal and absent ability to oligomerize.

Here we report extensive redesign of the rhodopsin binding surface of arrestin-1 that yielded mutants with significantly higher affinity for unphosphorylated Rh*. We identified further enhanced arrestins, constitutively monomeric forms, and a mutant that combines inability to self-associate with high Rh* binding, all of which are stable. These

proteins are promising candidates for in vivo evaluation of the potential of compensational gene therapy and for elucidation of the role of arrestin-1 oligomerization.

## Methods

### Mutagenesis and plasmid construction

For in vitro transcription mouse arrestin-1 (generous gift of Dr. Cheryl Craft, University of California) was subcloned into pGEM2 (Promega, Madison, WI) with "idealized" 5-UTR between NcoI and HindIII sites as described. All mutations were introduced in transcription construct by PCR using the strategy previously described. All constructs were confirmed by dideoxy sequencing. For the expression in HEK293 cells, coding sequences with 5′-UTR were excised from pGEM2 constructs using EcoRI and HindIII restriction sites and subcloned into pcDNA3 vector (Invitrogen) with a modified multiple cloning site as described previously. In vitro transcription, translation, and preparation of phosphorylated and unphosphorylated rhodopsin were performed as described recently.

A direct binding assay was performed as described. Briefly, 1 nM arrestin-1 (50 fmol) was incubated with 0.3 μg of P-Rh* in 50 μl of 50 mM Tris-HCL, pH 7.4, 100 mM potassium acetate, 1 mM EDTA, 1 mM DTT for 5 min at 37 °C under room light. Samples were cooled on ice, and bound and free arrestin-1 was separated at 4 °C by gel filtration on a 2-ml column of Sepharose 2B-CL. Arrestin-1 eluting with rhodopsin-containing membranes was quantified by liquid scintillation counting. Nonspecific "binding" was determined in samples where rhodopsin was omitted and subtracted.

### In vitro arrestin stability assay

Translated radiolabeled arrestin-1 was incubated for 0.5–4 h at the indicate

temperatures and cooled on ice. The binding of arrestin-1 in these samples to P-Rh* was compared with that of control sample kept on ice as described above except that 2 nM arrestin-1 (100 fmol/sample) was used.

**Cell-based stability assay**

HEK293 cells were maintained in Dulbecco's modified Eagle's medium supplemented with 10% serum as described. Cells were transfected with 3 μg of DNA per well of a 6-well plate using Lipofectamine according to manufacturer's instructions. After 36 h cells were serum-starved overnight and then kept at 37 °C (control) or at 40 °C for 3 h. Cells were washed with PBS and non-enzymatically detached from plates with 2 × 500 μl of Versene. Cells were pelleted by centrifugation at 4 °C for 10 min at 300 rpm (Eppendorf centrifuge 5417R) and resuspended in 400 μl of 50 mM Tris-HCl, pH 7.4, 100 mM NaCl, 1 mM EDTA, 1 mM DTT supplemented with Complete protease inhibitors mixture (Roche Applied Science) and 1 mM PMSF. Cells were lysed by sonication (Sonic Dismembrator Model 500, Fisher Scientific) 3 × 5 s at 30% power. Unbroken cells and debris were pelleted by centrifugation at 4 °C for 10 min at 14,000 rpm (Eppendorf centrifuge 5417R), and the supernatant was frozen in aliquots and stored at −80 °C until used. Total protein was measured using Bradford reagent (Bio-Rad), and the expression of different forms of arrestin-1 was determined by Western blot with anti-arrestin rabbit polyclonal antibody. To determine functionality of soluble arrestins, equal volumes of lysates (10 μl) were incubated with or without (nonspecific) 1 μg of P-Rh* in 50 μl of 50 mM Tris-HCL, pH 7.4, 100 mM potassium acetate, 1 mM EDTA, 1 mM DTT for 5 min at 37 °C in room light. The samples were cooled on ice, loaded onto 0.1 ml of 0.2 M sucrose in binding buffer, and centrifuged 20 min at 100,000 rpm in Beckman TL-120

tabletop ultracentrifuge (rotor TLA120.1). Supernatants were removed, and pellets were dissolved in 50 μl of SDS sample buffer. One-tenth of each sample along with one-tenth of the input were subjected to SDS-PAGE and analyzed by Western blot with anti-arrestin antibody followed by HRP-conjugated anti-rabbit secondary antibody, with detection by SuperSignal Pico [141]. Nonspecific binding (the amount of arrestin-1 pelleted in the absence of rhodopsin, likely due to aggregation, was subtracted from binding to P-Rh*. Protein survival was calculated as the ratio of the fraction of arrestin-1 in lysate of cells incubated at 40 °C that specifically bound to P-Rh* to the bound fraction in lysates of control cells kept at 37 °C.

**Arrestin-1 purification and analysis of its self-association**

Mouse arrestin-1 mutants were expressed in Escherichia coli and purified essentially as described. All light-scattering measurements were made with a DAWN EOS detector coupled to an Optilab T-rEX refractometer (Wyatt Technologies) after gel filtration on a QC-PAK GFC 300 column (7.8 mm inner diameter × 15 cm) (Tosoh Bioscience). The arrestin samples (100 μl) at different concentrations were incubated in fresh 5 mM DTT for 30 min at room temperature to disrupt covalent inter-arrestin disulfide bonds and injected onto the column at 25 °C at a flow rate of 0.6 ml/min in 50 mM MOPS, 100 mM NaCl, pH 7.2. The column did not resolve oligomeric species but simply acted as a filter to remove highly scattering particulates. Light scattering at 7 angles (72–126°), absorbance at 280 nm, and refractive index (at 658 nm) for each sample were taken for a narrow slice centered at the peak of the elution profile. The experimental weight-averaged molecular weight values were obtained from the protein concentration and light scattering data using ASTRA 5.3.4.20 software (Wyatt Technologies). The weight-

averaged molecular weight data were analyzed using the two-step monomer-dimer-tetramer (MDT) model, where M, D, and T are monomer, dimer, and tetramer, respectively. The data for arrestin-1 carrying F86A/F198A mutations did not fit the MDT model and was fitted using the monomer-dimer model instead. Details of the analysis have been previously described. Except where noted, the equilibrium constants are given in terms of the corresponding dissociation constants, $K_{D,dimer}$ ($K_{D,dim}$) and $K_{D,tetramer}$ ($K_{D,tet}$). The errors in equilibrium constants were determined from least-squares fitting of the data to MDT or monomer-dimer model taking into account an estimated error of ± 1 kDa in the computed values of the average molecular weight.

## Results and Discussion

### Elimination of phosphate binding positive charges does not enhance arrestin-1 binding to Rh*

Multiple positive charges in bovine arrestin-1, including Lys-14, Lys-15, Arg-18, Lys-163, Lys-166, Lys-167, Arg-171, and Arg-175 were shown to bind rhodopsin-attached phosphates. Mouse arrestin-1 also carries all of these positive charges: Lys-15, Lys-16, Arg-19, Lys-164, Lys-167, Lys-168, Arg-172, and Arg-176. Therefore, we hypothesized that a mismatch between the presence of these positive charges on the receptor binding surface of arrestin-1 and the absence of negatively charged phosphates on the C terminus of Rh* destabilized the complex. To test this idea, we replaced phosphate binding lysines and arginines (Figure 1A) with neutral hydrophilic glutamine with hydrogen-bonding capability, introducing K15Q, K16Q, R19Q, R172Q, K164Q, K167Q, and K168Q mutations. Although R176E mutation per se in mouse arrestin-1 significantly increases the binding to Rh*, it was not introduced because previously we

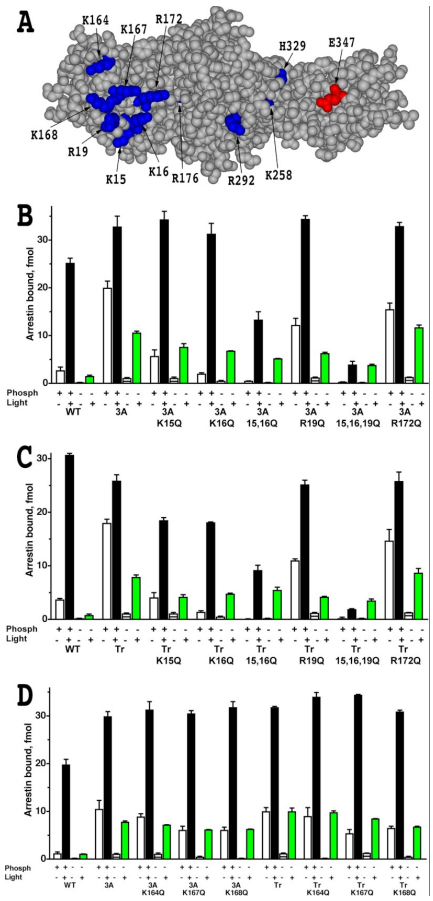


**Figure 1. Elimination of phosphate-binding residues does not improve the binding of phosphorylation-independent arrestin-1 mutants to Rh*.** A, the structural model of mouse arrestin-1 (based on bovine arrestin-1 crystal structure PDB 1CF1) shows surface residues mutated in this study (*blue*, positive charges; *red*, negative charge). B–D, shown is the binding of WT mouse arrestin-1 and indicated N-domain (residues 1–177) mutants, where positively charged phosphate binding residues were replaced with glutamine, constructed on the background of either arrestin-1-(L374A/V375A/F376A) (*3A*) or truncated arrestin-1-(1–377) (*Tr*) to four functional forms of rhodopsin. The colors of the bars are: *white*, dark P-Rh; *black*, P-Rh*; *horizontally striped*, *dark Rh*; *green*, Rh*. The means ± S.D. of two experiments, each performed in duplicate, are shown. Note that R172Q is the only mutation that marginally increases Rh* binding of parental L374A/V375A/F376A and truncated arrestin-1-(1–377) mutants.

found that it greatly reduces protein stability. Neutralizing mutations were introduced, singly or in groups, in the context of the two arrestin-1 mutants that were successfully expressed in transgenic mice, arrestin-1-3A and arrestin-1-(1–377). As expected, on both backgrounds, mutations eliminating phosphate binding charges significantly reduced arrestin-1 ability to interact with dark P-Rh (Figure 1). Combinations K15Q/K16Q and K15Q/K16Q/R19Q also reduced the binding to P-Rh*, but only R172Q mutation marginally enhanced Rh* binding (Figure 1 B, C, and D). These data suggest that the presence of phosphate binding-positive charges is not the main factor destabilizing the complex of enhanced arrestin-1 with Rh*.

**Selected mutations on arrestin-1 surface engaged by other parts of the receptor increase Rh* binding but reduce thermal stability**

Several mutations on the receptor binding surface of the C-domain, such as K257E and E346K, were previously shown to increase bovine arrestin-1 binding to Rh* in the context of WT protein. Therefore, we introduced homologous mutations K258E and E347K in mouse arrestin-1 (Figure 2A). These substitutions proved to act additively with the 3A mutation and the deletion of the C-tail, enhancing arrestin-1 binding to P-Rh* (Figure 2A), and especially to Rh* well beyond the level achieved by the 3A mutation or C-terminal deletion alone. Because the effects of all mutations tested were essentially the same on the background of arrestin-1-3A and arrestin-1-(1–377) (Figures 1 B, C, and D, and 2A), we focused on arrestin-1-3A, which showed higher expression levels in transgenic mice. On arrestin-1-3A background the addition of R172Q mutation to K258E, E347K, or K258E/E347K combination further increased Rh* binding without appreciably affecting the interaction with P-Rh* (Figure 2B). The best combination

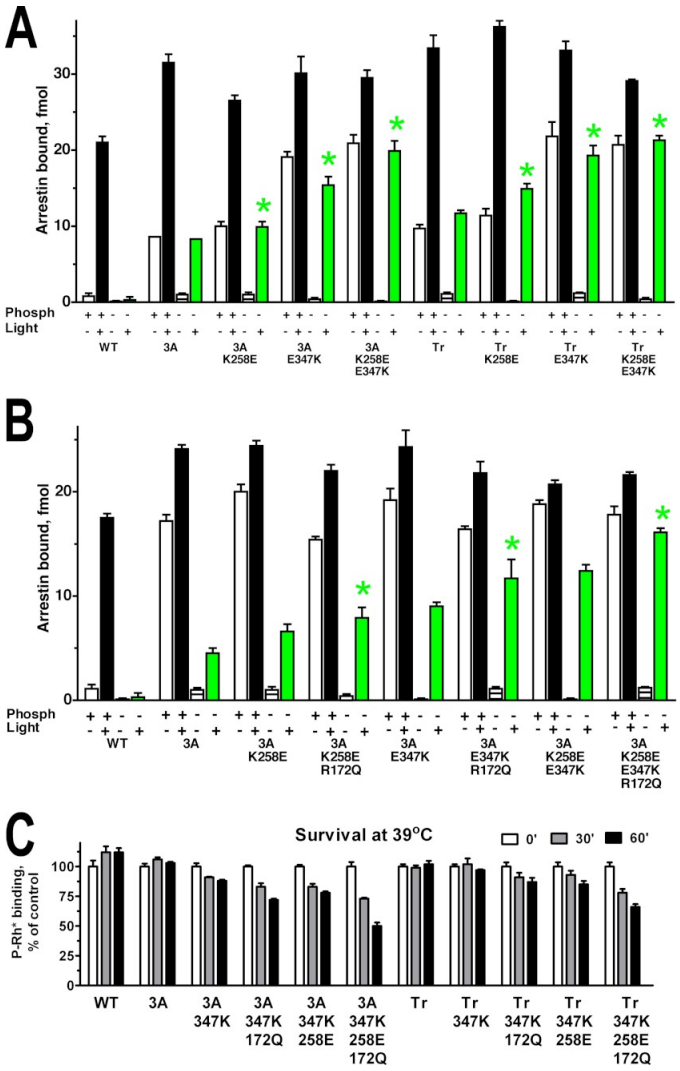


**Figure 2. Reengineering of the rhodopsin binding surface of the C-domain improves Rh* binding of phosphorylation-independent arrestin-1 base mutants but reduces protein stability.** A and B, shown is binding of WT mouse arrestin-1 and the indicated C-domain (residues 190–360) mutants constructed on the background of either arrestin-1-(L374A,V375A,F376A) (*3A*) or truncated arrestin-1-(1–377) (*Tr*) to four functional forms of rhodopsin. The colors of the bars are: *white*, dark P-Rh; *black*, P-Rh*; *horizontally striped*, *dark Rh*; *green*, Rh*. Statistical significance of the differences in Rh* binding ($p < 0.05$), as compared with parental L374A/V375A/F376A or truncated arrestin-1-(1–377) mutant, is indicated by *green star*. C, to determine protein stability, indicated translated arrestins were incubated for 30 or 60 min at 39 °C, and their specific binding to P-Rh* was compared with that of controls kept on ice (0 min). The means ± S.D. of two-three experiments, each performed in duplicate, are shown in all panels.

(3A+K258E/E347K/R172Q) yielded the level of Rh* binding virtually indistinguishable from that of WT arrestin-1 to P-Rh* (Figure 2B).

Because many activating mutations reduce arrestin-1 stability and only sufficiently stable proteins can be successfully expressed in vivo at physiologically relevant levels, next we tested the stability of these mutants (Figure 2C). To this end, radiolabeled WT mouse arrestin-1 and mutants produced in cell-free translation were incubated at elevated temperature for varying periods of time, and then their ability to specifically bind P-Rh* was compared with that of the control samples kept on ice. WT arrestin-1 as well as the 3A and truncated (1–377) mutants did not lose any activity after 60 min of incubation at 39 °C (Figure 2C). Mutations E347K, K258E, and their combination somewhat reduced arrestin-1 stability on both backgrounds, and the addition of R172Q to any mutation or combination further reduced arrestin-1 stability (Figure 2cC. Thus, the most potent ligands of Rh* in this series are less stable than the 3A mutant successfully used in vivo.

**Neutralization of surface charges is less detrimental for stability than charge reversal**

Surface residues in soluble proteins often stabilize the structure via intramolecular interactions with neighboring side chains. Therefore, we analyzed the available crystal structure of highly homologous bovine arrestin-1 and then ascertained that the residues of interest are conserved in the mouse protein (Figure 3A shows mouse residue numbers). R172Q reduced the stability of all arrestin-1 mutants tested (Figure 2). Arg-172 appears to form a salt bridge with Glu-149, which in turn contacts Lys-151. The R172Q mutation is likely to weaken or destroy the interaction of this residue with Glu-149, which would in this case become fully engaged by Lys-151. We reasoned that replacing Lys-151 with aspartic acid would likely prevent that, making the interaction via H-bond between Glu-

149 and Gln-172 more likely. Importantly, the homologous K150E mutation in bovine arrestin-1 did not significantly affect the binding to P-Rh* or other forms of rhodopsin. Another reason the R172Q mutation could reduce the stability is inappropriate H-bonding of Gln with some of the neighboring residues. We reasoned that replacing Arg-172 with an alanine should solve this problem. The K258E and E347K mutations also appear to be detrimental for arrestin-1 stability (Figure 2). Judging by bovine arrestin-1 structure, Lys-258 forms a salt bridge with Asp-139 (Figure 3A), which would be destroyed by K258E mutation introducing a negative charge that repulses Asp-139. The replacement of Lys-258 with a neutral glutamine would prevent the repulsion and likely create an opportunity for H-bonding to preserve the stabilizing effect of the salt bridge in the WT protein. Glu-347 forms a salt bridge with Lys-333 and H-bond with Thr-335 (Figure 3A). Lys-347, introduced by E347K mutation, would repulse Lys-333; in addition, its longer side chain allows the end amino group to reach all the way to Ser-345. The modeling shows that replacement of Glu-347 with glutamine, which has exactly the same geometry and no charge, would prevent both repulsion of Lys-333 and unnatural H-bonding to Ser-345. The replacement of Glu-347 with histidine, which has only a partial positive charge at neutral pH and shorter side chain, would moderate the repulsion of Lys-333 and also prevent H-bonding with Ser-345.

To test these predictions, on the arrestin-1-3A background we added K151D mutation to the R172Q/E347K and R172Q/K258E combinations, made the R172A/E347K combination to compare with R172Q/E347K, and generated three “milder” versions of the K258E/E347K combination: K258E/E347Q, K258E/E347H, and K258Q (Figure 3B). Because two additional mutations, R291E and Q328K, increased the binding of bovine

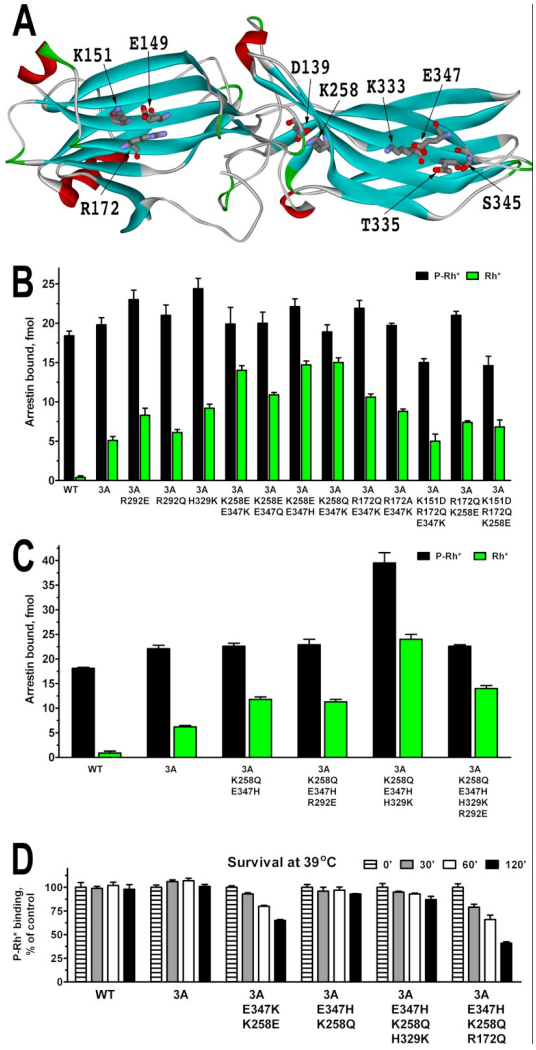


**Figure 3 Design of stable arrestin-1 mutants with high Rh* binding.** A, a structural model of mouse arrestin-1 (based on bovine arrestin-1 crystal structure 1CF1) show the residues mutated in this series. B and C, shown is binding of WT mouse arrestin-1 and the indicated mutants constructed on the background of arrestin-1-(L374A,V375A,F376A) (3A) to P-Rh* (black bars) and Rh* (green bars). D, indicated translated arrestins were incubated for 30, 60, or 120 min at 39 °C, and their specific binding to P-Rh* was compared with that of controls kept on ice (0 min). Note that charge neutralization mutations preserve the stability much better than charge reversals. The means ± S.D. of two experiments each performed in duplicate are shown in all panels.

arrestin-1 to Rh*, we constructed homologous mutants of mouse arrestin-1: R292E, its less drastic version R292Q, and H329K (note that in WT mouse protein bovine Gln-328 is replaced with His-329). The data show that the H329K and R292E mutations increase Rh* binding, whereas the R292Q does not; the R172A mutation is less effective than the R172Q; the K151D mutation decreases Rh* binding of any combination it is added to; the combinations K258Q/E347K and K258E/E347H work as well as the original K258E/E347K (Figure 3B). Based on these data, we generated several combinations of the most effective mutations and constructed the K258Q/E347H, K258Q/E347H/R292E, K258Q/E347H /H329K, and K258Q/E347H/R292E/H329K combination mutants on the arrestin-1-3A background (Figure 3C). We found that R292E does not act additively with the K258Q/E347H combination, whereas in the context of the K258Q/E347H/H329K mutant it actually reduces Rh* binding (Figure 3C). Interestingly, the H329K mutation significantly increased the binding of the K258Q/E347H mutant to both P-Rh* and Rh*. Moreover, the absolute level of the K258Q/E347H/H329K mutant binding to Rh* is even higher than achieved with P-Rh* by WT arrestin-1, making it by far the most potent Rh* ligand constructed (Figure 3C).

Next, we tested the stability of the combination mutants yielding high Rh* binding, extending the incubation time to 2 h to make the test more rigorous (Figure 3D). The results showed that the R172Q mutation reduces the stability of the K258E/E347H combination to the same extent as that of K258E/E347K (compare Figure 2C and 3D). We also confirmed that the K258E/E347K combination is significantly less stable than parental arrestin-1-3A and found that both the K258Q/E347H and K258Q/E347H/H329K mutants essentially retain the stability of arrestin-1-3A. Considering that the arrestin-1-

3A was successfully expressed in transgenic mice at fairly high levels, these data suggest that both the K258Q/E347H and K258Q/E347H/H329K mutants might be stable enough for in vivo expression.

**Mutant stability in cells follows the same pattern as in the in vitro assay**

To closer mimic the intracellular environment that these proteins will be facing in rod photoreceptors, we expressed several arrestins in HEK293 cells. We chose the K258Q/E347H+3A mutant, the K258Q/E347H/H329K+3A mutant, with stable WT arrestin-1 and the arrestin-1-3A mutant as positive controls as well as the much less stable K258E/E347H/R172Q+3A mutant for comparison. Three hours before lysis one plate with cells expressing each mutant was kept at 37 °C (control), whereas a second plate was incubated at 40 °C. The cells were lysed and centrifuged to remove debris and aggregated proteins. To measure possible loss due to aggregation during the 3-h incubation at 40 °C, 2 μg of total protein from each cell lysate was analyzed by Western blot with rabbit polyclonal anti-arrestin antibodies. We found a slight reduction of soluble arrestin-1 level in the lysates of cells incubated at 40 °C, which in no case exceeded that observed for WT protein (Figure 4A). Next, we tested the ability of these proteins to bind P-Rh* in our standard extensively characterized direct binding assay using lysates of cells expressing various mutants (Figure 4B). Arrestin-containing lysates were incubated for 5 min at 37 °C with or without 1 μg of P-Rh in room light, and rhodopsin-containing membranes were pelleted by centrifugation. We compared the total amount of arrestin-1 added (input (I)) with that bound to P-Rh* [140] or non-specifically aggregated (ns) in samples containing no rhodopsin. In all cases at least half of the arrestin added bound P-Rh*, and very little was pelleted in the absence of rhodopsin (Figure 4B). All mutants

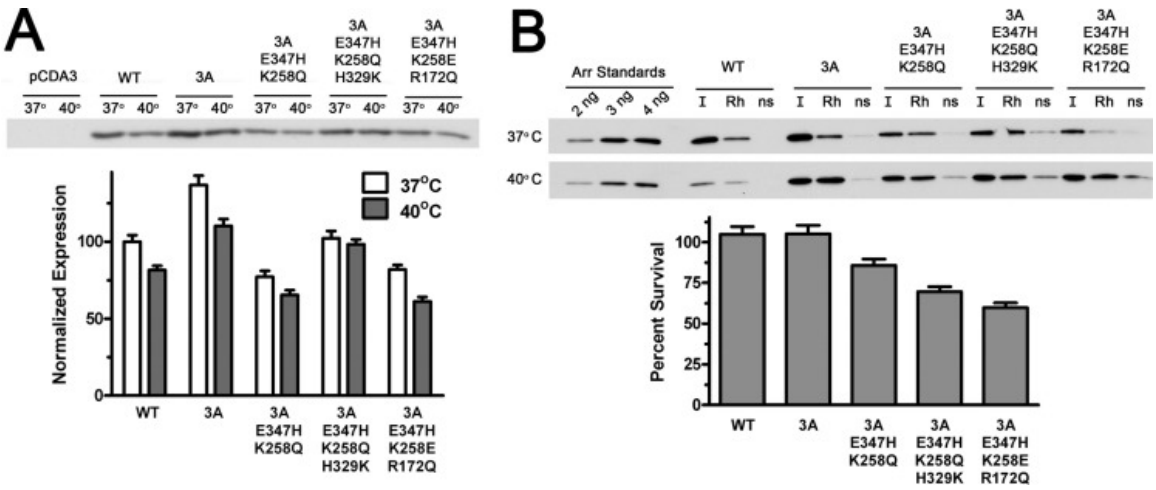


**Figure 4. Several mutants with the highest Rh* binding are stable in cellular environment.** A, indicated forms of mouse arrestin-1 were expressed in HEK293 cells. For the last 3 h before lysis the cells were kept either at regular (37 °C) or elevated (40 °C) temperature. The levels of soluble arrestin-1 in lysates were determined by Western blot (*upper panel*) and expressed as percent of the level of WT arrestin-1 in cells kept at 37 °C (*lower bar graph*). B, functional activity of soluble arrestin-1 in lysates is shown. Equal volumes of lysates (10 μl) were incubated with or without (*ns*) 1 μg of P-Rh*, and bound arrestin-1 was separated from free by centrifugation as described under "Experimental Procedures." One-tenth of each pellet and input (*I*) was analyzed by Western blot (*upper panel*). Protein survival was calculated as the ratio of the fraction of arrestin-1 in lysate of cells incubated at 40 °C that specifically bound to P-Rh* to the bound fraction in lysates of control cells kept at 37 °C. Nonspecific binding (the amount of arrestin-1 pelleted in the absence of rhodopsin, likely due to aggregation) was subtracted from specific binding to P-Rh*. The means ± S.D. of two independent experiments, each quantified in two blots, are shown in both panels.

performed similarly to WT, with the exception of the K258E/E347H/R172Q+3A mutant, which demonstrated increased nonspecific aggregation and lower specific binding, in agreement with its reduced stability in the in vitro survival test (Figure 3D). The ratio of specifically bound fraction of each arrestin from cells incubated at 40 and 37 °C was used to estimate protein survival (Figure 4B). This parameter was found to be ~100% for WT arrestin-1 and 3A mutant, >80% for the K258Q/E347H+3A mutant, and lower for the other two mutants (Figure 4B). These results match in vitro survival test (Figure 3D) remarkably well. Both tests suggest that the K258Q/E347H+3A mutant, with significantly higher Rh* binding than 3a (Figure 3C), demonstrates stability comparable to the 3A mutant (Figures 3D and 4B).

**Elimination of arrestin-1 self-association is compatible with enhanced Rh* binding**

Arrestin-1 that retains normal ability to bind P-Rh* but does not self-associate is necessary to test the biological role of its oligomerization in photoreceptors. Therefore, we performed both cell-based and in vitro stability tests with the two previously designed constitutively monomeric mouse arrestin-1 mutants, F86A/F198A and F86A/F198A/A349V. We found that these mutants express at least as well as WT arrestin-1 in HEK293 cells, and both survive 3 h of incubation of cells at 40 °C at least as well as WT (Figure 5A). The fraction of the two mutants in cell lysates that specifically bound P-Rh* was similar to that of WT arrestin-1 (Figure 5B). Both constitutively monomeric mutants showed essentially the same ~100% survival, estimated as the ratio of specifically bound fraction of WT and mutant arrestin-1 from cells incubated at 40 and 37 °C (Figure 5B). In full agreement with these data, the in vitro testing at 39 °C of both constitutive monomers demonstrated even higher stability than 3A mutant (Figure 5C).

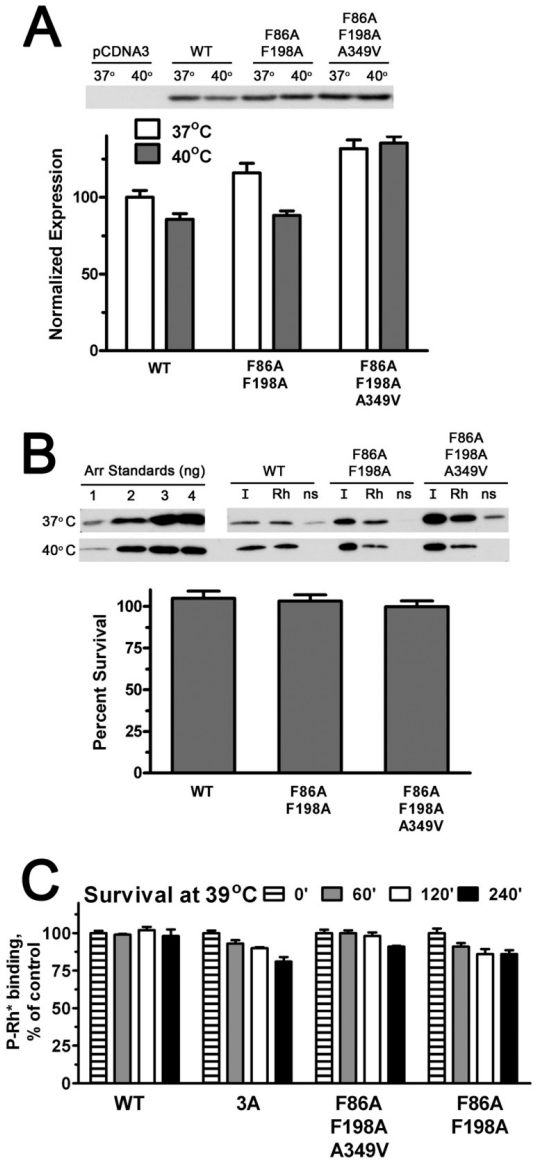


**Figure 5. High stability of constitutively monomeric forms of arrestin-1.** A, indicated forms of mouse arrestin-1 were expressed in HEK293 cells. For the last 3 h before lysis the cells were kept either at regular (37 °C) or elevated (40 °C) temperatures. The levels of soluble arrestin-1 in lysates were determined by Western blot (*upper panel*) and expressed as percent of the level of WT arrestin-1 in cells kept at 37 °C (*lower bar graph*). B, Protein survival was calculated as the ratio of the fraction of arrestin-1 in the lysate of cells incubated at 40 °C that specifically bound to P-Rh* to the bound fraction in lysates of control cells kept at 37 °C. Quantification in *panels A* and *B* represents the means of two independent experiments, each quantified in two blots. *ns*, without P-Rh*. C, the indicated translated arrestins were incubated for 60, 120, or 240 min at 39 °C, and their specific binding to P-Rh* was compared with that of controls kept on ice (0 min). The means ± S.D. of two independent experiments are shown.

Thus, in contrast to activating mutations, substitutions disabling self-association of arrestin-1 do not appear to adversely affect protein stability (Figures 3–5).

Mutations preventing oligomerization of arrestin-1 introduced on WT background were shown not to affect the binding to rhodopsin and microtubules. On the basis of the multifunctionality of arrestin proteins and demonstrated feasibility of changing individual functions without affecting others, it was suggested that combinatorial mutagenesis can generate arrestins with essentially any desired set of functional characteristics. To test this idea, we combined the double mutation F86A/F198A that renders arrestin-1 constitutively monomeric with several mutations enhancing binding to Rh*, including 3A, K258Q/E347H+3A and K258Q/E347H/H329K+3A, and compared these proteins with parental mutants where only a single function was changed (Figure 6). We found that although the addition of F86A/F198A to enhancing mutations does not appreciably affect P-Rh* interaction, the binding to Rh* of constitutively monomeric-enhanced arrestins was somewhat reduced compared with the parental forms where the same activating mutations were introduced on WT background (Figure 6A). However, arrestin-1 carrying combinations of K258Q/E347H+3A and K258Q/E347H/H329K+3A with F86A/F198A largely retained its high binding to unphosphorylated Rh* (Figure 6A). Finally, to determine the suitability of these mutants for in vivo testing, we performed harsher in vitro stability test, measuring the survival of these proteins at 42 °C (Figure 6B). At this temperature even WT arrestin-1 shows some inactivation, whereas the arrestin-1-3A mutant, which was successfully expressed in rods of transgenic mice, lost ~50% of activity by 4 h (Figure 6B). These conditions also revealed the difference between the two constitutive monomers: F86A/F198A is almost as stable as WT, whereas

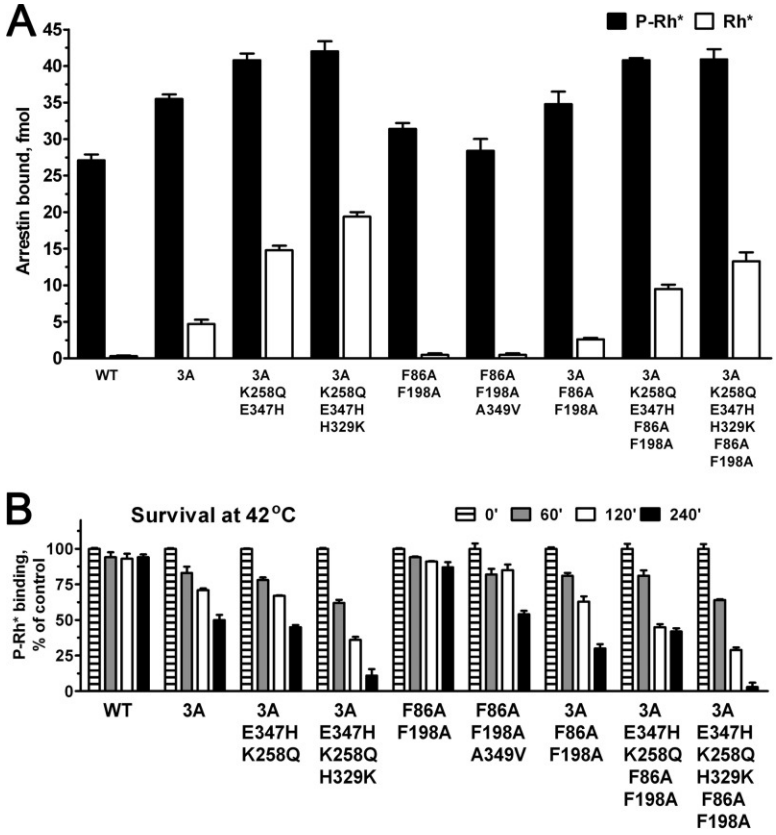


**Figure 6. Enhanced binding to Rh* can be achieved with and without ability to self-associate.** A, the binding of WT mouse arrestin-1 and the indicated mutants to P-Rh* (*black bars*) and Rh* (*white bars*) are shown. B, to rigorously compare protein stability, indicated translated arrestins were incubated for 60, 120, or 240 min at 42 °C, and their specific binding to P-Rh* was compared with that of controls kept on ice (0 min). The means ± S.D. of two independent experiments performed in duplicate are shown in *both panels*.

F86A/F198A/A349V demonstrated ~50% survival, similar to 3A (Figure 6B). The F86A/F198A double mutation somewhat reduced the stability of the less robust K258Q/E347H/H329K+3A, and it did not significantly affect the survival of K258Q/E347H+3A (Figure 6B). This test revealed that the stability of K258Q/E347H+3A on both WT and constitutively monomeric background is comparable to that of 3A mutant. Thus, both forms of enhanced K258Q/E347H+3A as well as constitutively monomeric mutants are suitable candidates for in vivo expression.

Because the effect of the F86A/F198A double mutation on arrestin-1 self-association was only tested on the WT background, we determined the ability to oligomerize of the enhanced K258Q/E347H+3A mutant and the combination of K258Q/E347H+3A with F86A/F198A. To this end both proteins were expressed in E. coli and purified, and their self-association was quantitatively tested by multiangle light scattering. We found that the K258Q/E347H+3A mutant retained the ability to form dimers and tetramers (Figure 7). However, its self-association was reduced relative to WT mouse arrestin-1. Although the data were readily fitted to the MDT model, log $K_{dim}$ and log $K_{tet}$ were 3.35 ± 0.05 and 3.85 ± 0.28, which translates into $K_{D,dim}$ and $K_{D,tet}$ of 447 ± 7 and 141 ± 10 μM, respectively. Similar to what we previously found for mouse arrestin-1-F86A/F198A, the data for the K258Q/E347H/H329K+3A + F86A/F198A combination mutant (Figure 7) could not be fitted by the MDT model but were fitted by a simpler monomer-dimer model, with log $K_{dim}$ = 2.43 + 0.16, which corresponds to $K_{D,dim}$ = 3,715 ± 245 μM. Thus, on both WT and the K258Q/E347H+3A background (Figure 7), the F86A/F198A double mutation reduced dimerization about 10-fold and totally eliminated tetramerization.

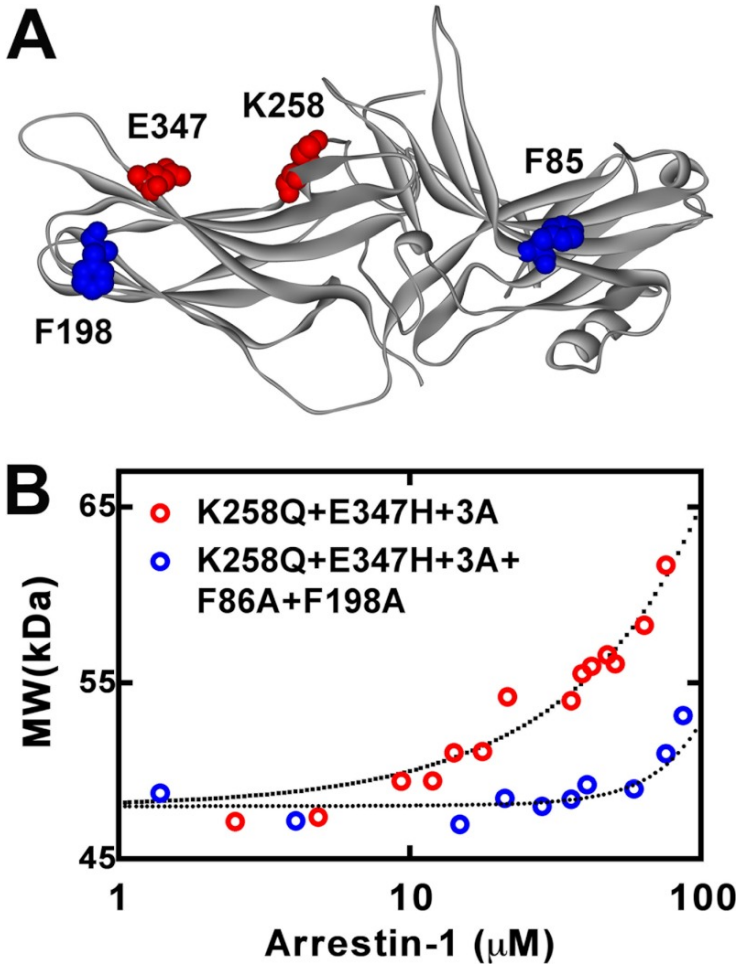


**Figure 7. Self-association of engineered mouse arrestin-1 mutants.** A, the structural model of mouse arrestin-1 (based on bovine arrestin-1 crystal structure 1CF1) shows two residues mutated to enhance Rh* binding (Lys-258 and Glu-347) in *red* and two phenylalanines (Phe-86 and Phe-198) mutated to alanines to block self-association in *blue*. B, the average molecular weight of the K258Q/E347H+3A (*red circles*) and K258Q/E347H+3A+F86A/F198A (*blue circles*) mouse arrestin-1 mutants as a function of total arrestin-1 concentration was determined from the light scattering data (*symbols*). Note that K258Q/E347H+3A+F86A/F198A mutant showed no detectable tetramerization, so that the resulting fit describes monomer-dimer equilibrium.

The data (Figures 6 and 7) show that self-association and binding to unphosphorylated Rh* are not completely independent of each other, which could be expected as the mutations necessary to change both functions localize to the concave sides of the two arrestin-1 domains (Figure 7A). Nonetheless, targeted reengineering of mouse arrestin-1 yielded new forms where two of its functional characteristics, the level of Rh* binding, and the ability to self-associate, were differentially affected, generating expected combinations.

# CHAPTER 6

## ARRESTIN-3 INTERACTION WITH DOWNSTREAM MAPK CASCADE

Much of this chapter is accepted for publication at *Scientific Reports* [ref]. Xuanzhi Zhan, Henriette Stoy, Tamer S. Kaoud, Nicole A. Perry, Alejandro Perez, Sylvia Els-Heindl, Jack V. Slagis, TM Iverson, Annette G. Beck-Sickinger, Eugenia V. Gurevich, Kevin N. Dalby, Vsevolod V. Gurevich contributed to the work.

## Introduction

The spatial and temporal organization of proteins within a cell is critical for coordinating essential activities [142]. Appropriate cellular response to external or internal stimuli often requires precise orchestration by scaffold proteins, which determine the specificity and precise time course of signaling. In particular, the specificity of signal transduction through mitogen activated protein kinase (MAPK) cascades is highly dependent on scaffold proteins [143-145]. MAPK signaling is involved in the regulation of key cellular behaviors, from proliferation to differentiation and apoptotic death [145]. The overall architecture of three-kinase MAPK cascades is conserved from yeast to mammals. Most cells have multiple MAPKs, MAPK kinases (MAPKKs), and MAPKK kinases (MAPKKKs), so signaling outcome is often determined by scaffolds organizing particular MAPKKK-MAPKK-MAPK complexes [143-146].

The c-Jun NH2-terminal protein kinases (JNKs) belong to the MAPK family. JNKs regulate normal physiological processes of cell proliferation, apoptosis, differentiation, and migration [147]. JNKs were also implicated in many diseases, from cancer to neurological and immunological disorders [148-150]. Full activation of all JNKs requires double phosphorylation of the T-X-Y motif in the activation loop by two upstream kinases, MKK4 (tyrosine) and MKK7 (threonine) [151]. Similar to other MAPKs, JNK

activation is dependent on scaffolding proteins, such as JIPs [152]. Arrestins, which specifically bind active phosphorylated G protein-coupled receptors (GPCRs), were first discovered as negative regulators of GPCR signaling via G proteins [40, 41]. Among the four arrestin subtypes expressed in vertebrates [126], only arrestin-3 promotes the activation of JNK3 [53], as well as ubiquitous JNK1/2 in cells [54], acting as a scaffold that brings together MAPKKK ASK1, MAPKKs MKK4 and MKK7, and several isoforms of JNK1/2/3 [50, 53-58]. Recently we identified the first 25 residues of arrestin-3 as the key JNK3 binding site [153]. Here we demonstrate that this short arrestin-3-derived peptide also binds ASK1 and MKK4/7 and facilitates JNK3 activation in intact cells. This is the smallest JNK cascade scaffold discovered so far. Its size paves the way to designing small molecule mimics that can be used as tools for targeted manipulation of anti-proliferative and often pro-apoptotic JNK signaling in cells.

## Methods

### MBP-fusion protein constructs in pMa and MBP pull-down

To make MBP-fusions containing arrestin-2/3 elements, the cDNAs encoding arrestin fragments were subcloned into pMal-p2T (generous gift from Dr. Keiji Tanaka, Tokyo Institute of Medical Science) between Eco RI and Xho I sites in frame with MBP, as described [153]. MBP-Arr3 (full-length arrestin-3) was created by subcloning the corresponding cDNA into pMal-p2T between Eco RI and Not I sites 23. All MBP-arrestin-3 fusion proteins contained the same TLVPRGSPGF linker between MBP and arrestin-3 or its fragments. The MBP protein used as negative control was purified using empty pMal-p2T vector containing the same linker with 10 additional residues: PGRLERPHRD. MBP fusions were purified, as described [153]. MBP pull-down was

performed, as described [153]. Briefly, Indicated MBP fusions (10-30 μg in 50 μL 20 mM Tris/150 mM NaCl) were immobilized on amylose resin (25 μL, 50% slurry, New England Biolabs) for 1 h at 4°C with slight rotation. Purified, as described [154], MKK4/7 (10 μg in 50 μL 20 mM Tris/150 mM NaCl) were added to the immobilized MBP fusions and rotated gently for 2 h at 4°C. Samples were transferred to centrifuge filters (Durapore®-PVDF-0.65μm), washed three times with 50 mM HEPES-Na, pH 7.3, 150 mM NaCl. The proteins were eluted by 100 μl of elution buffer (wash buffer containing 50 mM maltose) by gentle rotation for 5 min at 4°C. Eluates were analyzed by SDS-PAGE and Western blotting.

**Kinase purification and in vitro phosphorylation assay**

JNK3a2 and MKK4 and MKK7 were expressed in E. coli and purified as previously described [154]. The effect of arrestin-3 and MBP-T1A on the phosphorylation of JNK3α2 by MKK7 or MKK4 was analyzed by an in vitro kinase assay, as described [50, 58]. Briefly, the assays were conducted in 10 μL containing the following final concentrations: 50 nM active MKK7 or MKK4, 1μM JNK3α2, and indicated concentrations of arrestin-3 or T1A. The mixtures were incubated individually at 30°C for 10 sec. The reactions were stopped by the addition of 15 μL of Laemmli SDS sample buffer (Sigma) and 2 μl of total reaction sample was subjected to SDS-PAGE (8%) and transferred polyvinylidene difluoride (PVDF) membranes (Millipore, Bedford, MA). Phosphorylated JNK3α2 was visualized by rabbit anti-phospho JNK antibody (Cell Signaling) and the level of JNK phosphorylation was quantified.

**Peptide synthesis**

The T1A peptide (MGEKPGTRVFKKSSPNCKLTVYLGK), representing the first 25

residues of arrestin-3, was synthesized using automated synthesis robot (SyroI, MultiSyntech, Witten, Germany) on NovaSyn® TGR R resin (13.5 µmol, Novabiochem, Darmstadt, Germany) with a fluorenylmethyloxycarbonyl chloride (FMOC)/tert-butyl strategy, as described [155]. FMOC-amino acids were from Iris Biotech and Novabiochem (Marktredwitz, Germany). Amino acid side chain protecting groups were used as following: trityl (Trt) for Asn and Cys; tBu for Glu, Thr, Ser and Tyr; tert-butyloxycarbonyl [4] for Lys; and pentamethyl-2,3-dihydrobenzofuran-5-sufonyl (Pbf) for Arg. Automated FMOC deprotection was carried out with 40% (v/v) piperidine (Sigma-Aldrich, Taufkirchen, Germany) in N,N-dimethylformamide (DMF; Biosolve, Valkenswaard, The Netherlands) for 3 min and 20% (v/v) piperidine in DMF for 10 min. The coupling of the amino acids was carried out twice. FMOC-amino acids were pre-incubated with OxymaPure (Iris Biotech) for 2 min. Following the addition of N,N'-diisopropylcarbodiimide (DIC; Iris Biotech), reaction was incubated for 40 min. After successful synthesis, peptides were cleaved from the resin with 90% trifluoroacetic acid (TFA) and 10% 1,2-ethanedithiol/thioanisole (v/v 3:7). Methionines were reduced with 1,2-ethanedithiol and trimethylsilyl bromide in TFA. Subsequently, peptides were purified on a reversed-phase C18 column (Phenomenex Jupiter 10u Proteo 90 Å: 250 × 21.2 mm; 7.8 µm; 90 Å) and analyzed by MALDI-TOF mass spectrometry (UltraflexII, Bruker, Bremen, Germany) and analytical reversed-phase HPLC on columns Phenomenex Kinetex 5u XB-C18 100 Å (Phenomenex: 250 × 4.6 mm; 5 µm; 100 Å) and Phenomenex Jupiter 4u Proteo 90 Å (Phenomenex: 250 × 4.6 mm; 4 µm; 90 Å). Eluent A was 0.1% TFA in H2O and eluent B 0.08% TFA in ACN. On both columns, a gradient of

10% eluent B in A to 60% eluent B in A in 40 min was used. Following this procedure, the peptide was ⩾ 95% pure.

**Plasmids, cell culture, and transient transfection**

HA-tagged arrestins and their separated domains were constructed, as described [156]. Full-length arrestin-3 and its fragments with N-terminal YFP tag were constructed by subcloning the cDNA encoding YFP-arrestin-3 or YFP-tagged arrestin-3 fragments cDNAs into pcDNA3.1 between Eco RI and Hind III restriction sites.

COS-7 African green monkey cells were maintained in DMEM supplemented with 10% heat-inactivated FBS (Invitrogen), penicillin, and streptomycin at 37 °C in a humidified incubator with 5% CO2. The cells were plated at 80–90% confluence and transfected using Lipofectamine 2000 (Invitrogen) according to the manufacturer's instructions. Cells were used 48 h post-transfection and serum-starved overnight before experiments.

**Western Blotting and measurement of JNK phosphorylation in intact cells**

COS-7 cells were incubated with phosphatase inhibitors (50 mM NaF and 10 mM $Na_3VO_4$) in serum-free medium for 15 min at 37 °C; washed with cold PBS; and lysed with SDS lysis buffer containing 1% SDS, 10mM Tris (pH7.4), 10 mM NaF, 100 μM Na3VO4, 2 mM EDTA, 2 mM benzamidine and 1 mM PMSF. JNKs activity was assayed by Western blotting using an antibody specific for phosphorylated JNK to detect phophorylated (active) JNKs. Whole cell lysates were boiled for 5 min and centrifuged at 10,000 × g for 10 min, and the supernatants were used for Western blotting. Protein was measured using the Bio-Rad Coomassie Blue assay. The proteins were resolved on 8% SDS-PAGE and transferred to PVDF membrane (Millipore, Bedford, MA). Blots were

incubated with the primary antibodies (Cell Signaling Technology, Inc) anti-phospho-JNK, anti-JNK, anti-HA (6E2) (1:1000 to 1:5000), followed by appropriate HRP-conjugated secondary antibodies. Protein bands were detected by enhanced chemiluminescence (ECL, Pierce), followed by exposure to x-ray film. To quantify phopho-JNKs, we used serial dilutions of anisomycin (1μg/ml)-stimulated HEK-A cell lysates to ensure that all samples were in linear range. The values for these proteins are expressed in arbitrary units.

## Results and discussion

### T1A peptide directly interacts with MAPK kinases

We recently found that while three elements in both arrestin-3 domains are involved in JNK3 binding [153], the peptide representing the first 25 residues of arrestin-3 (T1A) is the key interaction site. This opens up three possibilities. First, if T1A only binds JNK3, but not the other kinases in the cascade, it could recruit JNK3 away from functional scaffolds, thereby suppressing JNK3 activation. Second, if T1A binds several kinases in the JNK3 activation module, but does not promote JNK3 phosphorylation, it might act as a dominant-negative silent scaffold, similar to arrestin-3-KNC mutant [133]. Finally, if T1A binds the same kinases as arrestin-3 and facilitates the signaling in the JNK3 cascade, it would be the smallest active MAPK scaffold known, which opens new avenues for the manipulation of MAPK signaling in cells for research and therapeutic purposes.

To determine the functional capabilities of T1A peptide we took advantage of the availability of purified MKK4 and MKK7, both of which activate JNK3 [151] and were shown to bind full-length arrestin-3 [58]. We expressed T1A in E. coli as an MBP-fusion

and purified it on an amylose column. The ability of purified GST-MKK4 or GST-MKK7 (Figure 1A), with GST as negative control, to bind MBP-T1A immobilized on an amylose column was tested in an in vitro pull-down assay, where MBP and MBP-arrestin-3 served as negative and positive controls, respectively (Figure 1B). T1A effectively retained both kinases, but not control GST (Figure 1B). Interestingly, similar to full-length arrestin-3, T1A peptide demonstrated stronger interaction with MKK4 than with MKK7 (Figure 1B, lower panel). Thus, in addition to JNK3, T1A peptide binds both MKKs known to phosphorylate it. Since the pull-down was performed with purified proteins, the data prove that the interactions of T1A with MKK4 and MKK7 are direct and do not involve any intermediaries or helpers. Next, we tested whether T1A binds the uppermost kinase in the cascade, ASK1. Because ASK1 is not available in purified form, we co-expressed HA-tagged ASK1 and YFP-tagged T1A (using YFP as a control) in COS7 cells, lysed the cells, and immunoprecipitated YFP constructs with anti-GFP antibody (Figure 1C). We found that HA-ASK1 was effectively co-immunoprecipitated with YFP-T1A, but not with control YFP (Figure 1C). Thus, in addition to JNK3, T1A peptide binds all upstream kinases of its activation cascade, ASK1, MKK4, and MKK7 (Figure1).

**T1A acts as a scaffold facilitating signaling *in vitro***

Next, we tested whether T1A acts as a scaffold facilitating signaling. To this end, we used experiments with purified proteins, because they provide the most definitive data supporting a direct interaction. As purified ASK1 is not available, we reconstituted MKK4-JNK3 and MKK7-JNK3 modules in the absence and presence of varying concentrations of synthetic purified T1A peptide and measured JNK3 phosphorylation

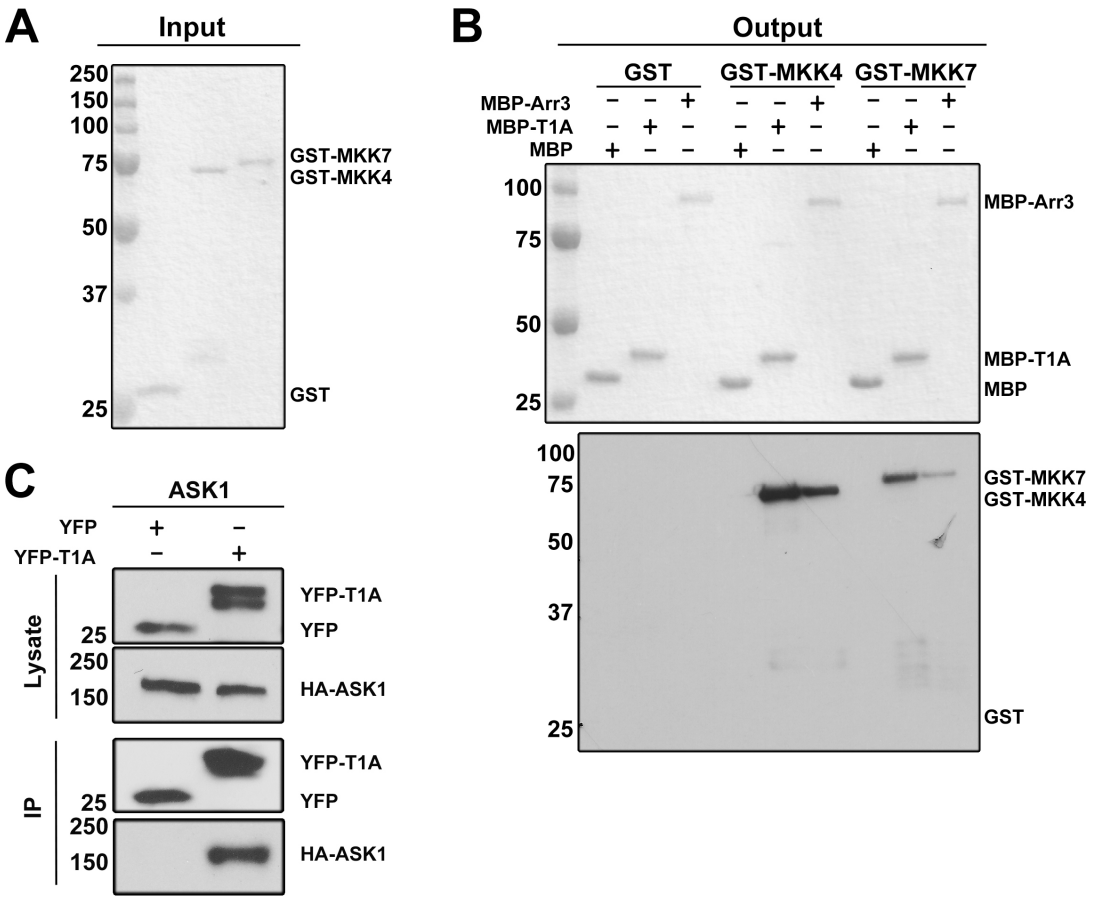


**Figure 1. The T1A peptide binds ASK1, MKK4, and MKK7. A.** Purified GST (control), GST-MKK4, and GST-MKK7 (Coomassie staining) **B.** Top: Coomassie staining of MBP (control), MBP-T1A, and MBP-arrestin-3 bait eluted from amylose beads. Lower blot: GST-MKK4 and GST-MKK7 retained by MBP-T1A and MBP-arrestin-3. Pull-down was performed as described in methods. **C.** HA-ASK1 was co-immunoprecipitated with YFP-T1A, but not the YFP control, from cells coexpressing these proteins (top blots: lysate; bottom blots: proteins immunoprecipitated with anti-GFP antibody).

(Figure 2A). In both cases we obtained bell-shaped curves reflecting JNK3 phosphorylation level as a function of T1A concentration (Figure 2B). This dependence, where signaling is increased at lower scaffold concentrations and decreased at higher, was also found for scaffolding of these modules by full-length arrestin-3 [58]. It is believed to be a characteristic of simple scaffolds, which act by bringing the enzyme and substrate together, as lower scaffold concentrations make the formation of complete scaffold-enzyme-substrate ternary complexes likely, whereas higher concentrations increase the probability of formation of incomplete enzyme-scaffold and substrate-scaffold binary complexes, suppressing the signaling [157, 158]. The optimal concentration of a scaffolding protein for signaling depends on its affinity for the proteins it scaffolds [58, 157, 158].

Our previous work suggested that the efficiency of JNK3 phosphorylation in the complex that includes MKK4 and arrestin-3 is higher than the efficiency of JNK3 phosphorylation by MKK4 in the absence of arrestin-3. Since these experiments were performed with pure components, the data show that simultaneous direct binding to T1A of MKK4/7 (Figure 1A) and their substrate JNK3 places MKKs into a favorable position to phosphorylate JNK3 (Figure 2A,B). Previously we found that the optimal concentrations of arrestin-3 for scaffolding MKK4-JNK3 and MKK7-JNK3 modules are ~0.6 μM and ~ 6 μM [58], reflecting lower affinity of arrestin-3 for MKK7 than for MKK4. Interestingly, the optimal concentration of T1A for promoting JNK3 phosphorylation by MKK4 is lower than for MKK7-JNK3 module (Figure 2B), in line with more avid binding of this peptide to MKK4 (Figure 1B). Intriguingly, in both cases optimal T1A concentrations were ~10-times lower than those of full-length arrestin-3.

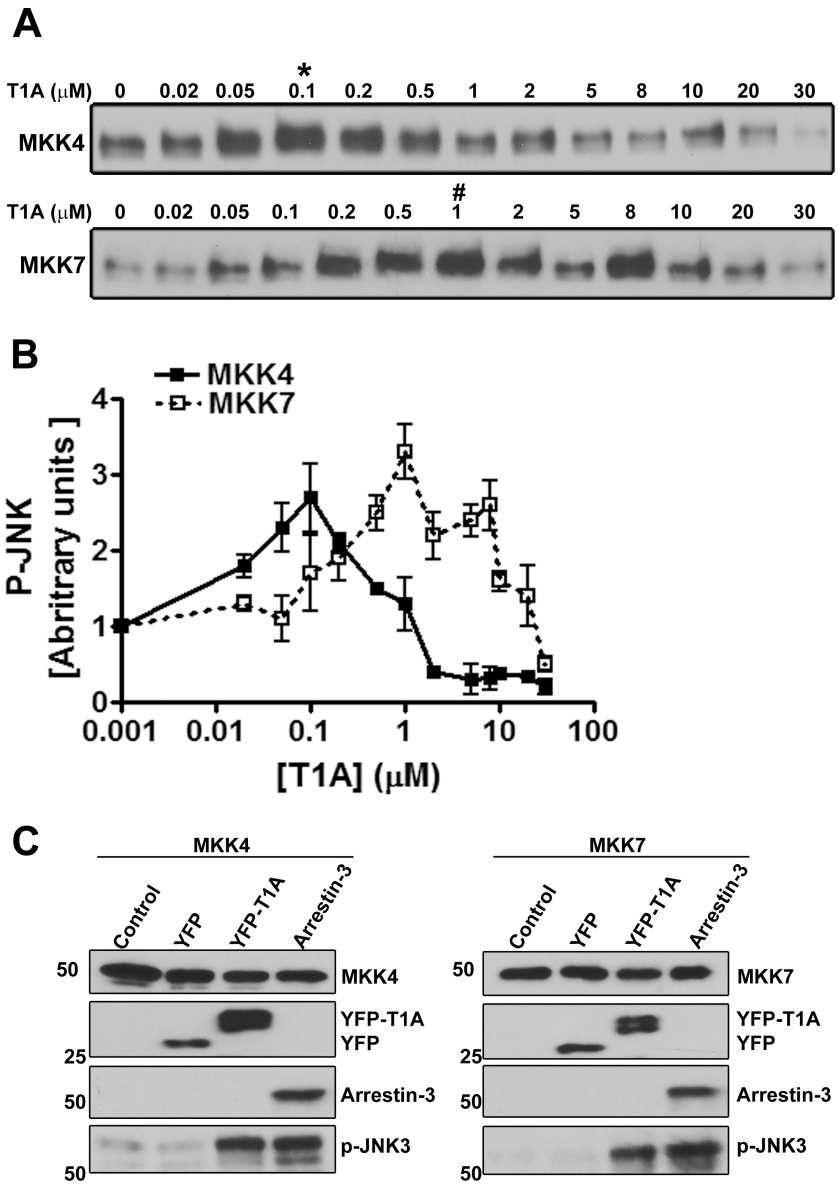


**Figure 2. T1A facilitates JNK3 phosphorylation by MKK4 and MKK7. A** Representative autoradiograms showing JNK3a2 phosphorylated by purified MKK4 (upper panel) and MKK7 (lower panel) at the indicated concentration of synthetic purified T1A peptide (10s incubation). **B** Quantification of JNK3a2 phosphorylation by MKK4 and MKK7. **C** JNK3a2 phosphorylation by MKK4 and MKK7 in HEK293 cells co-expressing JNK3a2 with MKK4 or MKK7 (control) and YFP, YFP-T1A, or arrestin-3.

These results suggest that T1A has higher affinity for MKKs and/or JNK3, in line with its ability to retain more MKKs than arrestin-3 (Figure 1B). This phenomenon might be explained by greater accessibility of T1A peptide when it is free and not in the context of full-length arrestin-3, where it is partially shielded by other elements of the N-domain.

**T1A acts as a scaffold facilitating signaling *in vivo***

To test whether T1A can promote JNK3 phosphorylation by MKKs in cells, we co-expressed MKK4 or MKK7 with YFP-T1A in COS7 cells, using YFP and full-length arrestin-3 as negative and positive controls, respectively (Figure 2C). We found that YFP-T1A, but not YFP, increases JNK3 phosphorylation by both MKKs, similar to arrestin-3. Thus, T1A is necessary and sufficient to promote the signaling in MKK4/7-JNK3 modules both in vitro and in intact cells.

T1A constitutes a small part of the arrestin-3 N-domain [132]. All arrestins consist of two domains, which fold independently, can be expressed separately, and retain certain functions [27, 132, 159]. Therefore, we tested whether separated domains of arrestin-3, as well as the other ubiquitously expressed non-visual subtype, arrestin-2, which also binds kinases of the JNK3 activation cascade [56], can promote JNK3 phosphorylation in cells. To this end, we expressed in COS7 cells both arrestins and their individual domains with the same HA-tag (to compare their expression on the same blot) along with ASK1 and JNK3 (Figure 3). We confirmed that arrestin-3 expression significantly increases JNK3 phosphorylation in cells, whereas arrestin-2 does not, and found no effect of the separated domains of either arrestin (Figure 3).

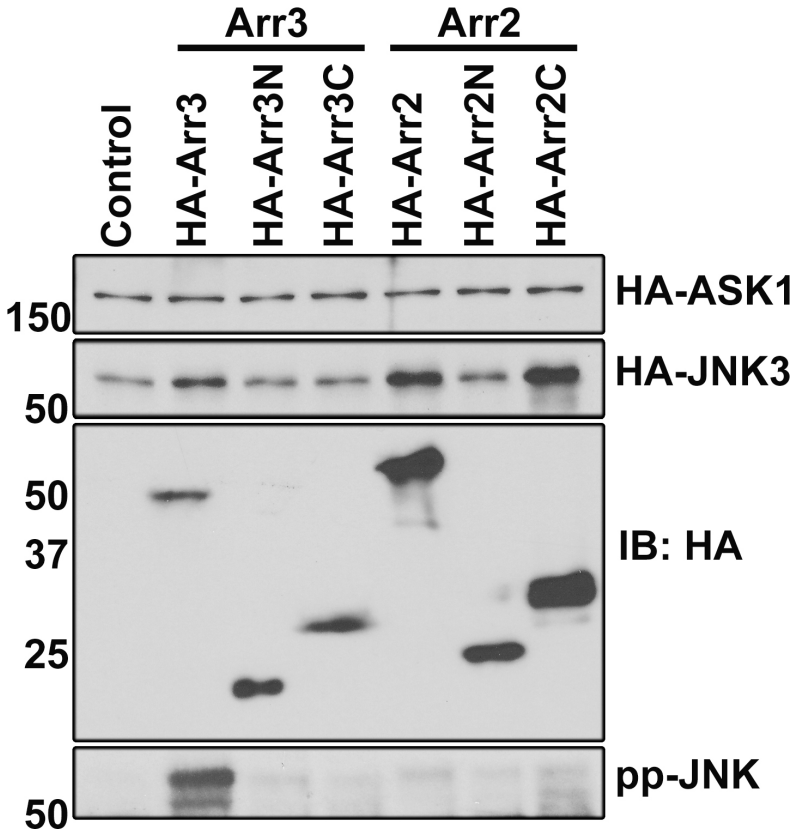


**Figure 3. Separated arrestin domains do not promote JNK activation.** Western blot of lysates of HEK293 cells co-expressing HA-ASK1 and HA-JNK3a2 (Control), or with HA-tagged full-length arrestin-3 (Arr3), arrestin-2 (Arr2), or separated N- and C-domains of the two non-visual arrestins (Arr3N, Arr2N, Arr3C, Arr2C). Phospho-JNK blot shows that among these constructs only full-length arrestin-3 facilitates JNK3a2 phosphorylation in cells.

T1A effectively enhanced JNK3 phosphorylation by MKK4 and MKK7 (Figures. 1,2), whereas full-length arrestin-3 facilitates JNK3 phosphorylation upon co-expression with ASK1 [53, 55, 56, 153], which phosphorylates and activates MKKs. If the arrestin-3 N-domain fails to promote the activation of JNK3 because it can only scaffold MKK4/7-JNK3 modules, then the T1A peptide, which constitutes only a part of the arrestin-3 N-domain [132], would not be expected to promote JNK3 phosphorylation in the presence of ASK1 in cells. To test this, we co-expressed YFP fusions of T1A, two other JNK3-binding peptides T3 and T6 (Figure 4A) [132], with JNK3 and ASK1 in COS7 cells and monitored JNK3 phosphorylation, using YFP and arrestin-3 as negative and positive controls, respectively (Figure 4B). As expected, arrestin-3 increased the level of JNK3 phosphorylation (Figure 4B). T1A, but not other peptides, was also active, and the effect of T1A was greater than that of full-length arrestin-3 (Figure 4B). To test whether T1A still functions as a simple scaffold in intact cells in the presence of over-expressed ASK1, as in case of MKK4/7-JNK3 signaling modules (Figure 2), we co-expressed ASK1 and JNK3 with YFP (control) and varying amounts of YFP-T1A (Figure 4C). The dose-response curve for T1A in these experiments was also biphasic, with a clear optimum, indicating that T1A is a simple scaffold of the three-kinase cascade, similar to full-length arrestin-3 [50].

**T1A mediated MAPK activation is specific**

To test the specificity of T1A action, we compared its ability to bind purified MKK4, MKK7, and JNK3 with that of B1A, a homologous N-terminal peptide from closely related arrestin-2, which differs from T1A only in four positions (Figure 5). We found that while both peptides comparably bind MKK4, B1A demonstrates less robust

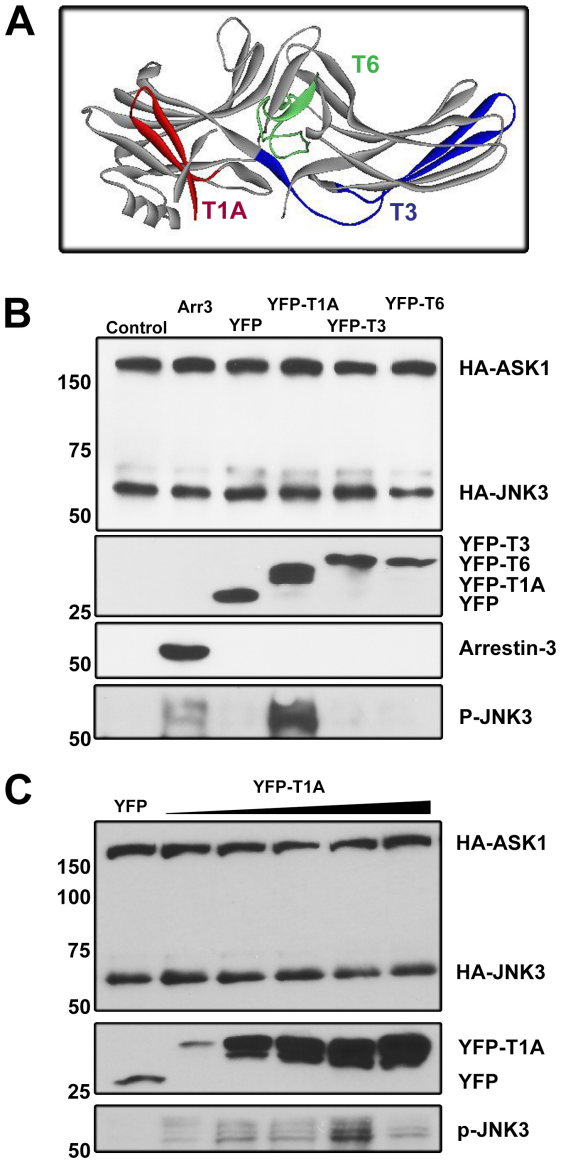


**Figure 4. T1A facilitates JNK3 activation in cells. A** The structure of arrestin-3 (PDB: 3P2D) with the three peptides implicated in JNK3 binding shown in red (T1A), blue (T3), and green (T6). **B** HEK293 cells co-expressed HA-ASK1 and HA-JNK3a2 without (Control) or with full-length arrestin-3 (Arr3), YFP, or indicated YFP-tagged JNK3-binding peptides. The upper three blots show expression levels of indicated proteins; the lower blot shows that T1A facilitates JNK3a2 phosphorylation more efficiently than full-length arrestin-3. **C** HEK293 cells co-expressed HA-ASK1 and HA-JNK3a2 with YFP (Control) or different concentrations of YFP-T1A. The upper two blots show expression levels of indicated proteins; the lower blot shows biphasic dependence of JNK3a2 phosphorylation on T1A level.

interaction with JNK3 and its other upstream activator, MKK7 (Figure 5). To test whether this difference in binding translates into differential activity in cells, we compared the ability of YFP-T1A and YFP-B1A to facilitate JNK3 activation in cells over-expressing ASK1, using YFP-arrestin-3 and YFP as positive and negative controls, respectively. We found that in contrast to T1A, arrestin-2-derived B1A does not functionas a scaffold of ASK1-MKK4/7-JNK3 cascade in cells (Figure 5e), indicating that specific sequence, rather than simple accessibility of this part of arrestins, determines its functional capabilities.

Thus, the first 25 residues contained in the T1A peptide are primarily responsible for the ability of arrestin-3 to scaffold the ASK1-MKK4/7-JNK3 signaling module. The lack of the activity of the arrestin-3 N-domain (Figure 3), which contains the T1A peptide, along with facilitation of JNK3 phosphorylation in exactly the same experimental paradigm by T1A (Figure 4), clearly indicates that when separated, this peptide is a lot more accessible than in the context of arrestin-3 or its N-domain. It is tempting to speculate that receptor binding of arrestin-3 stimulates its ability to promote JNK3 activation [53] by increasing the accessibility of the T1A element to relevant kinases. Significant flexibility of receptor-bound arrestins revealed by biophysical methods supports this idea. While the crystal structure of arrestin-3 in complex with any GPCR is not available, the only existing structure of the arrestin-receptor complex, that of visual arrestin-1 bound to rhodopsin, is consistent with this hypothesis. Arrestin-3 elements that promote signaling leading to the activation of other MAPKs, such as ERK1/2 and p38, also need to be identified. The activation of these two kinases is strictly dependent on arrestin binding to the receptor, suggesting that arrestin elements that

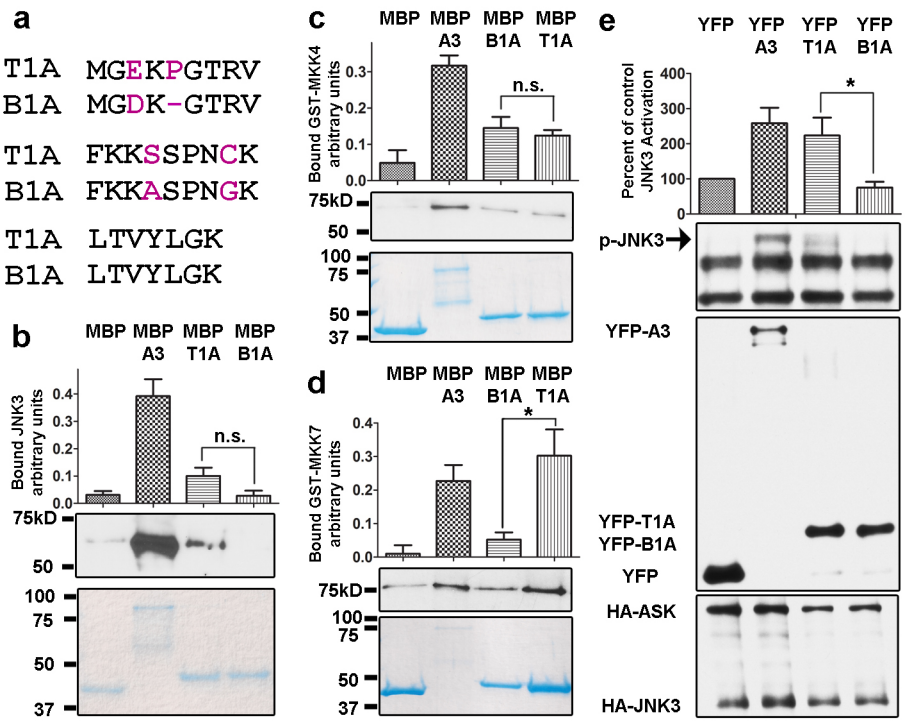


**Figure 5. T1A activity is specific. a** Sequence comparison of arrestin-3-derived T1A and B1A, derived from arestin-2, which does not facilitate JNK3 activation . Residues that differ between T1A and B1A are shown in magenta.**b, c, d** Pull-down of purified JNK3 (**b**), MKK4 (**c**), and MKK7 (**d**) by MBP (negative control), MBP-arrestin-3 (positive control), MBP-T1A, and MBP-B1A, was performed, as described in Methods. Lower panels, Coomassie gels of loaded MBP-fusions; middle panels, Western blots of retained JNK3 (**b**), MKK4 (**c**), and MKK7 (**d**); upper panels, quantification of Western blots from 3-4 independent experiments. Note that B1A binds MKK4 like T1A, but does not appreciably interact with JNK3 or MKK7.**e** HEK293 cells co-expressed HA-ASK1 and HA-JNK3a2 with YFP (negative control), YFP-arrestin-3 (Arr3, positive control), YFP-T1A, or YFP-B1A. Lower two blots show expression levels of indicated proteins; upper blot and bar graph (quanitification of JNK3a2 phosphorylation in four independent experiments) show that T1A facilitates JNK3a2 phosphorylation, whereas B1A does not. *, $p<0.05$; n.s., not significant.

change conformation and/or become more exposed upon GPCR interaction are likely the prime suspects. Our data identify a relatively short arrestin-3-derived peptide as an effective scaffold of the ASK1-MKK4/7-JNK3 signaling cascade, making it the smallest MAPK scaffold ever reported. Its limited size opens the prospect of designing peptides and/or non-peptide small molecule mimics that can be used as tools to manipulate MAPK signaling for research and therapy. Many human disorders are caused by excessive cell proliferation (e.g., cancer) or death (e.g., Alzheimer's, Parkinson's, and other neurodegenerative diseases). Targeted activation of JNK family kinases usually has anti-proliferative effect, whereas the activation of ERK1/2 promotes cell survival. Scaffolds facilitating signaling in these pathways might be easier to dose than direct pharmacological activators, making them safer intervention tools. The identification of the shortest active form of the T1A-derived peptide must be the next step in this direction.

# Chapter 7

## THE OLIGOMERIZATION OF ARRESTINS AND THE FUNCTIONAL CONSEQUENCES

Much of this chapter has been published as a review in the *Handbook of Experimental Pharmacology* [160]. Ya Zhuo , Miyeon Kim , Susan M. Hanson, Derek J. Francis, Sergey A. Vishnivetskiy, Christian Altenbach, T. M. Iverson, Candice S. Klug, Wayne L. Hubbell, Vsevolod V. Gurevich contributed to this work.

### Visual arrestin-1: the discovery of oligomerization

The beginning of arrestin history is rather convoluted: the first member of what we now call the arrestin family was originally discovered as an antigen against which patients with uveitis have antibodies [161]. Therefore, this protein was named S-antigen, and its gene is still called Sag in the HUGO database. The ability of this protein to oligomerize was described when it was identified, isolated, and characterized [161]. A soluble protein with an apparent molecular weight of ~48 kDa was later found to bind light-activated phosphorylated rhodopsin (P-Rh*) [162] and suppress its signaling [16]. Later it was established that the 48-kDa protein and S-antigen are one and the same protein; it was named arrestin for its ability to "arrest" rhodopsin signaling. Despite active functional work with this protein, its oligomerization was largely ignored until two groups independently found that arrestin crystallizes as a tetramer under different conditions (Figure 1) [27, 163]. Its self-association was further analyzed by analytical centrifugation, which suggested that arrestin-1 forms dimers and tetramers in solution [90]. This was taken as an indication that the solution tetramer is likely similar to that in the crystal, and the data were interpreted accordingly [90]. Since it was clearly demonstrated earlier that at low nanomolar concentrations, where no self-association would be possible, arrestin-1 binds P-Rh* [29, 80, 97, 164], oligomers were hypothesized

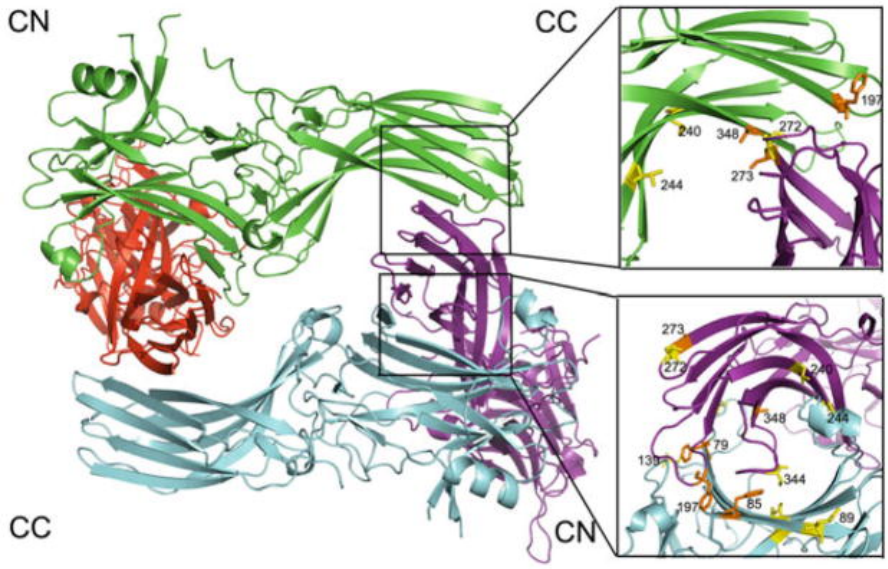


**Figure 1. The crystallographic tetramer of arrestin-1.** In the structure [PDB ID: 1CF1] each protomer is shown in a different color. The crystallographic tetramer is a dimer of dimers, where individual dimers are held together via C-to-N-domain interfaces, and the two dimers form a tetramer via C-to-C-domain interfaces (CC). The interfaces are enlarged on the right, with residues in positions probed by site-directed spin labeling EPR shown as stick models. Color coding: the residues in positions where the behavior of the spin label was consistent with predictions based on the crystal structure are shown in orange; those in positions where the behavior of the spin label was inconsistent with crystal structure are shown in yellow. Note that at least half of the positions fall into the latter category.

to be an inactive storage form [90]. Two subsequent studies of arrestin-1 oligomerization by small-angle X-ray scattering yielded surprisingly different self-association constants [89, 165]. Since the wavelength of X-rays is comparable to the size of arrestin, the small-angle X-ray scattering data could provide information about the shape of the solution tetramer, which was concluded to be the same as that in the crystal. One of these studies [89] proposed that visual arrestin-1 forms tetramers according to: $2M \rightleftarrows D$ ($K_1$), $2D \rightleftarrows T$ ($K_2$), where M, D, and T are monomer, dimer, and tetramer, respectively (MDT model). The oligomerization was found to be cooperative in the sense that the association constant $K_2 > K_1$. When the dimerization constant is much greater than the tetramerization constant, the concentration of dimers in the equilibrium mixture is small: it is dominated by tetramers.

**Crystal and solution tetramers of arrestin-1 have nothing in common**

Next, self-association of arrestin-1 in solution was analyzed by multi-angle laser light scattering (MALLS) [166]. The advantages of this method include high resolution to within a few hundred Daltons, wide molecular mass range, relatively small sample size, and high sample throughput. Importantly, because the wavelength of light is large compared to the dimensions of arrestin-1 monomer or any oligomer, no assumptions regarding the shape of solution tetramer are necessary for data interpretation [167]. The results confirmed the earlier proposed MDT model of monomer–dimer–tetramer equilibrium and the cooperativity of self-association, although it yielded different constants for the same bovine arrestin-1: $K_1 = 2.7 \pm 0.1 \times 104$, $K_2 = 1.3 \pm 0.1 \times 105$, which translates into $K_{D,dim} = 1/K1 = 37$ μM and $K_{D,tet} = 1/K2 = 7.5$ μM [166]. Interestingly, mutations that were predicted to disrupt self-association based on the

crystal tetramer did not affect oligomerization, whereas many others that would not be expected to affect protomer interactions in the crystal had profound effects [166].

Continuous wave (CW) electron paramagnetic resonance [78] spectroscopy can be used to monitor the mobility of a spin label on the surface of a protein [2]. If a particular element happens to be on the protomer–-protomer interaction interface, its mobility would decrease upon oligomer formation. A spin-label side chain (R1) introduced at many positions where significant immobilization was expected based on the crystal structure showed little to no change in mobility, whereas spin labels in several positions that are not on the crystal interfaces were immobilized upon tetramer formation. Collectively, the light scattering and EPR data showed that residues 79, 85, 173, 197, 244, and 348 are involved in inter-subunit interactions in the solution tetramer. While this result would be expected for 79, 85, 197, and 348 based on the crystal tetramer, the strong immobilization of 173R1 and the strong perturbation of self-association due to 244R1 were not predicted by the crystal tetramer (Figure 1). Neither the native Leu173 and Val244 nor the R1 side chain modeled at these positions in the crystal tetramer makes contacts with neighboring subunits [27].

Relatively small perturbations and lack of immobilization of R1 at sites 60, 272, and 344, which are deeply buried at the CN, CC, and CN interfaces, respectively, were also inconsistent with the crystal tetramer, where residue 344 is buried to the extent that the R1 side chain cannot be modeled without major rearrangement of the structure (Figure 1). Importantly, the 344R1 does not perturb the formation of oligomers [166]. The weak perturbation of self-association by 89R1 and lack of spectral change of 89R1, located directly at the NN interface in the crystal (Figure 1), do not support its existence.

These results clearly indicate that the tetramer in solution is quite different from that observed in the crystal.

Double electron–electron resonance (DEER), a pulse EPR technique [168], is a powerful method for measuring distances between paramagnetic centers in the range of ~19–60 Å [169], complementing CW EPR methods that determine distances between 10 and 20 Å [170]. DEER was used to measure distances between unique spin labels on each protomer within the solution tetramer, which were placed at eight non-perturbing or mildly perturbing sites in the tetramer (74, 108, 139, 173, 240, 272, 273, and 344). Only in one case (273R1) were the experimentally determined inter-spin distances close to the predictions based on the crystal structure, whereas the data for the other sites were clearly incompatible with the crystal tetramer [166]. Thus, several lines of evidence independently suggested that the shape of the solution tetramer must be different.

These unexpected findings made it necessary to elucidate the structure of the physiologically relevant solution tetramer, which holds clues to the functional role of arrestin-1 self-association. Since crystallography was misleading in this regard, the shape of the solution tetramer was deduced using inter-spin distances in the oligomer and the positions where the spin label was immobilized upon self-association. These data were used as inputs for Rosetta modeling [171-174]. Several iterations yielded a model for a tetramer consistent with all experimental data [88], which turned out to be symmetrical diamond shaped, with two nearly identical CC and NN interfaces, where all the interaction interfaces on each protomer are engaged by sister subunits (Figure 2). Since modeling per se does not yield unambiguous information, this model was subjected to rigorous post hoc testing.

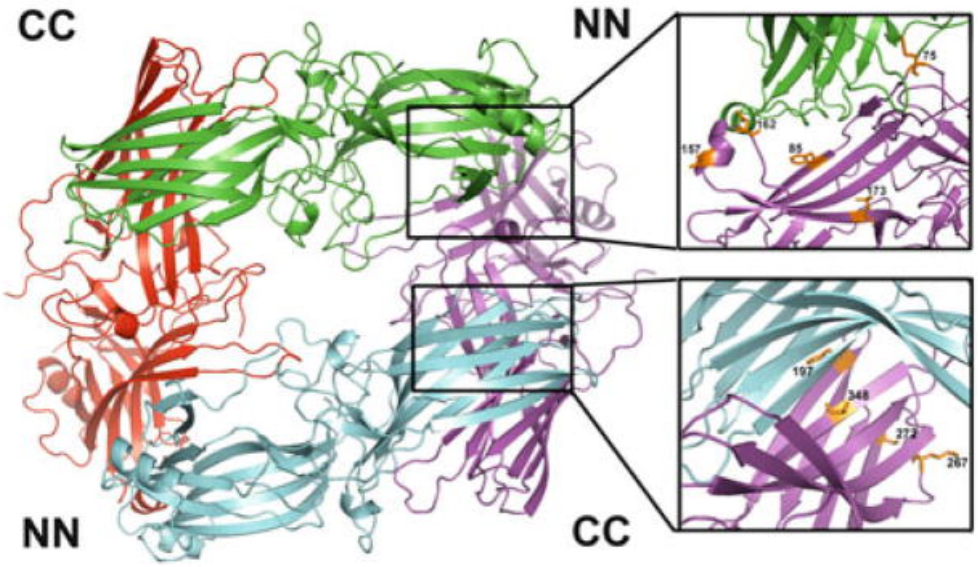


**Figure 1 Solution tetramer of arrestin-1.** Studies using site-directed spin labeling EPR, long-range inter-subunit distance measurements by DEER spectroscopy, site-directed mutagenesis, Rosetta modeling, and inter-subunit disulfide bridge formation lead to the conclusion that the solution tetramer of arrestin-1 is a symmetrical closed diamond, where adjacent protomers interact via two types of interfaces: C-to-C domain (CC) and N-to-N domain (NN). Enlarged interfaces are shown on the right, with residues in positions experimentally tested by various methods shown as stick models.

First, the R1 side chain was introduced either directly at the putative interface (position 75) or outside it (positions 376 and 381). CW EPR showed immobilization of the label at 75, with no evidence of immobilization at 376 or 381, consistent with the model [88]. The residues Phe197 and Ala348 in the CC interface and Thr157 and Asp162 in the NN interface in the model are very close to their counterparts in the adjacent monomer (Figure 2). In the crystal tetramer, all of these residues are far from their counterparts in other protomers (>20 Å). In contrast, residue Leu173 in the NN interface and Ser272 in the CC interface are far from their counterparts in the model. To test these predictions, single cysteine mutants were created and their ability to form inter-subunit disulfide bonds in solution was determined. In the presence of DTT, each arrestin ran as a single band on SDS-PAGE at a molecular weight (MW) corresponding to the arrestin monomer. However, in the absence of DTT, the Thr157Cys, Asp162Cys, Phe197Cys, and Ala348Cys mutants showed a second band corresponding to the expected mobility of the arrestin dimer. This suggests that residues 157, 162, 197, and 348 are close enough to their counterparts in the arrestin oligomer to self-cross-link in solution. As predicted, the absence of DTT did not induce cross-linking of Leu173Cys and Ser272Cys. These data strongly support the orientation of the NN and CC interfaces in the model, since disulfide cross-linking only occurs at very short (~5 Å) Cβ–Cβ distances between the two residues.

Finally, the model was tested via targeted disruption of arrestin-1 self-association by mutations directly affecting predicted inter-subunit interfaces. Since the introduction of a spin label per se constitutes a mutation, first the effects of cysteine substitution followed by spin labeling at positions 85 in the predicted NN interface, as well as at positions 197 and 267 in the predicted CC interface, were evaluated. The labeling at all

three positions reduced arrestin-1 self-association, confirming that these residues are in the inter-protomer interfaces. Importantly the effects of spin labeling at 197 and 267 were not additive, so that simultaneous labeling of both produced the same effect as the more detrimental to self-association 197R1 [88]. This is consistent with both side chains being at the same interface. In contrast, the combination of 85R1 and 197R1 was much more disruptive than the labeling of either of these two sites alone, consistent with their localization in two different interfaces [88]. Interestingly, the resulting 85R1/197R1 protein virtually lost the ability to self-associate. In the native structure both positions are occupied by phenylalanines. The replacement of Phe85 or Phe197 with alanine reduces self-association, whereas simultaneous substitution of both yields arrestin-1 that is essentially unable to oligomerize [88]. Thus, three independent lines of evidence strongly support the model of solution tetramer (Figure 2). Most importantly, these studies lead to the generation of a constitutively monomeric form of arrestin-1, which is necessary to elucidate the biological role of arrestin-1 self-association.

The proposed structure of the solution tetramer explains several observations that were inconsistent with the crystal tetramer. First, it explains the observed cooperativity [89, 166]: the interaction between two dimers engages two interfaces, whereas dimer formation involves only one. In contrast, in the crystal tetramer interfaces of comparable size mediate both dimerization and the interaction between two dimers in the tetramer [27, 89, 163]. Second, the circular "closed" configuration engages all self-association interfaces, explaining why arrestin-1 self-association stops at tetramer, so that larger oligomers are never formed. In contrast, in the crystal tetramer two protomers are left "dangling" with unused potential interaction interfaces that could mediate the binding of

additional monomers. Finally, in the solution tetramer all arrestin-1 elements implicated in receptor binding, which were identified by numerous groups using a variety of methods [2, 32, 104-107, 175-178], are either directly engaged or shielded by sister protomers, which explains why only monomeric arrestin-1 can bind rhodopsin. Moreover, the proposed structure of the solution tetramer (Figure 2) adequately explains the recent finding that manipulation of the receptor-binding surface of arrestin-1 to enhance its ability to interact with unphosphorylated rhodopsin significantly changes self-association parameters [179].

**The mechanism of arrestin-1 self-association is conserved in mammalian evolution**

All these mechanistic studies were performed with bovine arrestin-1, which was purified first both from its native source [180] and upon overexpression in Escherichia coli [181]. However, most of the physiological insights into rod function have been obtained in genetically modified mice [182, 183], with the ultimate goal of translating the findings to human therapy [94]. The key biologically relevant facts about arrestin-1 were established in mice: (1) that it is the second (after rhodopsin) most abundant protein in rods [83, 87]; (2) that it undergoes light-dependent redistribution in rod photoreceptors; and [43] that it is unexpectedly abundant in cones, where it represents ~98 % of total arrestin complement, whereas cone-specific arrestin-4 accounts for only ~2 % [184]. Thus, it was critically important to test whether mouse and human arrestin-1 self-associate and to determine the parameters of its oligomerization in these species.

Purified mouse arrestin-1 was found to form dimers and tetramers, similar to its bovine homolog [86]. Interestingly, both dimerization ($K_{D,dim}$ = 57.5 ± 0.6 μM) and tetramerization ($K_{D,tet}$ = 63.1 ± 2.6 μM) dissociation constants of mouse protein were

significantly higher than the corresponding values for bovine arrestin-1 [37.2 ± 0.2 μM and 7.4 ± 0.1 μM, respectively]. Moreover, whereas self-association of bovine arrestin-1 is cooperative ($K_{D,tet} < K_{D,dim}$), both constants are roughly equal for mouse arrestin-1, eliminating cooperativity. The dramatic differences in self-association constants of arrestin-1 from these two mammalian species made it imperative to determine the properties of human arrestin-1. Purified human arrestin-1 was also found to self-associate and form dimers and tetramers. However, it demonstrated strikingly different constants compared to bovine and mouse proteins: remarkably low $K_{D,dim}$ = 2.95 ± 0.02 μM and relatively high $K_{D,tet}$ = 224 ± 5 μM [86]. Importantly, if the overall concentration of arrestin-1 in the cell body of mammalian dark-adapted rod photoreceptors is similar to that measured in mouse (~2 mM), it greatly exceeds all measured dissociation constants. Therefore, despite these differences in self-association parameters the concentration of monomeric arrestin-1 in human, bovine, and mouse rods would be in a fairly narrow range, 30–90 μM. As the majority of arrestin-1 would exist in the form of tetramer in all three species, the tetramer concentration in the rod would vary by no more than 30 %, and the most striking difference would be in the expected dimer concentrations, varying from ~60 μM in bovine to ~280 μM in human rod [86].

Nonetheless, measured $K_{D,dim}$ between human and mouse arrestin-1 differs ~20-fold, and $K_{D,tet}$ of bovine and human proteins is ~30-fold different. The magnitude of these differences raises the possibility that arrestin-1 in these three species could use distinct interaction interfaces. In this scenario phenomenological similarity of self-association could represent convergent evolution, rather than direct conservation of the molecular mechanism. The nature of the interaction interfaces in the solution tetramer of

bovine arrestin-1 was strongly supported by the observation that the combination of two mutations predicted to disrupt NN (Phe85Ala) and CC (Phe197Ala) self-association interfaces makes the protein essentially a constitutive monomer, with $K_{D,dim}$ = 525 μM and no detectable tetramerization. To test whether interaction interfaces are conserved in mouse protein, self-association of the double mutant carrying homologous substitutions Phe86Ala + Phe198Ala was tested. This mutation yielded the same phenotype as in bovine protein: mouse arrestin-1-Phe86Ala + Phe198Ala demonstrated dramatically impaired self-association, with $K_{D,dim}$= 537 μM and no tetramer formation. The finding that homologous mutations in bovine and mouse arrestin-1 similarly disrupt their self-association strongly suggests that both proteins use the same interfaces for oligomerization. Thus, strikingly different self-association constants reflect the difference in the energy of interactions between the subunits, whereas the organization of the solution tetramer is likely the same in all mammals. Importantly, the elimination of these two phenylalanines does not appreciably affect arrestin-1 binding to its two best-characterized partners, P-Rh* and microtubules [86]. This finding suggests that these residues are strictly conserved in all mammalian arrestin-1 proteins because they facilitate self-association, indicating that robust arrestin-1 oligomerization is a biologically important aspect of its function in photoreceptor cells [93].

**Possible biological role of arrestin-1 self-association**

Unambiguous demonstration that only monomeric arrestin-1 is capable of binding rhodopsin [90] confirmed the earlier hypothesis that dimers and tetramers are storage forms. Although rod photoreceptors express many signaling proteins at levels several orders of magnitude higher than “normal” cells [185], and arrestin-1 is the second most

abundant protein in the rod [83-85], no other signaling protein in photoreceptors has an inactive storage form. Thus, arrestin-1 propensity to form inactive oligomers calls for an explanation.

The first glimpse into a possible role of this phenomenon emerged from unexpected quarters. In an attempt to compensate for defects in rhodopsin phosphorylation, two transgenic lines were created expressing the enhanced phosphorylation-independent arrestin-1-3A mutant [186] at ~50 and ~240 % of normal WT level [94]. It turned out that the lower expressor line actually showed the expected compensation, whereas rod photoreceptors in the other degenerated even faster than in arrestin-1 knockout mice [94, 187]. To achieve light sensitivity at the physical limit of single photons [10], rods express very high levels of all signaling proteins [185], maintaining a fairly precarious balance. As a result, overexpression of a perfectly normal WT protein can often lead to photoreceptor death, as has been shown for rhodopsin [188]. However, it was found that the expression of WT arrestin-1 at essentially the same level, ~220 % of WT, is harmless [84], indicating that it is the mutant nature of arrestin-1-3A that makes it toxic for rods. The analysis of the 3A mutant by MALLS showed that while this enhanced mouse arrestin-1 binds Rh* much better than WT, its self-association is partially compromised: $K_{D,dim}$ increased from 57.5 ± 0.6 μM of WT protein [86] to 135 ± 2 μM, with a simultaneous increase of $K_{D,tet}$ from 63.1 ± 2.6 μM to 380 ± 79 μM [187]. Calculations based on these constants, relative volumes of rod compartments [189], and arrestin-1 distribution in dark-adapted rod indicate that the concentration of arrestin-1 monomer in the cell body of WT mouse rod is ~95 μM (out of ~2,000 μM of total arrestin-1). Due to robust self-association, a 2.2-fold increase of WT arrestin-1 to ~4,400

μM results in only a modest increase in free monomer, to ~104 μM. In contrast, the expression of arrestin-1-3A at 240 % of WT level would yield ~270 μM of monomer, almost three times more than in WT rods [187]. Importantly, the expression of the same mutant at ~50 % of WT level yields only ~115 μM monomer, which is not dramatically different from WT overexpressors, consistent with the relatively good health of photoreceptors in these animals, at least until they reach the age of 32 weeks [187]. WT arrestin-1 was shown to effectively recruit mutants with partially compromised oligomerization into tetramers. Thus, if too high monomer concentration adversely affects rods, co-expression of WT arrestin-1 with the mutants would be expected to protect them. Indeed, it was shown that WT arrestin-1 expressed in rods with high levels of arrestin-1-3A affords partial protection against the mutant, slowing down photoreceptor death [187]. Interestingly, arrestin-1 was shown to interact with N-ethylmaleimide-sensitive factor (NSF) [190], a protein involved in exocytosis of neurotransmitter in the synapses. Indeed, synaptic terminals of rods expressing high levels of 3A mutant showed early damage, and their protection by WT arrestin-1 was very robust [187]. Collectively, the existing evidence is consistent with the idea that a relatively low level of monomeric arrestin-1 is optimal for photoreceptor health, whereas an excess of monomer induces cell death.

This hypothesis explains why arrestin-1 developed the ability to self-associate: rods need sufficient amounts of arrestin-1 to quench virtually all rhodopsin, yet can tolerate only fairly low levels of monomer [187]. Thus, to solve this problem rods store the bulk of arrestin-1 in the form of “safe” oligomers. Cytotoxicity of the monomer can also explain the relatively low expression of arrestin-4 [191], which is outnumbered by

arrestin-1 in cones by ~50:1 [184]. Arrestin-4, a cone-specific subtype, appeared early in vertebrate evolution [126]. In contrast to other subtypes that form tight relatively long-lived complexes with their cognate GPCRs [21, 192], arrestin-4 forms only low-affinity fairly transient complexes with cone opsins [159]. Functionally, this is perfectly suited for cones operating at high levels of illumination, which makes recycling and immediate reuse of cone opsins a necessity. Like rods, cones need enough arrestin to stop the signaling by all expressed photopigment. However, arrestin-4 is the only subtype that is self-association deficient, a natural constitutive monomer [193]. If the monomer is toxic, cones simply cannot afford to express sufficient amounts of arrestin-4 and therefore keep the majority of their arrestin complement in the form of safely self-associating arrestin-1.

Thus, it appears that self-association of arrestin-1 is a cytoprotective mechanism, reducing the concentration of toxic monomer in photoreceptor cells. While it remains to be elucidated whether monomer toxicity arises from excessive binding to NSF [190], inappropriate engagement of clathrin adaptor AP2 [194], or some other partner, it appears that arrestin-1 oligomerization prevents harmful interactions [187].

**Oligomerization of nonvisual arrestins: mechanism and consequences**

Whereas arrestin-1 is expressed at very high levels in rods and cones, with concentrations reaching ~2 mM in the body of dark-adapted photoreceptors [84], intracellular concentrations of nonvisual arrestins are much lower. Even in mature neurons, which express both at higher levels than most cells, the concentrations of arrestin-3 and -2 reach only ~30 and 200 nM, respectively [195, 196]. However, arrestins are fairly evenly distributed only in the non-stimulated cell [57]. Both arrestin-2 and -3 are recruited to active phosphorylated GPCRs in all cell types and were shown to become

concentrated in the vicinity of the plasma membrane and endosomes upon GPCR activation [57]. By virtue of their binding to polymerized tubulin, nonvisual arrestins also appear to be concentrated in the vicinity of microtubules [197]. Thus, local concentration in particular cell compartments under certain circumstances can greatly exceed estimated averages. Indeed, arrestin-2 and -3 expressed at near-physiological levels were reported to form homo- and hetero-oligomers in cells [129, 139]. Hetero-oligomerization of arrestin-3, which has a functional nuclear export signal in it C-terminus [198, 199], with arrestin-2 that does not, appears to help the removal of arrestin-2 from the nucleus [129].

Inositol-hexakisphosphate ($IP_6$), an abundant metabolite present in many cells in concentrations of 15–100 μM [200], was shown to greatly enhance self-association of both nonvisual arrestins [139]. Even though full-length arrestin-2 crystallizes as a monomer [136], solving the structure of crystals soaked with IP6 revealed that IP6 bridges neighboring molecules in a head-to-tail configuration via interactions with two sites, one in the N-domain and the other in the C-domain of arrestin-2 [136]. Direct binding studies combined with extensive mutagenesis showed that the C-domain site has a much higher affinity ($K_D$ ~ 40 nM) than the N-domain site ($K_D$ ~ 1 μM) for IP6, but both are well within the range of physiological $IP_6$ concentrations in the cell [136].

Elimination of positively charged residues critical for $IP_6$ binding increased the arrestin-2 presence in the nucleus, suggesting that oligomers are largely cytoplasmic [136]. Both IP6 binding sites appear to be localized on the receptor-binding surface of arrestins identified by many groups using various methods [2, 29, 80, 102-106, 175], indicating that simultaneous binding of receptor and $IP_6$ is impossible. This finding suggested that, as in the case of arrestin-1, oligomers represent an inactive storage form,

whereas monomeric arrestins are recruited to GPCRs, as well as translocated to the nucleus [136]. Interestingly, while $IP_6$ greatly increases self-association of nonvisual subtypes [136, 193], it significantly inhibits the oligomerization of arrestin-1 [193], indicating that the interfaces involved and overall shape of the oligomers formed by visual and nonvisual arrestins are different.

Experiments with purified proteins and cells expressing $IP_6$ binding-deficient mutants of both arrestin-2 and -3 also suggested that they form oligomers larger than dimer [136]. However, while arrestin-1 was shown to stop at tetramer, in which all interaction interfaces are engaged by sister subunits [88], it remained unclear whether arrestin-2 and -3 also stop at a particular size of oligomer, or can form "infinite" chains, as suggested by $IP_6$-soaked arrestin-2 crystal structure [136]. This issue was addressed using pure arrestins in the presence of $IP_6$ by MALLS [136]. In the absence of $IP_6$, arrestin-2 and -3 have a low tendency to self-associate with a $K_D$ around 100 μM (Figure 3). $IP_6$ promotes their self-association, and the KDs decrease to 5.5 and 7.8 μM for arrestin-2 and -3, respectively.

Despite high homology arrestin-2 and -3 form distinct oligomers in the presence of $IP_6$: arrestin-3 forms dimers; in contrast, arrestin-2 forms long chains that go beyond tetramer. The average molecular weight of arrestin-2 keeps growing without obvious saturation. At the highest concentration tested (84 μM), the average molecular weight of arrestin-2 oligomers reached ~202 kDa, which exceeded the expected molecular weight for the arrestin-2 tetramer (184 kDa) (Figure 3). Due to the formation of higher order oligomers MALLS data do not fit into the MDT model. Instead, a liner polymerization model ($M_{[n]} + M \leftrightarrow M_{[n+1]}$) fit arrestin-2 oligomerization data very well. This

suggested that arrestin-2 might form an infinite chain mediated by $IP_6$, as in the arrestin-2 crystals soaked with $IP_6$. However, the crystal structure does not necessarily reflect that which exists in solution, since in that study the orientation of arrestin-2 molecules relative to each other was fixed by crystallization in the absence of $IP_6$. Therefore, DEER was used to probe the structure of the solution oligomer of arrestin-2 in the presence of $IP_6$. Thirteen sites on arrestin-2 were selected on both the N-domain (Leu33, Lys49, Leu68, Val70, Leu71, Leu73, Val81, Ile158, and Val167) and the C-domain (Ser234, Tyr238, Thr246, and Cys269). These sites were located on the receptor-binding concave side (Lys49, Ile158, Val81, Leu68, Val70, Leu71, Leu73, Val167, Thr246, Tyr238, and Ser234) and the convex side (Leu33 and Cys269) to obtain a comprehensive characterization of the solution oligomer of arrestin-2 in the presence of $IP_6$. A nitroxide spin label (R1) at selected sites in arrestin-2 was introduced by chemical modification of these unique cysteines and the inter-subunit distances were measured using the DEER spectroscopy. The measured DEER distances matched remarkably well with the expected nitroxide-to-nitroxide distances between adjoining protomers in the crystal structure. All but two sets of data matched to within 3 Å of the expected crystallographic distances. Importantly, the sites with closer distances (<50 Å) clustered in the central parts of the concave receptor-binding side, which suggested that $IP_6$ mediates the interaction between the N- and C-domains of arrestin-2, so that only the central parts of the concave side come close together (Figure 3). Collectively, these data clearly suggest that the arrangement of protomers in the arrestin-2 crystals soaked with $IP_6$ closely resembles the structure of the solution oligomer of arrestin-2, further supporting the hypothesis that

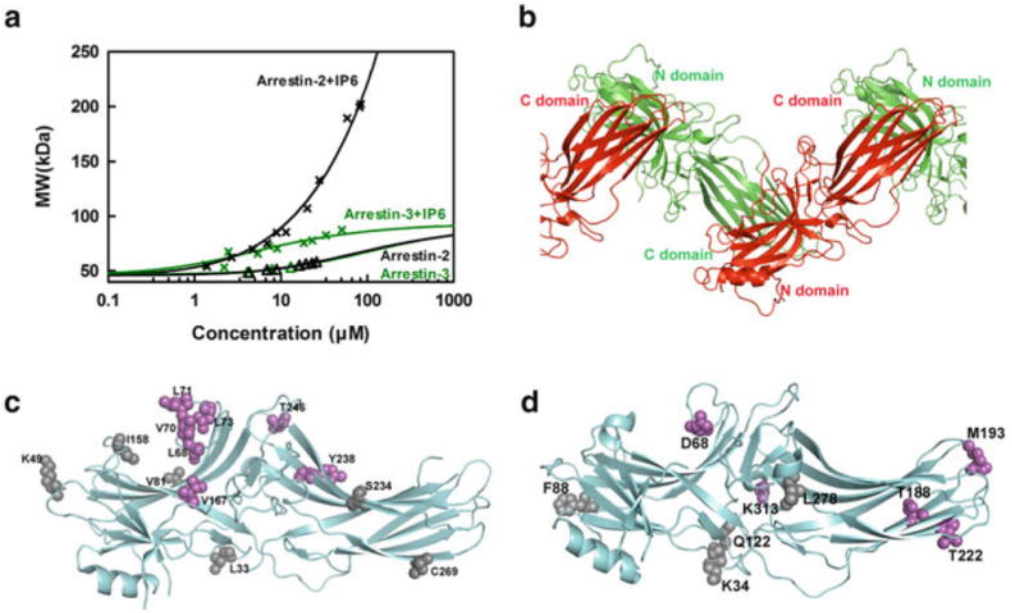


**Figure 3. The two nonvisual arrestins form distinct oligomers.** (a) The average molecular weight of arrestin-2 and arrestin-3 in the presence (crosses) and absence (triangles) of 100 μM IP6 as a function of total arrestin concentration was measured by MALLS. Arrestin-2 data were fit by a linear polymerization model (black line), while arrestin-3 data were fit by a monomer–dimer model (green line). Neither nonvisual arrestin showed a propensity to self-associate at physiologically relevant concentrations in the absence of IP6. (b) The crystal structure of arrestin-2 in complex with IP6 [PDB ID: 1ZSH] shows that arrestin-2 forms "infinite" chains through C-to-N-domain interactions mediated by IP6. (c) The positions of spin-labeled sites are shown as spheres on the crystal structure of arrestin-2 [PDB ID: 1ZSH]. The sites with inter-subunit distances shorter than 50 Å (Leu68, Val70, Leu71, Leu73, Val167, Tyr238, and Thr246), as measured by DEER spectroscopy in the presence of IP6, are colored magenta, and the ones with inter-subunit distance longer than 50 Å (Leu33, Lys49, Val81, Ile158, Ser234, and Cys269) are colored gray. (d) The positions of spin-labeled sites are shown as spheres on the crystal structure of arrestin-3 [PDBID: 3P2D]. The sites with inter-subunit distance shorter than 50 Å (Asp68, Thr188, Met193, Thr222, and Lys313), as measured by DEER spectroscopy in the presence of IP6, are colored magenta, while the ones with inter-subunit distance longer than 50 Å (Lys34, Phe88, Gln122, and Leu278) are colored gray.

arrestin-2 forms "infinite" chains in the presence of $IP_6$ in solution, similar to those observed in the crystal. In contrast, MALLS data showed that the average molecular weight of arrestin-3 oligomers in the presence of $IP_6$ did not exceed that of a dimer (Figure 3). Since the saturation was not reached due to concentration limitations, a higher order oligomer could not be excluded. However, the fact that the data could not be fit to either an MDT model or a polymerization model, but fit well to monomer–dimer equilibrium model suggested that the formation of higher order oligomers of arrestin-3 in the presence of IP6 was not favored. DEER was used to probe the structure of arrestin-3 oligomers in solution in the presence of $IP_6$. The distances measured with several arrestin-3 mutants in the presence of $IP_6$ aligned moderately well with the expected distances based on the arrestin-2 $IP_6$ crystallographic oligomer, but they were not as clearly matched as the arrestin-2 data. Interestingly, the sites in arrestin-3 with distances shorter than 50 Å are clustered not only in the central crest (Asp68, Lys313), but also in the C-domain, including the distal part of the C-domain (Thr188, Met193, Thr222), while the sites in the N-domain (Lys34, Phe88, and Gln122) had much longer distances, beyond the range of reliable measurement by DEER spectroscopy. These data suggested that $IP_6$ might mediate the interaction between the C-domains of two arrestin-3 molecules, so that the sites on the C-domain are in close contact, whereas the sites on the N-domain remain far apart. This model would explain why arrestin-3 stops at a dimer, since the interfaces mediating $IP_6$-assisted interaction are no longer exposed upon the formation of the C-to-C-domain dimer. This is in contrast to arrestin-2, in which only the sites in the central crest on the concave side come close to each other in the presence of $IP_6$. Though more data are needed to generate a high-resolution model for the arrestin-3 dimer (or larger

oligomer, if it exists), it is very clear that in the presence of $IP_6$ arrestin-2 and arrestin-3 form structurally distinct oligomers. Since nonvisual arrestins were reported to form mixed oligomers, it remains to be elucidated whether these resemble arrestin-2 chains or arrestin-3 C-to-C dimers or have a unique shape and size distinct from both.

**Do arrestin oligomers have specific functions?**

It was shown that mutations disrupting self-association of arrestin-1 do not significantly affect its ability to bind its preferred form of rhodopsin, P-Rh*, or microtubules [86]. However, the same mutations somewhat reduced the binding of an enhanced phosphorylation-independent mutant to Rh*, in agreement with the finding that distinct arrestin-1 elements are involved in its interactions with different functional forms of rhodopsin [179]. This difference might also reflect distinct stoichiometry of the arrestin-1-rhodopsin interactions in these cases. While arrestin-1 was shown to bind the P-Rh* monomer in nanodiscs [77, 78, 177, 201] and bicelles [202], a possibility of an alternative mode of interaction was reported in native disc membranes with a high fraction of light-activated rhodopsin, where arrestin-1 appears to engage two rhodopsin molecules simultaneously [203, 204]. Even though in these situations arrestin-1 binds only one rhodopsin molecule with high enough affinity to stabilize its active conformation [203, 204], the engagement of one or two rhodopsin molecules, one of which might be unphosphorylated, could be one of the mechanistic differences in arrestin-1 binding to P-Rh* and Rh*. In either case, it appears that only monomeric arrestin-1 can bind rhodopsin. Interestingly, while rhodopsin binding induces the dissociation of all arrestin-1 oligomers, indicating that only monomeric arrestin-1 can bind the receptor [166], the monomer and all oligomers appear to bind tubulin

comparably, so that in the presence of a sufficient concentration of microtubules to bind all arrestin-1 the inter-subunit distances reporting the presence of oligomers do not appear to be affected [166].

In the case of nonvisual arrestins, we know even less about specific functions of the oligomeric forms. Oligomerization-deficient mutants were found to bind clathrin, clathrin adaptor AP2, and ERK1/2 normally [139], in agreement with the localization of binding sites for these partners away from residues that mediate $IP_6$ binding [139]. However, an arrestin-3 mutant that did not bind IP6 was found to lack tight association with another partner, ubiquitin ligase Mdm2, and in contrast to WT arrestin-3, these presumably monomeric mutants did not suppress Mdm2-dependent degradation of p53 [205]. While it was proposed that arrestin-3 oligomers provide more interaction sites for putative dimers of Mdm2, another plausible explanation is that since Mdm2 preferentially binds arrestins in the basal conformation, oligomerization might simply stabilize this conformational state of nonvisual arrestins, which are inherently more flexible than arrestin-1. One study suggested that monomeric nonvisual arrestins are more likely to enter the nucleus, whereas another found comparable levels of arrestin oligomers in the nucleus and cytoplasm [205], although in the latter case it remained unclear whether arrestin oligomers can enter the nucleus, or arrestins self-associate after entering it as monomers and/or dimers.

It is entirely possible that nonvisual arrestins self-associate for the same reason as arrestin-1 to prevent the buildup of a cytotoxic monomeric form [187], but this idea needs to be tested experimentally. It is clear that more experimentation is necessary before we

will be able to unambiguously determine specific functions of nonvisual arrestin oligomers and sort out cellular processes affected by their impaired self-association.

# CHAPTER VII

## BROAD IMPLICATIONS AND FUTURE DIRECTIONS OF THIS WORK

My thesis study is focused on elucidating the structural basis of arrestin signaling. In particular, I am trying to answer the following questions: 1. What is the conformation of arrestin in the active form? 2. How does arrestin activate downstream signaling? 3. How is the receptor activation allosterically linked to the effector binding in arrestin? I have used NMR, EPR, crystallography and various techniques to look at arrestin dynamics and have determined the structure of active arrestin-3. Collectively, my results revealed the high dynamic of arrestin and identified key elements for receptor and downstream effector binding.

One characteristic feature of arrestin-receptor binding is that it requires the receptor to be both phosphorylated and activated [36, 206]. Thus it is critical to map the phosphate sensor and activation sensor of arrestin, which recognize the receptor-attached phosphates and receptor active conformation, respectively [41]. We applied NMR to look at arrestin-1 binding to rhodopsin in different states [202]. It offered a unique chance to look at both low and high affinity receptor-arrestin binding dynamically. Through this study, we were able to identify the structural elements of arrestin that either directly interacts with receptor or receptor attached phosphates or that undergoes significant conformational changes due to allosteric regulation [202]. Importantly, we showed that the receptor-attached phosphates are able to trigger the release of arrestin C terminus regardless the activation state of the receptor [202]. It was later verified by different groups that the receptor phosphorylated C terminus occupies the same place where the arrestin C terminus is, resulting in C terminus displacement [28, 128]. This

leads to the conclusion that the N domain cleft where both arrestin C terminus and receptor phosphorylated C terminus bind to is the receptor phosphate sensor.

Another characteristic feature of arrestin-receptor binding is that two non-visual arrestins are capable of mediating the signaling of ~800 different GPCRs without any observable conserved binding site [38, 207]. Very limited structural information is available for receptor-arrestin complex, making it very challenging to reveal the mechanism underlying the board receptor recognition of arrestins. Interestingly, we crystalized arrestin-3 in its trimeric form and the crystallographic three-fold provides a hydrophobic core similar to receptor cytoplasmic crevice opened upon activation. More importantly, it stabilizes arrestin-3 in its active form. Comparison between different active structures reveals that the finger loop of arrestin directly interacts with active receptor [22, 28, 128]. The receptor binding induces the helix formation of the finger loop, resulting in two conserved leucines facing the hydrophobic core for high affinity binding. Moreover, it is on a flexible tether, which give it flexibility to 'wiggle' around in distinct receptor cytoplasmic crevices for high affinity binding. Our study provides one possible explanation for the board receptor recognition of arrestin. It is that any hydrophobic core can induce the helix formation of arrestin finger loop and the flexibility, helixity and hydrophobicity is critical for receptor high affinity binding.

There are two functional consequences upon arrestin binding to GPCRs: arrestin can either terminate G protein dependent signaling or initiates its own signaling [127] [208]. It has been discovered that two non-visual arrestins have more than 100 interaction partners [43]. However very little information is available about the structural basis how arrestin interacts with many downstream effectors. We show the very first evidence that

arrestin-1 gains significant conformational flexibilities upon high affinity receptor binding [202]. This provides the fundamental basis how arrestin can accommodate up to 200 different downstream effectors. Moreover, we stabilized arrestin-3 in one specific active state and identified key conformational changes in the effector-binding region by comparing our active structure with the basal structure. This includes rearrangement of poly-proline motif, register shift and increased local dynamic.

Arrestin is tied to GPCRs ever since its discovery and it got the name of arrestin because it attenuates or 'arrests' GPCR signaling [38]. It is usually considered that arrestin is in its basal state in the absence of a receptor agonist. Our study suggests that inositol hexakisphosphate ($IP_6$) may serve as an alternative cytoplasmic activator for arrestin-3. $IP_6$ triggers the release of arrestin C terminus, which is one of the hallmarks of arrestin-3 activation. Arrestin-3 crystal structure in the presence of $IP_6$ shows that $IP_6$ induces the activation of arrstin-3 by mimicking receptor attached phosphates and providing a hydrophobic core by mediating trimerization. This also provides a possible mechanism how arrstin mediates receptor independent signaling.

Despite the 78% sequence identity between arrestin-2 and arrestin-3, each isoform has its unique function, for example, arrestin-3, but not arrestin-2, functions as a scaffold promoting the activation of JNK family kinases [53]. The underlying mechanism of the functional divergence between these two isoforms is unrevealed. Our study reveals that the arrestin-3 oligomerization mediated by $IP_6$ is critical for scaffolding and that distinct oligomeric states of arrestin-2 and -3 might underlie the functional difference in JNK activation. It is the very first evidence demonstrating that the oligomeric state of arrestin regulates scaffolding, and that the arrestin-3 oligomer can be a functional unit.

Following my thesis study, I'd like to focus on the following topics for my future investigation.

**Does arrestins bind to lipid membrane and if yes, how does the membrane-arrestin interaction affect receptor binding?**

GPCRs are located in the lipid bilayer and transduce the signaling across the membrane. It is not surprising that lipid–protein interactions exert a considerable influence [209] on GPCR signaling given that the signal transduction is membrane-associated and therefore lipid-related. G proteins and GRKs are anchored to the membrane through various ways: the lipid modification, ionic interaction, membrane binding domain and so on [210] [211]. However, whether there is interaction between lipid and arrestin is largely unknown. It has been reported that in vitro system, 30% of negatively charged lipid are needed for the highly affinity binding of arrestin to phosphorylated active rhodopsin indicating that lipid composition is critical for arrestin-receptor binding [21]. Interestingly, in the arrestin-3-IP6 structure, we detected one phosphate-binding site in the distal C domain and it aligns with the membrane binding sites of arrestin-1 in the arrestin-1-rhodopsin structure. We could identify two sites (Lys 227 and Arg 332) that are directly in contact with the phosphates in $IP_6$ and I hypothesize that these two sites in arrestins interacts with the phosphate head group of the lipid in the cell membrane and thus anchoring arrestins in the membrane through electrostatic interaction.

We have demonstrated that both bicelles and nanodics are suitable model systems for arrestin-receptor study [1, 21]. With these two model systems, we can manipulate the lipid composition to include either positively charged lipid or the negatively charged lipid

and test the binding of rhodopsin. We have shown that in nanodics, negatively charged lipids significantly enhance receptor binding. I anticipate that charge neutralization of these two potential lipid-binding sites will diminish the preference to the negatively charged lipid while reverse the charge of these will make arrestin favors the positively charged lipid. We can also use BRET assay to test how it affects the receptor binding in cells. If my hypothesis is right, charge reversal and neutralization will significantly decrease the receptor binding.

**What is the conformation of receptor-arrestin or arrestin-effector complex?**

A long-term challenge in the field is to understand how structural states correlate with different signaling outcomes, and one way to accomplish this is by visualizing the key functional complexes. In terms of arrestin signaling, the structure of arrestin in complex with G protein coupled receptors or downstream effectors, for example JNK3, Src, or Mdm2 would have tremendous impact on our understanding of biology. Moreover, the structures of these types of complexes can identify the molecular details of potentially druggable pharmacological targets, perhaps with the development of an activation-state biased arrestin ligand.

Crystallography offers the atomic resolution of a single state the complex, and requires the protein to be conformational homogenous [212]. The likely dynamic nature of arrestin-receptor complex [35, 202] therefore makes this complex challenging for crystallography. However, several methods can be used to stabilize the complex in one specific functional state. First, single-domain, conformationally-selective nanobodies have been successfully used for β2 adrenergic receptor-G protein complex crystallization. These nanobodies both stabilize the complex and have historically provided additional

soluble surface area that can mediate crystal contacts. Some of the future diretions of my work include the use of nanobodies to stabilize the native phodphorhodopsin-arrestin-1 complex. In collaboration with Jan Steyaert lab, we have immunized llamas with the crosslinked arrestin-phosphorhodopsin complex and collected the pool ready for yeast display and screening. Second, photo-activable crosslinkers can be used to trap the complex in one specific state [213]. One method to incorporate unnatural amino acids is by introducing an Amber codon into a site that is predicted to be within 9.5 Å of the binding partner in the complex [213]. This technique has the advantage of being highly specific. Paired cysteines can also be introduced to form disulfide bond to fix a certain region in one conformation. With further purification after crosslinking, it is possible to collect a homogenous sample of a protein-protein complex ready for crystallization. Third, thermo-stabilization of the complex is a possibility. Receptor thermo-stabilization has been shown to be very effective in aiding receptor crystallization [214]. The complex with higher thermo stability is more likely to form diffractive crystals. Even with all the possibility of stabilizing the complex, it remains very challenging to obtain complex crystals. Cyro electron microscope (EM) has less limitation in sample preparation as compared to crystallography and recent breakthroughs have allowed the resolution to be even lower than 4 Å [215]. It will also be tried to visualize the complex.

## REFERENCES


1. Chen, Q., et al., *The rhodopsin-arrestin-1 interaction in bicelles.* Methods Mol Biol, 2015. **1271**: p. 77-95.

2. Hanson, S.M., et al., *Differential interaction of spin-labeled arrestin with inactive and active phosphorhodopsin.* Proc Natl Acad Sci USA, 2006. **103**: p. 4900-4905.

3. Vishnivetskiy, S.A., et al., *The role of arrestin alpha-helix I in receptor binding.* J. Mol. Biol., 2010. **395**: p. 42-54.

4. Bockaert, J. and J.P. Pin, *Molecular tinkering of G protein-coupled receptors: an evolutionary success.* EMBO J, 1999. **18**(7): p. 1723-9.

5. West, C. and A.C. Hanyaloglu, *Minireview: Spatial Programming of G Protein-Coupled Receptor Activity: Decoding Signaling in Health and Disease.* Mol Endocrinol, 2015. **29**(8): p. 1095-106.

6. Ma, P. and R. Zemmel, *Value of novelty?* Nat Rev Drug Discov, 2002. **1**(8): p. 571-2.

7. Overington, J.P., B. Al-Lazikani, and A.L. Hopkins, *How many drug targets are there?* Nat Rev Drug Discov, 2006. **5**(12): p. 993-6.

8. Bjarnadottir, T.K., et al., *Comprehensive repertoire and phylogenetic analysis of the G protein-coupled receptors in human and mouse.* Genomics, 2006. **88**(3): p. 263-73.

9. Molday, R.S., *Photoreceptor membrane proteins, phototransduction, and retinal degenerative diseases. The Friedenwald Lecture.* Invest Ophthalmol Vis Sci, 1998. **39**(13): p. 2491-513.

10. Baylor, D.A., T.D. Lamb, and K.W. Yau, *Responses of retinal rods to single photons.* J Physiol, 1979. **288**: p. 613-34.

11. Sampath, A.P. and F. Rieke, *Selective transmission of single photon responses by saturation at the rod-to-rod bipolar synapse.* Neuron, 2004. **41**(3): p. 431-43.

12. Filipek, S., et al., *G protein-coupled receptor rhodopsin: a prospectus.* Annu Rev Physiol, 2003. **65**: p. 851-79.

13. Gether, U. and B.K. Kobilka, *G protein-coupled receptors. II. Mechanism of agonist activation.* J Biol Chem, 1998. **273**(29): p. 17979-82.

14. Meng, E.C. and H.R. Bourne, *Receptor activation: what does the rhodopsin structure tell us?* Trends in Pharmacological Sciences, 2001. **22**(11): p. 587-593.

15. Fung, B.K., J.B. Hurley, and L. Stryer, *Flow of information in the light-triggered cyclic nucleotide cascade of vision.* Proc Natl Acad Sci U S A, 1981. **78**(1): p. 152-6.

16. Wilden, U., S.W. Hall, and H. Kühn, *Phosphodiesterase activation by photoexcited rhodopsin is quenched when rhodopsin is phosphorylated and binds the intrinsic 48-kDa protein of rod outer segments.* Proc Natl Acad Sci USA, 1986. **83**: p. 1174-1178.

17. Krupnick, J.G., V.V. Gurevich, and J.L. Benovic, *Mechanism of quenching of phototransduction. Binding competition between arrestin and transducin for phosphorhodopsin.* Journal of Biological Chemistry, 1997. **272**: p. 18125-31.

18. Liebman, P.A. and E.N. Pugh, Jr., *ATP mediates rapid reversal of cyclic GMP phosphodiesterase activation in visual receptor membranes.* Nature, 1980. **287**(5784): p. 734-6.

19. Gurevich, V.V. and E.V. Gurevich, *The molecular acrobatics of arrestin activation.* Trends Pharmacol Sci, 2004. **25**(2): p. 105-11.

20. Vishnivetskiy, S.A., et al., *Regulation of arrestin binding by rhodopsin phosphorylation level.* Journal of Biological Chemistry, 2007. **282**(44): p. 32075-32083.

21. Bayburt, T.H., et al., *Monomeric Rhodopsin Is Sufficient for Normal Rhodopsin Kinase (GRK1) Phosphorylation and Arrestin-1 Binding.* J. Biol. Chem., 2011. **286**(2): p. 1420-1428.

22. Kang, Y., et al., *Crystal structure of rhodopsin bound to arrestin determined by femtosecond X-ray laser.* Nature, 2015. **523**: p. 561-567.

23. Szczepek, M., et al., *Crystal structure of a common GPCR-binding interface for G protein and arrestin.* Nat Commun, 2014. **5**: p. 4801.

24. Rasmussen, S.G., et al., *Crystal structure of the beta2 adrenergic receptor-Gs protein complex.* Nature, 2011. **477**(7366): p. 549-55.

25. Scheerer, P., et al., *Crystal structure of opsin in its G-protein-interacting conformation.* Nature, 2008. **455**(7212): p. 497-U30.

26. Granzin, J., et al., *Crystal Structure of p44, a Constitutively Active Splice Variant of Visual Arrestin.* J Mol Biol, 2012. **416**(5): p. 611-618.

27. Hirsch, J.A., et al., *The 2.8 angstrom crystal structure of visual arrestin: A model for arrestin's regulation.* Cell, 1999. **97**(2): p. 257-269.

28. Kim, Y.J., et al., *Crystal structure of pre-activated arrestin p44.* Nature, 2013. **497**(7447): p. 142-146.

29. Gurevich, V.V. and J.L. Benovic, *Visual arrestin binding to rhodopsin: diverse functional roles of positively charged residues within the phosphorylation-recignition region of arrestin.* J. Biol. Chem., 1995. **270**(11): p. 6010-6016.

30. Vishnivetskiy, S.A., et al., *How does arrestin respond to the phosphorylated state of rhodopsin?* J. Biol. Chem., 1999. **274**: p. 11451-11454.

31. Vishnivetskiy, S.A., et al., *An additional phosphate-binding element in arrestin molecule: implications for the mechanism of arrestin activation.* J. Biol. Chem., 2000. **275**(52): p. 41049-41057.

32. Zhuang, T.D., et al., *Involvement of distinct arrestin-1 elements in binding to different functional forms of rhodopsin.* Proc Natl Acad Sci USA, 2013. **110**(3): p. 942-947.

33. Kim, M., et al., *Conformation of receptor-bound visual arrestin.* Proceedings of the National Academy of Sciences of the United States of America, 2012. **109**(45): p. 18407-18412.

34. Vishnivetskiy, S.A., et al., *Critical role of the central 139-loop in stability and binding selectivity of arrestin-1.* J. Biol. Chem., 2013. **288**(17): p. 11741-11750.

35. Shukla, A.K., et al., *Visualization of arrestin recruitment by a G-protein-coupled receptor.* Nature, 2014. **512**(7513): p. 218-22.

36. Benovic, J.L., et al., *Functional desensitization of the isolated beta-adrenergic receptor by the beta-adrenergic receptor kinase: potential role of an analog of the retinal protein arrestin (48-kDa protein).* Proc Natl Acad Sci U S A, 1987. **84**(24): p. 8879-82.

37. Pfister, C., et al., *Retinal S antigen identified as the 48K protein regulating light-dependent phosphodiesterase in rods.* Science, 1985. **228**(4701): p. 891-3.

38. Lohse, M.J., et al., *beta-Arrestin: a protein that regulates beta-adrenergic receptor function.* Science, 1990. **248**(4962): p. 1547-50.

39. Attramadal, H., et al., *Beta-arrestin2, a novel member of the arrestin/beta-arrestin gene family.* J Biol Chem, 1992. **267**(25): p. 17882-90.

40. Carman, C.V. and J.L. Benovic, *G-protein-coupled receptors: turn-ons and turn-offs.* Curr Opin Neurobiol, 1998. **8**: p. 335-344.

41. Gurevich, V.V. and E.V. Gurevich, *The structural basis of arrestin-mediated regulation of G protein-coupled receptors.* Pharm Ther, 2006. **110**: p. 465-502.

42. Bowick, G.C., et al., *Identification of differentially activated cell-signaling networks associated with pichinde virus pathogenesis by using systems kinomics.* J Virol, 2007. **81**(4): p. 1923-33.

43. Xiao, K., et al., *Functional specialization of beta-arrestin interactions revealed by proteomic analysis.* Proc Natl Acad Sci U S A, 2007. **104**(29): p. 12011-6.

44. Shenoy, S.K., et al., *Regulation of receptor fate by ubiquitination of activated beta 2-adrenergic receptor and beta-arrestin.* Science, 2001. **294**(5545): p. 1307-13.

45. Shenoy, S.K. and R.J. Lefkowitz, *Trafficking patterns of beta-arrestin and G protein-coupled receptors determined by the kinetics of beta-arrestin deubiquitination.* J Biol Chem, 2003. **278**(16): p. 14498-506.

46. McDonald, P.H., et al., *Beta-arrestin 2: a receptor-regulated MAPK scaffold for the activation of JNK3.* Science, 2000. **290**(5496): p. 1574-7.

47. Miller, W.E., et al., *Identification of a motif in the carboxyl terminus of beta -arrestin2 responsible for activation of JNK3.* J Biol Chem, 2001. **276**(30): p. 27770-7.

48. Luttrell, L.M., et al., *Beta-arrestin-dependent formation of beta2 adrenergic receptor-Src protein kinase complexes.* Science, 1999. **283**(5402): p. 655-61.

49. DeFea, K.A., et al., *The proliferative and antiapoptotic effects of substance P are facilitated by formation of a beta -arrestin-dependent scaffolding complex.* Proc Natl Acad Sci U S A, 2000. **97**(20): p. 11086-91.

50. Zhan, X., et al., *Non-visual arrestins function as simple scaffolds assembling MKK4- JNK3α2 signaling complex.* Biochemistry, 2011. **50**: p. 10520-10529.

51. Bohn, L.M., et al., *Enhanced morphine analgesia in mice lacking beta-arrestin 2.* Science, 1999. **286**(5449): p. 2495-8.

52. Kohout, T.A., et al., *beta-Arrestin 1 and 2 differentially regulate heptahelical receptor signaling and trafficking.* Proc Natl Acad Sci U S A, 2001. **98**(4): p. 1601-6.

53. McDonald, P.H., et al., *Beta-arrestin 2: a receptor-regulated MAPK scaffold for the activation of JNK3.* Science, 2000. **290**: p. 1574-1577.

54. Kook, S., et al., *Arrestin-3 binds JNK1α1 and JNK2α2 and facilitates the activation of these ubiquitous JNK isoforms in cells via scaffolding.* J Biol Chem, 2013. **288**: p. 37332-37342.

55. Miller, W.E., et al., *Identification of a motif in the carboxyl terminus of beta -arrestin2 responsible for activation of JNK3.* J Biol Chem, 2001. **276**: p. 27770-27777.

56. Song, X., et al., *How does arrestin assemble MAPKs into a signaling complex?* J Biol Chem, 2009. **284**: p. 685-695.

57. Song, X., et al., *Visual and both non-visual arrestins in their "inactive" conformation bind JNK3 and Mdm2 and relocalize them from the nucleus to the cytoplasm.* J Biol Chem, 2006. **281**: p. 21491-9.

58. Zhan, X., et al., *JNK3 binding to arrestin-3 differentially affects the recruitment of upstream MAP kinase kinases.* J Biol Chem, 2013. **288**: p. 28535-28547.

59. Brown, M.F., *Modulation of rhodopsin function by properties of the membrane bilayer.* Chem Phys Lipids, 1994. **73**(1-2): p. 159-80.

60. Jastrzebska, B., et al., *Role of membrane integrity on G protein-coupled receptors: Rhodopsin stability and function.* Prog Lipid Res, 2011. **50**(3): p. 267-77.

61. Durr, U.H.N., M. Gildenberg, and A. Ramamoorthy, *The Magic of Bicelles Lights Up Membrane Protein Structure.* Chemical Reviews, 2012. **112**(11): p. 6054-6074.

62. Sanders, C.R., et al., *Magnetically-Oriented Phospholipid Micelles as a Tool for the Study of Membrane-Associated Molecules.* Progress in Nuclear Magnetic Resonance Spectroscopy, 1994. **26**: p. 421-444.

63. Sanders, C.R. and R.S. Prosser, *Bicelles: a model membrane system for all seasons?* Structure with Folding & Design, 1998. **6**(10): p. 1227-1234.

64. Ujwal, R. and J.U. Bowie, *Crystallizing membrane proteins using lipidic bicelles.* Methods, 2011. **55**(4): p. 337-341.

65. Rasmussen, S.G., et al., *Crystal structure of the human beta2 adrenergic G-protein-coupled receptor.* Nature, 2007. **450**(7168): p. 383-7.

66. Beaugrand, M., et al., *Lipid concentration and molar ratio boundaries for the use of isotropic bicelles.* Langmuir, 2014. **30**(21): p. 6162-70.

67. Ye, W.H., et al., *Characterization of the Morphology of Fast-Tumbling Bicelles with Varying Composition.* Langmuir, 2014. **30**(19): p. 5488-5496.

68. Thompson, A.A., et al., *GPCR stabilization using the bicelle-like architecture of mixed sterol-detergent micelles.* Methods, 2011. **55**(4): p. 310-317.

69. Zocher, M., et al., *Cholesterol increases kinetic, energetic, and mechanical stability of the human beta2-adrenergic receptor.* Proc Natl Acad Sci USA, 2012. **109**(50): p. E3463-72.

70. Rim, J. and D.D. Oprian, *Constitutive Activation of Opsin - Interaction of Mutants with Rhodopsin Kinase and Arrestin.* Biochemistry, 1995. **34**(37): p. 11938-11945.

71. Degrip, W.J., *Thermal-Stability of Rhodopsin and Opsin in Some Novel Detergents.* Methods in Enzymology, 1982. **81**: p. 256-265.

72. Reeves, P.J., J. Hwa, and H.G. Khorana, *Structure and function in rhodopsin: kinetic studies of retinal binding to purified opsin mutants in defined phospholipid-detergent mixtures serve as probes of the retinal binding pocket.* Proc Natl Acad Sci USA, 1999. **96**(5): p. 1927-31.

73. McKibbin, C., et al., *Opsin stability and folding: modulation by phospholipid bicelles.* J Mol Biol, 2007. **374**(5): p. 1319-32.

74. Gurevich, V.V. and E.V. Gurevich, *How and why do GPCRs dimerize?* Trends Pharmacol Sci, 2008. **29**: p. 234-40.

75. Bayburt, T.H., et al., *Transducin activation by nanoscale lipid bilayers containing one and two rhodopsins.* J. Biol. Chem., 2007. **282**(20): p. 14875-14881.

76. Whorton, M.R., et al., *Efficient coupling of transducin to monomeric rhodopsin in a phospholipid bilayer.* J. Biol. Chem., 2008. **283**: p. 4387-4394.

77. Vishnivetskiy, S.A., et al., *Constitutively active rhodopsin mutants causing night blindness are effectively phosphorylated by GRKs but differ in arrestin-1 binding.* Cell Signal, 2013. **25**(11): p. 2155-2162.

78. Singhal, A., et al., *Insights into congenital night blindness based on the structure of G90D rhodopsin.* EMBO Rep, 2013. **14**(6): p. 520-526.

79. Kuhn, H., *Light-regulated binding of rhodopsin kinase and other proteins to cattle photoreceptor membranes.* Biochemistry, 1978. **17**: p. 4389-95.

80. Gurevich, V.V. and J.L. Benovic, *Visual arrestin interaction with rhodopsin. Sequential multisite binding ensures strict selectivity toward light-activated phosphorylated rhodopsin.* J. Biol. Chem., 1993. **268**(16): p. 11628-38.

81. Binder, B.M., M.S. Biernbaum, and M.D. Bownds, *Light activation of one rhodopsin molecule causes the phosphorylation of hundreds of others. A reaction observed in electropermeabilized frog rod outer segments exposed to dim illumination.* J Biol Chem, 1990. **265**: p. 15333-40.

82. Binder, B.M., et al., *Phosphorylation of non-bleached rhodopsin in intact retinas and living frogs.* J Biol Chem, 1996. **271**: p. 19826-30.

83. Hanson, S.M., et al., *Each rhodopsin molecule binds its own arrestin.* Proc Nat Acad Sci USA, 2007. **104**: p. 3125-8.

84. Song, X., et al., *Arrestin-1 expression in rods: balancing functional performance and photoreceptor health.* Neuroscience, 2011. **174**: p. 37-49.

85. Strissel, K.J., et al., *Arrestin translocation is induced at a critical threshold of visual signaling and is superstoichiometric to bleached rhodopsin.* J Neurosci, 2006. **26**: p. 1146-1153.

86. Kim, M., et al., *Robust self-association is a common feature of mammalian visual arrestin-1.* Biochemistry, 2011. **50**: p. 2235-2242.

87. Nair, K.S., et al., *Light-dependent redistribution of arrestin in vertebrate rods is an energy-independent process governed by protein-protein interactions.* Neuron, 2005. **46**: p. 555-567.

88. Hanson, S.M., et al., *A model for the solution structure of the rod arrestin tetramer.* Structure, 2008. **16**: p. 924-34.

89. Imamoto, Y., et al., *Concentration-dependent tetramerization of bovine visual arrestin.* Biophys J, 2003. **85**: p. 1186-1195.

90. Schubert, C., et al., *Visual arrestin activity may be regulated by self-association.* J Biol Chem, 1999. **274**: p. 21186-21190.

91. Najafi, M., N.A. Maza, and P.D. Calvert, *Steric volume exclusion sets soluble protein concentrations in photoreceptor sensory cilia.* Proc Natl Acad Sci U S A, 2012. **109**: p. 203-208.

92. Gross, O.P. and M.E. Burns, *Control of rhodopsin's active lifetime by arrestin-1 expression in mammalian rods.* J Neurosci, 2010. **30**: p. 3450-3457.

93. Gurevich, V.V., et al., *The functional cycle of visual arrestins in photoreceptor cells.* Prog Retin Eye Res, 2011. **30**: p. 405-430.

94. Song, X., et al., *Enhanced Arrestin Facilitates Recovery and Protects Rod Photoreceptors Deficient in Rhodopsin Phosphorylation.* Curr Biol, 2009. **19**: p. 700-705.

95. Shi, Y. and J. Wu, *Structural basis of protein-protein interaction studied by NMR.* J Struct Funct Genomics, 2007. **8**(2-3): p. 67-72.

96. Zhuang, T.D., et al., *Elucidation of Inositol Hexaphosphate and Heparin Interaction Sites and Conformational Changes in Arrestin-1 by Solution Nuclear Magnetic Resonance.* Biochemistry, 2010. **49**(49): p. 10473-10485.

97. Gurevich, V.V. and J.L. Benovic, *Cell-free expression of visual arrestin. Truncation mutagenesis identifies multiple domains involved in rhodopsin interaction.* J. Biol. Chem., 1992. **267**: p. 21919-21923.

98. Ernst, O.P., et al., *Monomeric G protein-coupled receptor rhodopsin in solution activates its G protein transducin at the diffusion limit.* Proc. Natl. Acad. Sci. USA, 2007. **104**(26): p. 10859-10864.

99. Kaya, A.I., et al., *Coupling Efficiency of Rhodopsin and Transducin in Bicelles.* Biochemistry, 2011. **50**(15): p. 3193-3203.

100. Popot, J.L., *Amphipols, Nanodiscs, and Fluorinated Surfactants: Three Nonconventional Approaches to Studying Membrane Proteins in Aqueous Solutions.* Annual Review of Biochemistry, Vol 79, 2010. **79**: p. 737-775.

101. Gurevich, V.V. and J.L. Benovic, *Visual Arrestin Interaction with Rhodopsin - Sequential Multisite Binding Ensures Strict Selectivity toward Light-Activated Phosphorylated Rhodopsin.* Journal of Biological Chemistry, 1993. **268**(16): p. 11628-11638.

102. Gurevich, V.V., et al., *Arrestin interaction with G protein-coupled receptors. Direct binding studies of wild type and mutant arrestins with rhodopsin, b2-adrenergic, and m2 muscarinic cholinergic receptors.* J Biol Chem, 1995. **270**: p. 720-731.

103. Hanson, S.M. and V.V. Gurevich, *The differential engagement of arrestin surface charges by the various functional forms of the receptor.* J Biol Chem, 2006. **281**: p. 3458-3462.

104. Ohguro, H., et al., *Topographic study of arrestin using differential chemical modifications and hydrogen/deuterium exchange.* Protein Sci., 1994. **3**: p. 2428-2434.

105. Pulvermuller, A., et al., *Interactions of metarhodopsin II. Arrestin peptides compete with arrestin and transducin.* J. Biol. Chem., 2000. **275**: p. 37679-37685.

106. Vishnivetskiy, S.A., et al., *Few residues within an extensive binding interface drive receptor interaction and determine the specificity of arrestin proteins.* J Biol Chem, 2011. **286**: p. 24288-24299.

107. Vishnivetskiy, S.A., et al., *Mapping the arrestin-receptor interface: structural elements responsible for receptor specificity of arrestin proteins.* J. Biol. Chem., 2004. **279**(2): p. 1262-1268.

108. Mendez, A., et al., *Rapid and reproducible deactivation of rhodopsin requires multiple phosphorylation sites.* Neuron, 2000. **28**: p. 153-164.

109. Choe, H.W., et al., *Crystal structure of metarhodopsin II.* Nature, 2011. **471**: p. 651-655.

110. Li, J., et al., *Structure of bovine rhodopsin in a trigonal crystal form.* J Mol Biol, 2004. **343**: p. 1409-1438.

111. Park, J.H., et al., *Crystal structure of the ligand-free G-protein-coupled receptor opsin.* Nature, 2008. **454**: p. 183-7.

112. Scheerer, P., et al., *Crystal structure of opsin in its G-protein-interacting conformation.* Nature, 2008. **455**: p. 497-502.

113. Pulvermuller, A., et al., *Functional differences in the interaction of arrestin and its splice variant, p44, with rhodopsin.* Biochemistry, 1997. **36**: p. 9253-60.

114. Schleicher, A., H. Kuhn, and K.P. Hofmann, *Kinetics, binding constant, and activation energy of the 48-kDa protein-rhodopsin complex by extra-metarhodopsin II.* Biochemistry, 1989. **28**(4): p. 1770-1775.

115. Palczewski, K., et al., *Phosphorylated rhodopsin and heparin induce similar conformational changes in arrestin.* J Biol Chem, 1991. **266**: p. 18649-18654.

116. Tugarinov, V. and L.E. Kay, *Methyl groups as probes of structure and dynamics in NMR studies of high-molecular-weight proteins.* Chembiochem, 2005. **6**(9): p. 1567-1577.

117. Redfield, C., *Using nuclear magnetic resonance spectroscopy to study molten globule states of proteins.* Methods, 2004. **34**: p. 121-123.

118. Hofmann, K.P., et al., *The role of arrestin and retinoids in the regeneration pathway of rhodopsin.* J Biol Chem, 1992. **267**: p. 15701-15706.

119. Sommer, M.E., K.P. Hofmann, and M. Heck, *Distinct loops in arrestin differentially regulate ligand binding within the GPCR opsin.* Nat Commun, 2012. **3**: p. 995.

120. Vogel, R. and F. Siebert, *Conformations of the active and inactive states of opsin.* J Biol Chem, 2001. **276**: p. 38487-38493.

121. Emeis, D., et al., *Complex formation between metarhodopsin II and GTP-binding protein in bovine photoreceptor membranes leads to a shift of the photoproduct equilibrium.* FEBS Lett, 1982. **143**: p. 29-34.

122. Pervushin, K., et al., *Attenuated T2 relaxation by mutual cancellation of dipole-dipole coupling and chemical shift anisotropy indicates an avenue to NMR structures of very large biological macromolecules in solution.* Proc Natl Acad Sci USA, 1997. **94**: p. 12366-12371.

123. Tsukamoto, H., et al., *Monomeric Rhodopsin Is the Minimal Functional Unit Required for Arrestin Binding.* J Mol Biol, 2010. **399**: p. 501-511.

124. Kovacs, H., D. Moskau, and M. Spraul, *Cryogenically cooled probes—a leap in NMR technology.* Prog NMR Spectr, 2005. **46**: p. 131–155.

125. Luo, D.G., T. Xue, and K.W. Yau, *How vision begins: an odyssey.* Proc Natl Acad Sci U S A, 2008. **105**: p. 9855-9862.

126. Gurevich, E.V. and V.V. Gurevich, *Arrestins are ubiquitous regulators of cellular signaling pathways.* Genome Biol, 2006. **7**: p. 236.

127. Gurevich, V.V. and E.V. Gurevich, *The new face of active receptor bound arrestin attracts new partners.* Structure, 2003. **11**(9): p. 1037-42.

128. Shukla, A.K., et al., *Structure of active beta-arrestin-1 bound to a G-protein-coupled receptor phosphopeptide.* Nature, 2013. **497**(7447): p. 137-41.

129. Storez, H., et al., *Homo- and hetero-oligomerization of beta-arrestins in living cells.* J Biol Chem, 2005. **280**(48): p. 40210-5.

130. Bunce, C.M., et al., *Comparison of the levels of inositol metabolites in transformed haemopoietic cells and their normal counterparts.* Biochem J, 1993. **289 ( Pt 3)**: p. 667-73.

131. Sasakawa, N., M. Sharif, and M.R. Hanley, *Metabolism and biological activities of inositol pentakisphosphate and inositol hexakisphosphate.* Biochem Pharmacol, 1995. **50**(2): p. 137-46.

132. Zhan, X., et al., *Crystal structure of arrestin-3 reveals the basis of the difference in receptor binding between two non-visual arrestins.* J Mol Biol, 2011. **406**: p. 467-478.

133. Breitman, M., et al., *Silent scaffolds: inhibition of c-Jun N-terminal kinase 3 activity in the cell by a dominant-negative arrestin-3 mutant.* J Biol Chem, 2012. **287**: p. 19653-19664.

134. Gimenez, L.E., et al., *Manipulation of very few receptor discriminator residues greatly enhances receptor specificity of non-visual arrestins.* J Biol Chem, 2012. **287**(35): p. 29495-29505.

135. Oldham, W.M. and H.E. Hamm, *Structural basis of function in heterotrimeric G proteins.* Q Rev Biophys, 2006. **39**(2): p. 117-66.

136. Milano, S.K., et al., *Scaffolding functions of arrestin-2 revealed by crystal structure and mutagenesis.* Biochemistry, 2002. **41**(10): p. 3321-8.

137. Vishnivetskiy, S.A., et al., *Transition of arrestin into the active receptor-binding state requires an extended interdomain hinge.* J Biol Chem, 2002. **277**(46): p. 43961-7.

138. Westblade, L.F., et al., *Structural basis for the bacterial transcription-repair coupling factor/RNA polymerase interaction.* Nucleic Acids Res, 2010. **38**(22): p. 8357-69.

139. Milano, S.K., et al., *Nonvisual arrestin oligomerization and cellular localization are regulated by inositol hexakisphosphate binding.* J Biol Chem, 2006. **281**(14): p. 9812-23.

140. Ostermaier, M.K., et al., *Functional map of arrestin-1 at single amino acid resolution.* Proc Natl Acad Sci USA, 2014. **111**(5): p. 1825-1830.

141. Luttrell, L.M., et al., *Activation and targeting of extracellular signal-regulated kinases by beta-arrestin scaffolds.* Proc Natl Acad Sci U S A, 2001. **98**: p. 2449-54.

142. Lim, W.A., *Designing customized cell signalling circuits.* Nat Rev Mol Cell Biol, 2010. **11**: p. 393-403.

143. Burack, W.R. and A.S. Shaw, *Signal transduction: hanging on a scaffold.* Curr Opin Cell Biol, 2000. **12**: p. 211-216.

144. Dhanasekaran, D.N., et al., *Scaffold proteins of MAP-kinase modules.* Oncogene, 2007(22): p. 3185-3202.

145. Keshet, Y. and R. Seger, *The MAP kinase signaling cascades: a system of hundreds of components regulates a diverse array of physiological functions.* Methods Mol Biol, 2010. **661**: p. 3-38.

146. Good, M.C., J.G. Zalatan, and W.A. Lim, *Scaffold proteins: hubs for controlling the flow of cellular information.* Science, 2011. **332**: p. 680-686.

147. Davis, R.J., *Signal transduction by the JNK group of MAP kinases.* Cell, 2000. **103**: p. 239-252.

148. Flemming, A., *Alzheimer's Disease: JNK3 as new target in AD?* Nat Rev Drug Discov, 2012. **11**: p. 829.

149. Sabapathy, K., *Role of the JNK pathway in human diseases.* Prog Mol Biol Transl Sci, 2012. **106**: p. 145-169.

150. Yoon, S.O., et al., *JNK3 perpetuates metabolic stress induced by Aβ peptides.* Neuron, 2012. **75**: p. 824-837.

151. Lawler, S., et al., *Synergistic activation of SAPK1/JNK1 by two MAP kinase kinases in vitro.* Curr Biol, 1998. **8**: p. 1387-1390.

152. Yasuda, J., et al., *The JIP group of mitogen-activated protein kinase scaffold proteins.* Mol Cell Biol, 1999. **19**: p. 7245-7254.

153. Zhan, X., et al., *Arrestin-3 binds the MAP kinase JNK3α2 via multiple sites on both domains.* Cell Signal, 2014. **26**: p. 766-776.

154. Zhan, X., et al., *Arrestin-3-Dependent Activation of c-Jun N-Terminal Kinases (JNKs).* Curr Protoc Pharmacol, 2015. **68**: p. 2.12.1-2.12.26.

155. Els, S., A.G. Beck-Sickinger, and C. Chollet, *Ghrelin receptor: high constitutive activity and methods for developing inverse agonists.* Methods Enzymol, 2010. **485**: p. 103-21.

156. Ahmed, M.R., et al., *Ubiquitin ligase parkin promotes Mdm2-arrestin interaction but inhibits arrestin ubiquitination.* Biochemistry, 2011. **50**: p. 3749-3763.

157. Levchenko, A., J. Bruck, and P.W. Sternberg, *Scaffold proteins may biphasically affect the levels of mitogen-activated protein kinase signaling and reduce its threshold properties.* Proc Natl Acad Sci U S A, 2000. **97**: p. 5818-5823.

158. Levchenko, A., J. Bruck, and P.W. Sternberg, *Regulatory modules that generate biphasic signal response in biological systems.* Syst Biol (Stevenage), 2004. **1**: p. 139-148.

159. Sutton, R.B., et al., *Crystal Structure of Cone Arrestin at 2.3Å: Evolution of Receptor Specificity.* J Mol Biol, 2005. **354**: p. 1069-1080.

160. Chen, Q., et al., *Self-association of arrestin family members.* Handb Exp Pharmacol, 2014. **219**: p. 205-23.

161. Wacker, W.B., et al., *Experimental allergic uveitis. Isolation, characterization, and localization of a soluble uveitopathogenic antigen from bovine retina.* J Immunol, 1977. **119**: p. 1949-1958.

162. Kuhn, H., S.W. Hall, and U. Wilden, *Light-induced binding of 48-kDa protein to photoreceptor membranes is highly enhanced by phosphorylation of rhodopsin.* FEBS Lett., 1984. **176**: p. 473-478.

163. Granzin, J., et al., *X-ray crystal structure of arrestin from bovine rod outer segments.* Nature, 1998. **391**(6670): p. 918-921.

164. Gurevich, V.V. and J.L. Benovic, *Mechanism of phosphorylation-recognition by visual arrestin and the transition of arrestin into a high affinity binding state.* Mol Pharmacol, 1997. **51**: p. 161-169.

165. Shilton, B.H., et al., *The solution structure and activation of visual arrestin studied by small-angle X-ray scattering.* Eur J Biochem, 2002. **269**(15): p. 3801-3809.

166. Hanson, S.M., et al., *Structure and function of the visual arrestin oligomer.* EMBO J, 2007. **26**: p. 1726-36.

167. Mogridge, J., *Using light scattering to determine the stoichiometry of protein complexes.* Methods Mol Biol, 2004. **261**: p. 113-118.

168. Jeschke, G., *Distance measurements in the nanometer range by pulse EPR.* Chemphyschem, 2002. **3**: p. 927-932.

169. Pannier, M., et al., *Dead-time free measurement of dipole-dipole interactions between electron spins.* Journal of Magnetic Resonance, 2000. **142**(2): p. 331-340.

170. Altenbach, C., et al., *Estimation of Inter-Residue Distances in Spin Labeled Proteins at Physiological Temperatures: Experimental Strategies and Practical Limitations.* Biochemistry, 2001. **40**: p. 15471-15482.

171. Gray, J.J., et al., *Protein–protein docking with simultaneous optimization of rigid-body displacement and side-chain conformations.* J Mol Biol, 2003. **331**: p. 281-299.

172. Gray, J.J., et al., *Protein-protein docking predictions for the CAPRI experiment.* Proteins, 2003. **52**(1): p. 118-22.

173. Schueler-Furman, O., et al., *Progress in modeling of protein structures and interactions.* Science, 2005. **310**(5748): p. 638-42.

174. Wang, C., O. Schueler-Furman, and D. Baker, *Improved side-chain modeling for protein-protein docking.* Protein Sci, 2005. **14**(5): p. 1328-39.

175. Dinculescu, A., et al., *Insertional mutagenesis and immunochemical analysis of visual arrestin interaction with rhodopsin.* J Biol Chem, 2002. **277**: p. 11703-11708.

176. Gurevich, V.V., et al., *Binding of wild type and chimeric arrestins to the m2 muscarinic cholinergic receptor.* J Biol Chem, 1993. **268**(23): p. 16879-82.

177. Kim, M., et al., *Conformation of receptor-bound visual arrestin.* Proc Nat Acad Sci USA, 2012. **109**: p. 18407-18412.

178. Zhuang, T., et al., *Elucidation of inositol hexaphosphate and heparin interaction sites and conformational changes in arrestin-1 by solution nuclear magnetic resonance.* Biochemistry, 2010. **49**(49): p. 10473-85.

179. Vishnivetskiy, S.A., et al., *Engineering visual arrestin-1 with special functional characteristics.* J. Biol. Chem., 2013. **288**(17): p. 11741-11750.

180. Wilden, U., et al., *Rapid affinity purification of retinal arrestin (48 kDa protein) via its light-dependent binding to phosphorylated rhodopsin.* FEBS Lett, 1986. **207**(2): p. 292-295.

181. Gray-Keller, M.P., et al., *Arrestin with a single amino acid sustitution quenches light-activated rhodopsin in a phosphorylation0independent fasion.* Biochemistry, 1997. **36**: p. 7058-7063.

182. Arshavsky, V.Y. and M.E. Burns, *Photoreceptor signaling: supporting vision across a wide range of light intensities.* J Biol Chem, 2012. **287**(3): p. 1620-1626.

183. Makino, C.L., X.H. Wen, and J. Lem, *Piecing together the timetable for visual transduction with transgenic animals.* Curr Opin Neurobiol, 2003. **13**(4): p. 404-412.

184. Nikonov, S.S., et al., *Mouse cones require an arrestin for normal inactivation of phototransduction.* Neuron, 2008. **59**: p. 462-74.

185. Pugh, E.N., Jr. and T.D. Lamb, *Phototransduction in vertebrate rods and cones: Molecular mechanisms of amplification, recovery and light adaptation.*, in *Handbook of Biological Physics. Molecular Mechanisms in Visual Transduction*, D.G. Stavenga, W.J. DeGrip, and E.N. Pugh, Jr., Editors. 2000, Elsevier: Amsterdam. p. 183-255.

186. Gurevich, V.V., *The selectivity of visual arrestin for light-activated phosphorhodopsin is controlled by multiple nonredundant mechanisms.* J. Biol. Chem., 1998. **273**: p. 15501-15506.

187. Song, X., et al., *Rapid degeneration of rod photoreceptors expressing self-association-deficient arrestin-1 mutant* Cell Signal, 2013: p. in review.

188. Tan, E., et al., *The relationship between opsin overexpression and photoreceptor degeneration.* Invest Ophthalmol Vis Sci, 2001. **42**: p. 589-600.

189. Peet, J.A., et al., *Quantification of the cytoplasmic spaces of living cells with EGFP reveals arrestin-EGFP to be in disequilibrium in dark adapted rod photoreceptors.* J Cell Sci, 2004. **117**: p. 3049-59.

190. Huang, S.P., B.M. Brown, and C.M. Craft, *Visual Arrestin 1 acts as a modulator for N-ethylmaleimide-sensitive factor in the photoreceptor synapse.* J Neurosci, 2010. **30**: p. 9381-9391.

191. Chan, S., et al., *Functional comparisons of visual arrestins in rod photoreceptors of transgenic mice.* Invest. Ophthalmol. Vis. Sci., 2007. **48**: p. 1968-1075.

192. Gurevich, V.V., et al., *Agonist-receptor-arrestin, an alternative ternary complex with high agonist affinity.* J Biol Chem, 1997. **272**: p. 28849-28852.

193. Hanson, S.M., et al., *Opposing effects of inositol hexakisphosphate on rod arrestin and arrestin2 self-association.* Biochemistry, 2008. **47**: p. 1070-5.

194. Moaven, H., et al., *Visual arrestin interaction with clathrin adaptor AP-2 regulates photoreceptor survival in the vertebrate retina.* Proc Natl Acad Sci U S A, 2013. **110**(23): p. 9463-9468.

195. Gurevich, E.V., J.L. Benovic, and V.V. Gurevich, *Arrestin2 and arrestin3 are differentially expressed in the rat brain during postnatal development.* Neuroscience, 2002. **109**: p. 421-436.

196. Gurevich, E.V., J.L. Benovic, and V.V. Gurevich, *Arrestin2 expression selectively increases during neural differentiation.* J Neurochem, 2004. **91**: p. 1404-1416.

197. Hanson, S.M., et al., *Arrestin mobilizes signaling proteins to the cytoskeleton and redirects their activity.* J Mol Biol, 2007. **368**: p. 375-87.

198. Scott, M.G., et al., *Differential nucleocytoplasmic shuttling of beta-arrestins. Characterization of a leucine-rich nuclear export signal in beta-arrestin2.* J Biol Chem, 2002. **277**(40): p. 37693-37701.

199. Wang, P., et al., *Subcellular localization of beta-arrestins is determined by their intact N domain and the nuclear export signal at the C terminus.* J Biol Chem, 2003. **278**: p. 11648-11653.

200. Shears, S.B., *Assessing the omnipotence of inositol hexakisphosphate.* Cell Signal, 2001. **13**(3): p. 151-158.

201. Bayburt, T.H., et al., *Rhodopsin monomer is sufficient for normal rhodopsin kinase (GRK1) phosphorylation and arrestin-1 binding.* J. Biol. Chem., 2011. **286**: p. 1420-1428.

202. Zhuang, T., et al., *Involvement of Distinct Arrestin-1 Elements in Binding to Different Functional Forms of Rhodopsin.* Proc Nat Acad Sci USA, 2013. **110**(3): p. 942-947.

203. Sommer, M.E., K.P. Hofmann, and M. Heck, *Arrestin-rhodopsin binding stoichiometry in isolated rod outer segment membranes depends on the percentage of activated receptors.* J Biol Chem, 2011. **286**: p. 7359-7369.

204. Sommer, M.E., W.C. Smith, and D.L. Farrens, *Dynamics of arrestin-rhodopsin interactions: acidic phospholipids enable binding of arrestin to purified rhodopsin in detergent.* Journal of Biological Chemistry, 2006. **281**(14): p. 9407-17.

205. Boularan, C., et al., *beta-arrestin 2 oligomerization controls the Mdm2-dependent inhibition of p53.* Proc Natl Acad Sci U S A, 2007. **104**(46): p. 18061-18066.

206. Benovic, J.L., et al., *Regulation of G protein-coupled receptors by agonist-dependent phosphorylation.* Soc Gen Physiol Ser, 1990. **45**: p. 87-103.

207. Lohse, M.J., et al., *Multiple pathways of rapid beta 2-adrenergic receptor desensitization. Delineation with specific inhibitors.* J Biol Chem, 1990. **265**(6): p. 3202-11.

208. Luttrell, L.M. and D. Gesty-Palmer, *Beyond desensitization: physiological relevance of arrestin-dependent signaling.* Pharmacol Rev, 2010. **62**(2): p. 305-30.

209. Escriba, P.V., et al., *Lipid-protein interactions in GPCR-associated signaling.* Biochim Biophys Acta, 2007. **1768**(4): p. 836-52.

210. Garcia-Higuera, I., et al., *Association of the regulatory beta-adrenergic receptor kinase with rat liver microsomal membranes.* J Biol Chem, 1994. **269**(2): p. 1348-55.

211. Wedegaertner, P.B., P.T. Wilson, and H.R. Bourne, *Lipid modifications of trimeric G proteins.* J Biol Chem, 1995. **270**(2): p. 503-6.

212. McPherson, A., *Introduction to protein crystallization.* Methods, 2004. **34**(3): p. 254-65.

213. Fernandez, E.J., C. Abad-Zapatero, and K.W. Olsen, *Crystal structure of Lysbeta(1)82-Lysbeta(2)82 crosslinked hemoglobin: a possible allosteric intermediate.* J Mol Biol, 2000. **296**(5): p. 1245-56.

214. Lebon, G., et al., *Thermostabilisation of an agonist-bound conformation of the human adenosine A(2A) receptor.* J Mol Biol, 2011. **409**(3): p. 298-310.

215. Yan, C., et al., *Structure of a yeast spliceosome at 3.6-angstrom resolution.* Science, 2015. **349**(6253): p. 1182-91.